STUDIES ON INTERACTION FIELD DUE TO A TRANSVERSE SUPERSONIC JET INJECTION INTO A SUPERSONIC FLOW OVER A FLAT PLATE

By

Sreejith. K

DEPARTMENT OF AEROSPACE ENGINEERING

Indain Institute of Technology Kapnur

MAY, 2004

STUDIES ON INTERACTION FIELD DUE TO A TRANSVERSE SUPERSONIC JET INJECTION INTO A SUPERSONIC FLOW OVER A FLAT PLATE

A Thesis Submitted
in Partial Fulfillment of the Requirements
for the Degree of
Master of Technology

by

Sreejith. K

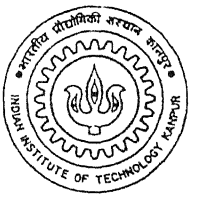

to the

Department of Aerospace Engineering
Indian Institute of Technology, Kanpur

May, 2004

Certificate

This is to certify that the work contained in the thesis entitled " *STUDIES ON INTERACTION FIELD DUE TO A TRANSVERSE SUPERSONIC JET INJECTION INTO A SUPERSONIC FLOW OVER A FLAT PLATE* ", by *Sreejith. K*, has been carried out under my supervision and that this work has not been submitted elsewhere for a degree.

May, 2004

(Dr. E. Rathakrishnan)
Department of Aerospace Engineering,
Indian Institute of Technology,
Kanpur.

Dedicated

to

My Beloved Parents

Acknowledgements

I take this opportunity to express my sincere gratitude towards my thesis supervisor Dr. E. Rathakrishnan for his invaluable guidance. It would have never been possible for me to take this project to completion without his innovative ideas and his relentless support and encouragement. I consider myself extremely fortunate to have had a chance to work under his supervision. Learning how to do research and problem solving methodology from him has being a life time experiences in itself.

I must acknowledge with a lot of gratitude, for the spontaneous assistance and cooperation extended by Mr. Suresh Mishra, Mr. Sharad Chuhan and Mr. Mahendra of High Speed Aerodynamics Laboratary, Dept. of Aerospace Engg.

I am very much thankful to Mr. Shibu, Mr. Sivaprasad, Mr. Lovaraju, Mr. Vinoth and Paparao, who helped me a lot during experimentation for the present investigation.

I would like to thank my friend Mr. Sumesh. P. T for his help towards the type setting during my report preparation.

I would like to thank my friends who helped me in various stages and for their mental support. The blessings of my parents and my family members have been an invaluable source of inspiration.

Sreejith. K

Abstract

The present experimental study aims at understanding the details of the flow which results when a transverse secondary supersonic jet discharges into a flow field over a flat plate which is established by a supersonic flow exiting a Laval nozzle flowing over the plate kept in-line with the bottom wall of the nozzle. The interaction flow field is investigated using optical visualizations and probe based measurement techniques. Results of wall pressure along the plate centerline and around the injection nozzle periphery are reported for a number of tests differing by main nozzle Mach number, secondary injection Mach number and the nozzle pressure ratio of the secondary jet. Shadowgraph visualizations documented the global characteristics of the interaction flow field. The quantitative and qualitative results are used to characterize the flow field on the plate due to the combined flow. The penetration and turning of the secondary jet is governed by the waves prevailing in the freestream flow and the expansion level of secondary jet, which is strongly influenced by the nozzle pressure ratio. The strong bow shock formed ahead of the secondary injection, causes the main flow to separate, and produce a high pressure zone ahead of the injection and a suction zone behind the secondary injection. It is found that the penetration height depends on the momentum flux of the secondary jet, which is a function of both injection Mach number and pressure ratio. The compression zone ahead and suction downstream of the injection port establishes a nosedown moment on the plate. The moment is found to increase with increase of secondary jet Mach number.

Experiments were conducted with Mach 1.72 and 1.95 main flow and the transverse secondary jet Mach numbers 1.35, 1.41 and 1.52. The main flow nozzles were operated at a constant NPR of 7 and the secondary jets were operated with NPR 4-9, in steps of 1 for every case of main flow. The secondary jet was located at one time the nozzle height, from the nozzle exit, along the axis.

Nomenclature

A_j Secondary nozzle exit area

A_∞ Main nozzle exit area

A_j^* Secondary nozzle throat area

c_p Specific heat

d Exit diameter of secondary nozzle

E Energy per unit length

F Force on the plate surface

h Penetration height

h_{j0} Specific enthalpy

K Shock correction factor

M Moment on the plate surface

M_{c0} Moment on the plate surface with out injection

M_∞ Freestream Mach number

M_j Secondary injection Mach number

$\dot{m}_j$ Mass flow rate

NPR Nozzle pressure ratio

P_a Atmospheric pressure

P_{c0} Pressure on the plate without injection

P_{0j} Stagnation pressure of secondary injection jet

P_0 Stagnation pressure

P_{0u} Stagnation pressure of freestream

P_0 Stagnation chamber pressure

R Gas constant

R_s Shock radius

R_{s0} Characteristic shock radius

T_0 Stagnation temparature

T_{0j} Staganation temparature for secondary jet

V_∞ Exit velocity of the jet

x Co-ordinate perpendicular to exit plane

List of Figures

Contents

Chapter 1

Introduction to Jet in Cross Flow

The jet-interaction flow field resulting from a gaseous jet injected transversely in to a supersonic freestream is a complex fluid dynamic problem and has been studied for quite some time. Examples of application of the jet interaction principles range from the very low speed regimes of a chimney plume in a cross flow to the very high speed of scramjet combustion and supersonic missile control systems and from the very low mass flow of boundarylayer control system to the high mass flow of V/STOL aircraft. An application of current interest for a transverse jet is as a fuel injector for a supersonic combustor. The development of supersonic combustors has been motivated by the desire to develop an air breathing hypersonic vehicle. For the injected fluid to mix well with the supersonic primary stream, the jet must have sufficient momentum to penetrate into the freestream. Because the trajectory of the injectant downstream of the Mach disk formed in the jet interaction flow field is nearly parallel to the surface through which the jet is injected, the height of the Mach disk has served as a measure of jet penetration into the freestream. The past work in the jet-interaction field consists primarily of correlation of experimental results for various injector and freestream parameters. Most commonly used parameters are the injectant to freestream stagnation pressure and momentum ratios, penetration height and shock radius. Several analytical models of the complex jet-interaction phenomena have been proposed[5–7]. However, they provide little information on the detailed structure of the interaction field. Many researchers have studied the jet-interaction problem with emphasis on the penetration of the injection fluid, in relation to fuel injection for supersonic combustion ramjet[8,9]. Some researchers have investigated the problem of supersonic jet injected into a supersonic freestream, with the aim of using

jet interaction as an aerodynamic control. Spaid and Zukoski[1] developed an analytical model by applying an integral momentum balance to predict the penetration of injectant into the freestream. The penetration height of the jet is one of the scaling factors for simply organizing the interaction between the supersonic freestream and the secondary jet. Schetz and Billing[5] suggested the concept of an effective back pressure, which was defined as an average static pressure around a jet. But the behavior of the effective back pressure has not been defined clearly yet. Also, it is very difficult to measure the effective back pressure in the cross flow interaction field. Shock radius is also a parameter used for the jet-interaction flow field study. The shape of the interaction shock is often important, as it determines the losses in fuel injection problems[1] and the surface pressure for attitude control applications. The radius of the induced bow shock can be treated as a function of the penetration height of the secondary jet or may be calculated from the blastwave analogy as presented by Collins[10]. The size and shape of the separation zone on the surface and the pressure distribution in that zone has been the subject of numerous studies.

Control of rockets, missiles and other flight vehicles by thrust deflection and jet reaction system has been the primary motivation for the present study. The present study focuses on the problem of normal injection of supersonic circular jets into a supersonic freestream over a flat plate, which is wave dominated. This configuration is a representative of a typical arrangement of an aerodynamic control system on a supersonic vehicle, such as missiles and interceptors. In the present work, the jet-interaction problem is analyzed over a flat plate rather than a body of revolution. Schematic representation of two typical flow fields observed experimentally by Dowdy and Newton[17]. The flow field is illustrated schematically in Fig. 1.1. As the jet is injected into the mainstream, it acts as an obstacle for the main flow. This obstruction results in the formation of a bow shock in the main flow upstream of the injector port. The resulting shock boundary layer interaction establishes a complex pressure field around the injection port, and a separation shock is also generated. The formation of the bow shock produces a high adverse pressure gradient in the flow field ahead of the injection port and causes boundary layer separation. If the jet coming out of the injection nozzle is highly underexpanded, after expanding at the injector nozzle exit, the jet fluid gets compressed through a barrel shock. As a result, Mach disks are formed and these Mach disks have very significant role in the jet penetration and mixing points of view. The secondary jet penetrates the mainstream to a certain height before it completely bent over and proceeds downstream with the primary fluid. The present study provides a preliminary estimate of the penetration height of

the secondary jet into the main flow, and some quantitative correlation for the shock radius with Broadwell's[16] blastwave analogy model of the interaction. Also, the force and moments acting on the plate due to the secondary injection are estimated using the surface pressure measurements on the plate.

1.1 Description of Flow Field

The problem of jet in a cross flow has attracted the attention of researchers, due to its vast raging application in different areas such as turbine blade cooling, V/STOL aircraft, control of missiles or chimney flows and so on. Investigation on the jet in a cross flow have started in the 1930s[18] with the mixing of chimney plumes. Since then there have been a numerous investigations on the jet in cross flow(JICF) leading to the perception that the JICF, in contrast to other flow configurations like the jet and mixing layer cannot be generalized in terms of self similarity and Reynolds number dependence due to strong non linear effects. The systematic analysis of JICF started in 1970s with the discovery and acceptance of coherent structures[19]. A clear definition of coherent structure cannot be given so far. Hussain[20] tried to define them as a "connected, large scale fluid mass with a phase correlated vorticity over its spatial extent", but still this definition is incomplete[21]. Most of the interest in research on JICF has been focused on the application to combustors. This is an interesting flow configuration with regard to mixing. It is one of the most effective way to mix two fluids in a limited space, which is superior to other flow constellations like the mixing layer or the jet in co-flow[16].

The flow pattern which results when a jet is introduced from a secondary nozzle in to a supersonic mainstream will be as shown in Fig. 1.2.The injected gas acts as an obstruction to the main stream or primary flow and produces a bow shock in the primary flow. The shock wave produces an adverse pressure gradient that causes the boundary layer on the wall to separate, and gives rise to a complex flow similar to that found upstream of a forward facing step. The disturbance propagates upstream through the boundary layer, causing a wedge like region of separated flow ahead of the jet, with its separation shock and elevated surface pressure. The injected secondary jet penetrates the primary stream to a certain height before it is completely bent over and proceeds downstream with the primary fluid. The level of expansion of the secondary jet plays a significant role on this complex flow field. The underexpanded jet expands in to the lower surrounding pressure and displays the characteristic Mach

disk of jets entering a quiescent medium. Since the injectant jet is turned downsream as a result of its interaction with the main stream flow, the Mach disk is inclined to the horizontal. The penetration height depends upon the charecteristics of the two jets and properties of the two fluids. A schematic of the three-dimensional flow field formed by normal injection into a supersonic cross flow over a flat plate is as shown in Fig. 1.3. This sketch illustrates the features of the flow field in a plane through the spanwise jet centerline, where a three dimensional-bow shock forms ahead of the jet and interacts with the approaching turbulent boundary layer resulting in separation. Two counter-rotating vortices form in the jet plume and contribute to the mixing of the injectant fluid with the freestream, mainly by entrainment of the freestream by the vortices. The fluid in the recirculation region cannot flow directly downstream along the center line due to the obstruction of the jet plume. This trapped fluid therefore forms a horse shoe vortex that starts in the recirculation region and trails downstream on the sides of the barrel shock.

In the jet interaction flow field, two primary mechanisms contribute to the production of the lateral forces. The first contribution comes directly from the thrust of the jet. The second contribution comes from the interaction of the jet with the cross flow. Figure 1.4 shows the typical pressure distribution along the centre line of the flat plate in the jet-interaction flow field. It is clear that, upstream of the injection is characterized by a high pressure zone and the downstream with a low pressure zone. The high pressures typical of recirculated flows augment the lateral force produced by the thrust of the jet. The low pressure zone behind the jet decreases the normal force on the plate created by the combined effects of the jet thrust and of the high pressure region ahead of the injector, and also it creates a couple with the high pressure zone and hence to produce a nose down moment about the injection point.

Most of the available literature is on the flow field of a secondary jet injected into an uniform main stream flow without wave domination. But to gain an insight into the flow field on a flying object like a missile due to the injection of a cross jet, it is imperative to have the freestream flow field similar to that on the flying body, which is wave dominated, due to the reflection of the waves generated at its nose cone from the free boundary. Such a field is essentially non-simple[22] with number of shock and expansion waves. Therefore in the present study, to simulate a field resembling that over a flying body with a nose cone followed by a parallel body, the flow from a Laval nozzle is made to flow over a flat plate attached to the lip of a nozzle exit.

1.2 Jets

Jet is a free shear flow driven by momentum introduced at the exit of, usually, a nozzle or an orifice which exhibits a characteristic, that the ratio of width to axial distance is a constant. The jet may also be defined as a fluid flow on either side of the tangential separation surfaces. Free jets can be defined as a pressure driven unrestricted flow of a fluid into a quiescent ambiance. Since a fluid boundary can't sustain a pressure difference across it, the jet boundary becomes a free shear layer, in which static pressure is constant throughout. The boundary layer at the exit of the nozzle develops as a free shear layer, mixing with the ambient fluid thereby entraining the ambient fluid into the jet stream. Thus, the mass flow at any cross-section of the jet progressively increases along the downstream direction. Hence, to conserve momentum the centerline velocity decreases with downstream distance. The vast quanta of knowledge presently available and the continuous research currently being carried out stand testimony to the importance associated with the jet flows. This is owing to their extensive nature of applicability, from household appliances to hi-tech rockets. High speed jets find application in numerous engineering fields; aircraft, rockets, missile, propulsive systems of aircraft, thrust augmenting ejectors and so on. In terms of academic interest, studies on jets have provided insight to the understanding of the jet dynamics of free shear layers and vortical structures. Jet flows are an important part of various mixing devices and propulsion systems, wherein enhanced rate of mixing or thrust augmentation is desirable. In combustion systems, both large and small scale mixing enhancement is sought since large scale mixing determines the rapidity of the mixing process and small scale or micro scale level mixing ensures effective molecular level mixing for efficient combustion. In combustion chambers with space constraint, the entire mixing process has to be completed within a short distance.

Basically jets can be classified into two categories namely incompressible and compressible jets. The jets with Mach number less than 0.3 upto which the compressible effects are negligible are called incompressible jets and these are subsonic jets. Compressible jets can be again subdivided into subsonic jets and supersonic jets. Supersonic jets are the jets with Mach number more than one, these can be further classified into overexpanded, underexpanded and correctly expanded jets. Compressible subsonic jets are with Mach numbers in between 0.3 to 0.8, and showing the following properties.

- The exit velocity is preserved upto some axial distance along the centerline from the exit of the nozzle known as potential core.

- The core extends about 6 times the nozzle exit diameter.
- Jet develops with an included angle of about 10 degrees.
- Subsonic jets are always correctly expanded.

A schematic diagram of a typical subsonic jet and the flow zones in it are shown in Fig. 1.5

1.2.1 Overexpanded Jets

If the pressure in the ambient medium is larger than that at the exit of the nozzle, the jet is said to be an overexpanded jet. In this oblique shock waves are formed at the edge of the nozzle exit. These oblique shocks will be reflected as wedge shaped expansion waves on the boundary of the jet. Figure. 1.6 shows a sketch of such a jet. If the pressure difference between exit pressure and back pressure is small, a periodic shock cell structure will exist in the jet and the wave length of these periodic structures will increase with Mach number.

When the flow is overexpanded the exhaust gas pressure, P_e, is higher than the supersonic isentropic exit pressure but lower than the ambient pressure, P_a. This causes an oblique shock (A) to form at the exit plane of the nozzle. To reach ambient pressure, the exhaust gas undergoes compression as it moves away from the nozzle exit and passes through the oblique shock wave standing at the exit plane.

Flow that has passed through the shock waves will be turned towards the center line (2). At the same time, the oblique shock wave, directed towards the centerline of the nozzle, can not penetrate the center plane since the center plane acts like a streamline. This causes the oblique shock wave to get reflected outwards (B) from the center plane. The gas flow goes through this reflected shocks and is further compressed but the flow is now turned parallel (3) to the center line. This causes the pressure of the exhaust gases to increase above the ambient pressure. Deflected shock wave now hits the free boundary called a contact discontinuity (or the boundary where outer edge of the gas flow meets the freestream air). Pressure is same across the boundary and so is the direction of the flow. Since the jet flow is at a higher pressure than the ambient pressure, the pressure must reduce. Thus, at the reflected shock wave-contact discontinuity intersection and expansion waves of the Prandtl-Meyer (P-M) type are set up (C) to reduce the pressure to P_a . These expansion waves turn the flow away from the center line (4). The P-M expansion waves in turn reflect from

the center plane towards the contact discontinuity (D). The gas flow passing through the reflected P-M waves is now turned back parallel to the center line but undergoes a further reduction of pressure. The reflected P-M waves now meet the contact discontinuity and reflect from the contact discontinuity towards the centerline as P-M waves (E). This allows the gas flow to pass through the P-M compression waves and increase its pressure to ambient pressure, but passes through the compression waves turns the flow back towards the centerline (6). The P-M compression waves now reflect from the centerline as compression waves (F) further increasing the pressure above ambient, but turn the flow parallel to the nozzle center line (7). The flow process is now back to when the flow had just passed through the reflected shock wave (B), i.e., the flow pressure is above the ambient pressure and the flow is parallel to the centerline (3). This process of expansion and compression wave formation continues until the pressure of the jet field is same as the ambient pressure and the flow is parallel to the centerline of the nozzle. These expansion and compression waves which interact with each other, lead to the diamond patterns termed as shock cells. Ideally this process would continue without end; but a turbulent shear layer created by the large velocity difference across the contact discontinuity will dissipate the wave patterns[24].

1.2.2 Underexpanded Jets

If the pressure in the ambient medium is lower than that at the exit of the nozzle, the jet is said to be un nderexpanded jet. If the back pressure is less than the nozzle exit pressure, wedge shaped expansion waves occur at the edge of the nozzle, these waves cross one another and get reflected from the opposite boundaries of the jet, as compression waves. The compression waves again cross one another and are reflected at the boundaries of the jet as expansion waves. Figure. 1.7 shows a sketch of such a jet.

1.2.3 Correctly Expanded Jets

If the nozzle exit pressure is equal to the back pressure then the jet is said to be correctly expanded. This jet is also wave dominated as imperfectly expanded jets, unlike what we think that there wont́ be any waves. The reason for this is that as the jet is issuing from the confined area to an infinite area, jet tries to expands through expansion waves and after that gets compressed through compression waves, which

results into a periodic wave structure.

1.3 Flow Visualization

Visualization of fluid flows proved to be an excellent tool for describing and calculating the flow properties in many problems of practical interest, in both subsonic and supersonic flow regimes. Researchers in this field have developed many techniques to visualize the motion of air. Smoke streams can be introduced into the flow to indicate not only its direction but also whether it is smooth or disturbed flow. Small tufts of wool even fine stands of hen-feathers or cat's whiskers can also be utilized to show direction oscillations in a down field. In the flow of water, aluminum powder sprinkled at the liquid surface will indicate local motions which can be photographed. Flow in water can also be studied by streams of hydrogen bubbles released by electrolysis from thin charged wires arranged across it. If attention is focused on the layer of air near a surface, chemical films can be applied on which the air will create patterns by evaporation, showing the direction and steadiness of the flow. In supersonic flows, the air density changes are sufficiently large to allow the air to be photographed directly using optical systems sensitive to density changes.

The general principle for flow visualization is to render the 'fluid particles' visible either by observing the motion of suitable selected foreign materials added to the flowing fluid or optical properties (such as refractive index) due to the variation of the properties of the flowing fluid itself. A third class of visualization technique is based on a combination of the above two principles. Each of these techniques is generally used for incompressible, compressible and low density gas flows, respectively. Some of popularly used visualization techniques to study flow problems of practical interest are the following[23].

- *Smoke flow visualization* is one of the popular techniques used in low speed flow fields with velocities upto 30 m/s. Smoke visualization is used to study problems like; boundary layer, air pollution problems, design of exhaust system of locomotives, cars, ships, topographical influence of disposal of stack grasses etc.

- *Tufts* are used to visualize flow fields in the speed range from 40–150 m/s. This technique is usually employed to study boundary layer flow, flow separation, stall spread, and so on.

- *Chemical coating* is used to visualize flow with medium speed in the range 40 to 150 m/s. Boundary layer flow, transition of the flow from laminar to turbulent and so on are usually described by this visualization technique.

- *Interferometry* is a technique to visualize high speed flows in the ranges of transonic and supersonic Mach numbers. This gives a qualitative estimate of flow density in the field.

- *Schlieren* is used to study high speed flows in the transonic and supersonic Mach number ranges. This again gives only a qualitative estimate of the density gradient of the field. This is used to visualize faint shock waves, expansion waves etc.

- *Shadowgraph* is yet another flow visualization technique meant for high speed flow with transonic and supersonic Mach numbers. This is employed for fields with strong shock waves.

1.3.1 The Direct Shadow/Shadowgraph Technique

This is admirably suited to the demonstration of compressibility phenomena, particularly to visualization of shock waves. The arrangement consists of a light source on one side of the tunnel and a screen on the other side. The visualization of the flow around a two-dimensional body in a wind tunnel, however , a more satisfactory arrangement is obtained by a collimating the light from the source into a parallel beam before it passes through the working section, by using a lens or mirror. The mechanism of the direct shadow is as follows. Let AB and CD be the undisturbed paths of two adjacent rays. In the disturbed field the rays are deflected, and if the refractive index gradient $\frac{\partial n}{\partial x}$ is constant, i.e. $\frac{\partial^2 n}{\partial x^2} = 0$. The deflected rays remain parallel. However, if $\frac{\partial^2 n}{\partial x^2}$ is positive the rays will diverge and if it is negative the rays will converge. Figure 1.8 shows the general nature of the variations of the density and its first and second derivatives through a shock wave. Thus at the front of the shock wave $\frac{\partial^2 n}{\partial x^2}$ is positive and the rays diverge, giving a region of decreased illumination on the screen, at the rear of the shock wave the rays converge and increase the illumination.

1.4 Application of Jets in Cross Flow

n practical engineering applications, jets in cross flow are found in both confined and nconfined environments.

Confined jets in cross flow include,

- Vertical and short Take-Off and Landing (V/STOL) aircraft in transition from hover to forward flight, in which case, the jets from its engine impinge on the ground surface.
- High altitude maneuvering of missiles, by injecting secondary jets from it's body.
- Thrust vector control of aircraft is commonly obtained with the use of fluid dynamic means such as secondary injection of gas or liquid into the exhaust nozzle.
- An important application of supersonic mixing enhancement is in scramjet combustion. Fuel can be efficiently mixed with supersonic air flow by injecting into the crossflow.
- Internal cooling of turbine blades by air jets impinging on the leading edge.

tion air jets in combustion chambers of gas turbine engines, where the are injected radially into the chamber, through discrete holes along its mference, inorder to stabilize the combustion process, and to dilute the combustion products near the end.

ined jets in cross flow include,

situation resulting from the action of cross winds on effluents from cooling rs, chimney stacks, or flames from petrochemical plants.

harge of sewage or waste heet into rivers or oceans.

mal plumes rising into cross winds in the atmosphere.

im of present investigation

tive of the present study is to understand the characteristics of the flow o the combination of supersonic main flow and a secondary jet, injected

transversely. Experimental study aims at understanding the effect of freestream Mach number, injection Mach number and injection NPR on flow characteristics like penetration height, shock strength and shock radius. Concentration was focused on the near flow field of injection jet to calculate the force and the moment generated due to the interaction of secondary supersonic injection into a supersonic freestream, which is used to control flying vehicles like missiles.

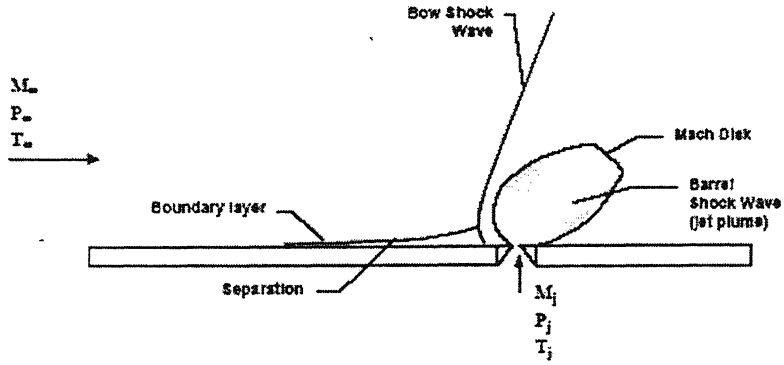

Figure 1.1 Schematic of the flow field due to the injection into a freestream

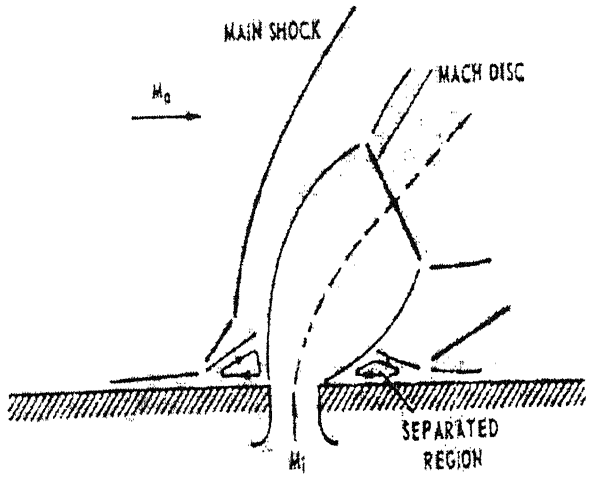

Figure 1.2 Schematic representation of flow field when a secondary jet injected into a supersonic flow

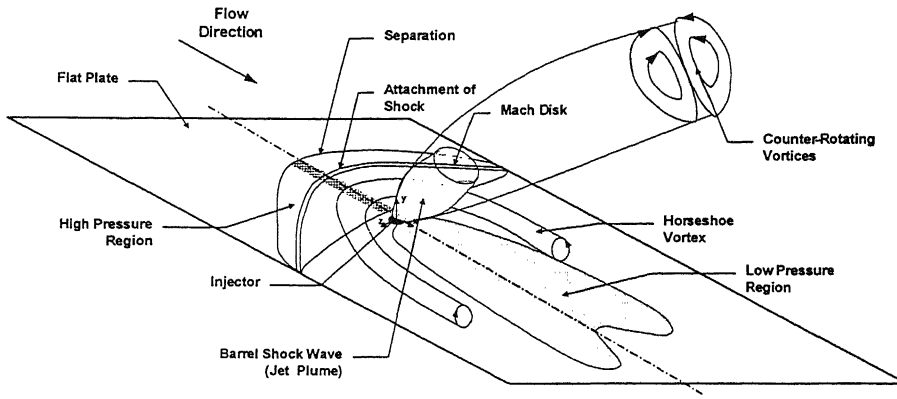

Figure 1.3 Three-dimensional schematic view of the flow field when a secondary jet injected into a supersonic cross flow

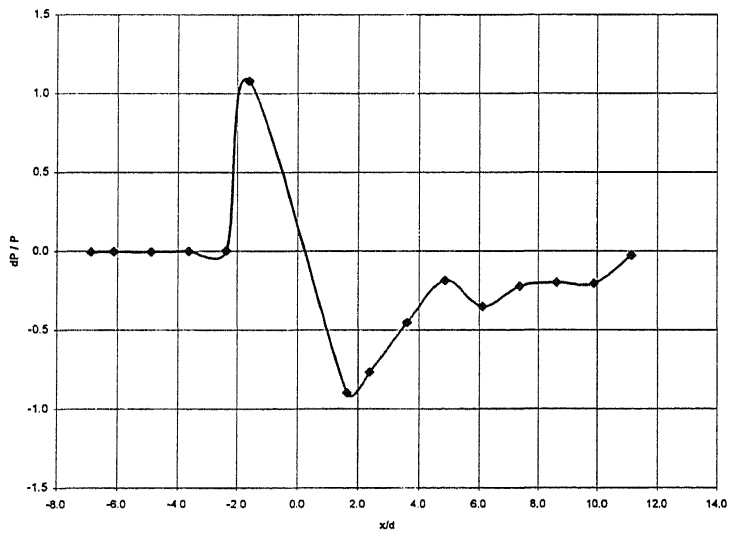

Figure 1.4 Typical pressure distribution along the plate centerline

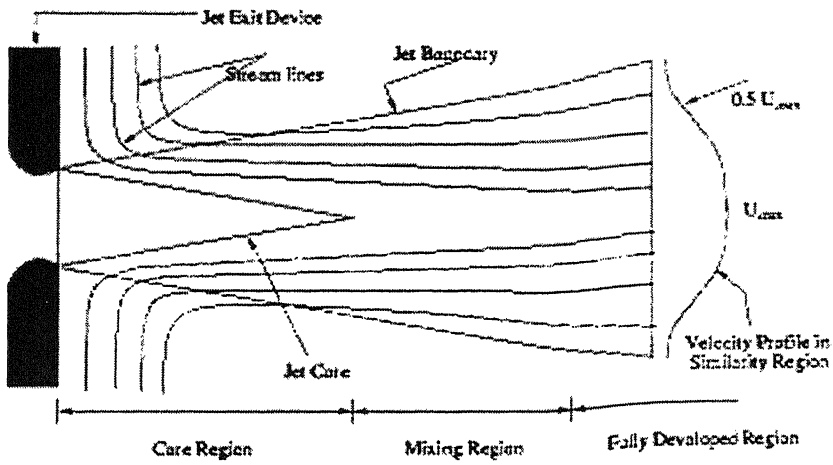

Figure 1.5 Schematic of subsonic jet flow and zones within jet

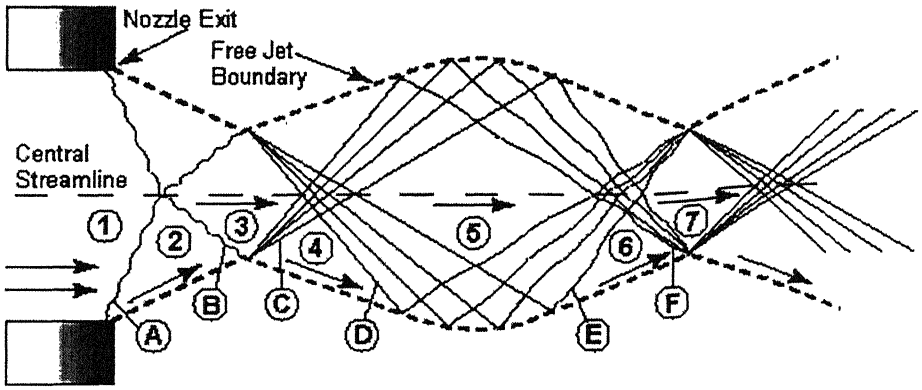

Figure 1.6 Schematic of overexpanded jet[20]

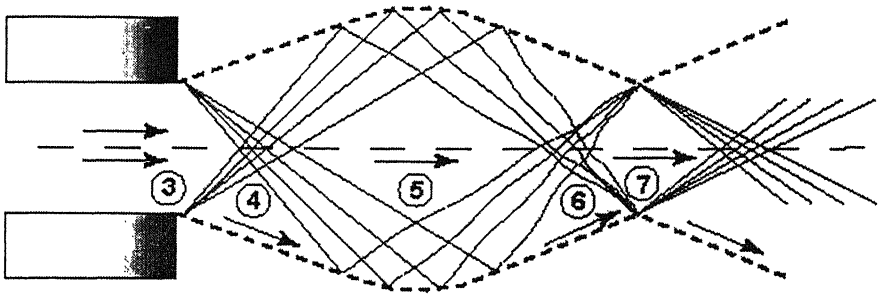

Figure 1.7 Schematic of underexpanded jet [24]

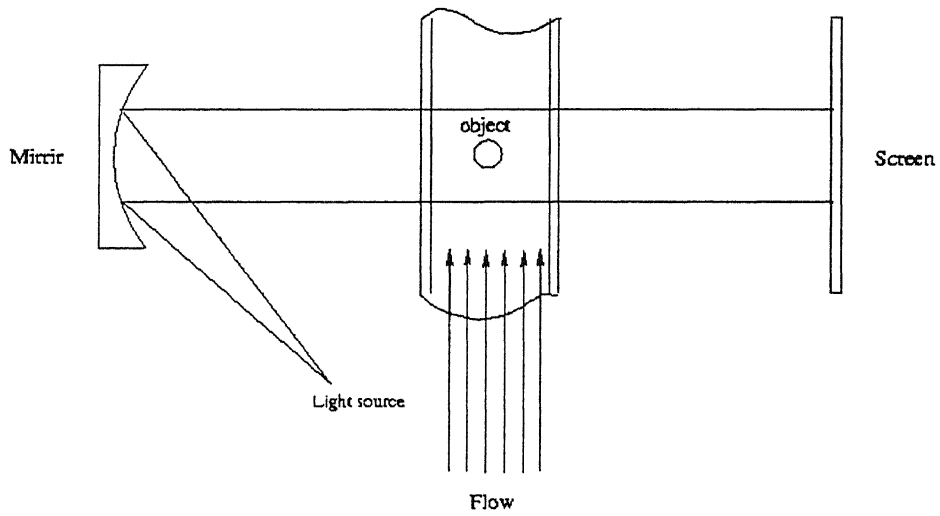

Figure 1.8 Schematic of shadowgraph arrangement

Chapter 2

Literature Review

The flow field dependence on fundamental values such as freestream Mach number, injector hole size, injectant gas composition, stagnation pressure ratio was studied by Spaid and Zukoski[1] and others in the 1960s. In their experiments freestream Mach number was varied between 1.38 to 4.54. The studied injectant gas included nitrogen, argon and helium into an uniform parallel stream of air. The secondary jets were sonic jets, issuing from a circular orifice in a plate, with the orifice axis normal to the plate surface. The surface pressure on the plate in the vicinity of the injector was studied via pressure taps drilled in the plate. Their study produced a general qualification of pressure over the surface, but did not produce a complete picture of the pressure field. Spaid and Zukoski in their investigation of injection phenomena, obtained the scaling laws for secondary injection by using an equivalent solid body model. An analytical model was developed by applying an integral momentum balance to predict the penetration of the secondary jet into the freestream. The line of maximum concentration of secondary jet rather than the jet boundary has been selected as the characteristic for the scale of the disturbance produced by the jet and was defined here as penetration height. The governing parameters for the prediction of penetration height of the secondary jet were the free stream Mach number and static pressure, as well as the injectant mass flow rate, stagnation temperature and gas constant. Measured values of the penetration height were not noticeably dependent on the state of the boundary layer.

Interaction of a supersonic stream and a transverse supersonic jet was investigated by Charwat and Allegre[2] through a series of experiments. The mixing region downstream of injection contains a horse shoe vortex separating the jet flow from the freestream flow near the nozzle wall. Their conclusions were, the penetration

and turning of the secondary jet is governed by the dynamics of the shock structure occurring in the free expansion plume and it is not a simple function of jet momentum, and the strength and location of the leading shock in the meridional plane is a function of the injected mass flow and the injection station Mach number only. They found some quantitative correlation with Broadwell's blast wave analogy model of the interaction. According to Charwat, the pressure jump across the leading shock does not depend explicitly on the stagnation pressure of the secondary jet and degree of expansion in the secondary nozzle bears little influence on the production of the main shock. With regard to mixing and penetration, Cohen[3] presented an experimental study of the interaction of a high velocity air stream with jets from single row multi hole wall injectors. Injected fluid included, helium, argon, and freon12. Cohen found out a correlation for the penetration height.

Study on the effects of momentum flux ratio, jet injectant pressure, and injected Mach number were performed by Orth and Funk[4]. They conducted a series of experiments in which hydrogen and nitrogen were injected at Mach numbers ranging between 1.0 and 1.67 from a nozzle in a flat plate, transversely in to a Mach 2.72 freestream of air. For these experiments the effective back pressure was taken to be the average static pressure around a cylindrical object on a flat plate in a supersonic flow. Conclusions from this were that, normalized penetration was found to be governed by both the ratio of the jet pressure to an effective back pressure and the ratio of the jet to freestream momentum. Absolute penetration was not substantially increased by increasing the stagnation pressure of sonic jets, but was increased by supersonic injection. Also, it was concluded from the study that the downstream region where the injectant behaves as a discrete jet with negligible mixing is quite short ($x/dj < 10$) and that most of the penetration occurs in this region.

Many analytical and numerical models representing the flow field of a supersonic injection into a supersonic freestream has been made by many investigators[5,6]. The secondary gas injected into a supersonic stream in the form of a highly underexpanded jet has been investigated by Schetz and Billing[5]. They contributed the first analytical model which considers jet spreading and momentum loss. The model is two-dimensional and predicts the jet trajectory by considering drag and centripetal force acting perpendicular to the trajectory of the jet. An analysis that does consider the structure of the secondary jet in the near downstream regions was developed. A solid body drag model was used to approximate the disturbance in the main stream caused by the behavior of the secondary jet near the injector, and the resulting drag

coefficient was used to determine the trajectory of the jet. They introduced the concept of effective back pressure, surrounding the injected jet. This back pressure is analogous to that around a jet injected in to quiescent air. The analysis developed is applied to a configuration study of a combustion chamber for a hypersonic ramjet with supersonic combustion.

Heister and Karagozian[6] describe an analytical model representing the deflection and mixing of a single gaseous jet in supersonic cross flow. The jet cross section is modeled in terms of a compressible vortex pair that results from viscous and impulsive forces acting at the periphery of the jet. The behavior of the vortex pair is then combined with mass and momentum balances along the axis of the jet to form a model that describes the trajectory and mixing of the injected fluid. Their model is however most appropriate for perfectly or slightly expanded jets and not suitable for highly underexpanded jets. Orth and Billing[7] presented the strengths and weaknesses of various physical and mathematical concepts that have been employed in the development of theories concerning transverse gaseous jet penetration in to a supersonic cross stream. A new unified model is presented and the development of the model rests on the similarity that exists between a jet discharging in to a quiescent medium and a jet discharging in to a cross flow. They obtained a correlation between the normal distance to the center of the Mach disk and the ratio of injection pressure to effective back pressure, by defining an effective back pressure concept. Other correlations are used to obtain the size and shape of the initial portion of the jet, and also calculated the complete trajectory of the injectant and one dimensional approximation of the mass-averaged properties at any point along the trajectory downstream of the Mach disk. In their study empirical relationships which describe the general characteristics of the structure of the jet in the quiescent medium were obtained and were used for the case with cross flow.

The role of interfacial eddies and large scale eddies in the flow field of a supersonic jet freestream interface has been studied by many investigators[8,9]. Gruber and Nejad[8] investigated the interaction between the upstream shock structure and the interfacial eddies in the jet fluid. Results indicate that the large structure strongly influences the near wall behavior of the bow shock, often resulting in severe curvature changes and positional fluctuations. Eddies exert a weaker influence on the bow shock further away from the wall. Lifting of the bow shock has been observed when the approaching boundary layer is relatively thick. Gruber and Goss[9] studied the effect of injector geometries on the jet free stream interface. They used pressure sensitive paint(PSP) to examine surface pressure in the flow fields created by transverse injection of air

through circular and elliptical nozzles in to a supersonic free stream. From their work it is evident that the injector geometry strongly affects the upstream extent of the separation region and the bow shock, and the character of the wake region downstream of the injection. Also the effective back pressure computed for elliptic injector cases were significantly higher than that for circular injector.

Chrans and Collins[10] investigated the effect of injectant stagnation temperature and molecular weight variation on the flow field generated from a secondary injection of a gas normal to a Mach 2.8 supersonic stream. Their conclusions were that, the depth of penetration of the secondary jet into the primary stream will be either jet mass or momentum dependent or a combination of both and shock radius varies with molecular weight and temperature ratio. Shock shape was correlated with the second order blast wave theory. Papamoschou and Hubbard[11] investigated the effect of sonic and supersonic jets normal to a supersonic cross flow. Their conclusion was that, penetration of secondary jet strongly depend on momentum ratio, weakly dependent on freestream Mach number and independent of jet Mach number. Pressure sensitive paint technique was used to determine the continuous surface pressure field around a sonic jet injected transversely in to a supersonic freestream of Mach 1.6 by Everett et. al[12]. In their study, maximum static pressure upstream of the jet injection site was observed to increase with increasing momentum flux ratio. Also, penetration of the jet was found to be controlled primarily by the magnitude of the jet to cross flow momentum flux ratio.

Chapter 3

Experimental Setup and Procedure

This chapter gives an overview of the test facility, describes the measurements carried out, the experimental arrangements, and various tools developed for the present study.

3.1 The Test Facility

The experiments were conducted in the free jet facility at high speed aerodynamic laboratory, Indian Institute of Technology Kanpur, India. The layout of the lab is shown in the Fig. 3.1. The test facility consists of (1) compressor, (2) storage tanks and (3) Jet test facility.

A two stage reciprocating compressor, capable of delivering 360 cfm of air at a pressure 500 psig is being used in this laboratory. The compressor used in present investigation is driven by a 150 hp 3 phase induction motor. A cooling water circuit, driven by an independent pump, cools the compressed air through an inter- cooler. The compressed air is then passed through a pre filter consisting of porous stone candles, to remove solid contaminants, like rust particles and oil droplets. An activated carbon filter is used for finer filtering. The compressed air is dried in a dual-tower semi-automatic silica gel dryer. While one tower is in use, a portion of the dried air is heated and used to reactivate the other. A diaphragm type back pressure valve operated by pressure relief pilot permits the dryer to operate at 500 psig, while the pressure in the storage tanks builds up from atmospheric to storage pressure. The compressed air is stored in three tanks, having total capacity of 3000 ft^3 at 300 psig.

The air enters the settling chamber through the tunnel section with a gate valve followed by a pressure regulating valve and a mixing length of 3" diameter. The settling chamber is connected to the mixing length by a wide angle diffuser. The flow

is further conditioned inside the settling chamber by closely meshed grids meant for minimizing turbulence. The settling chamber is a constant area circular section of 300 mm inside diameter and 600 mm length. The test models are fixed at the end of the settling chamber by a slot holder arrangement, which is a short pipe like protrusion with embedded O- ring to prevent leakage. Model to be studied is placed over the O-ring, over which an annular retaining sleeve with internal threads is screwed tightly. Fig. 3.2 shows a view of the free jet test facility at high speed aerodynamics lab IIT Kanpur, India.

3.2 Instrumentation for Pressure Measurement

The pressure sensed by Pitote and static probe was measured using a PSI model 9010, 16- channel pressure transducer (interfaced with a Pentium 4 computer loaded with VI based software for data acquisition). The model 9010 transducer is capable of measuring pressures upto 300 psig which is approximately 20 atm.

The system 9010 intelligent pressure scanner is a pressure measuring device intended for use in test and production environments. It consists of 16 channels and is working in differential mode. It has an asynchronous RS 422/485 host communication interface. It also has a standard RS-232 diagnostic interface that may also be used as host interface. The optomux style command set is used to send commands and receives response form all ports. It may be configured to communicate in the multidrop network communication always at selected baud rate using the optomux protocol. The multidrop communication always operates with no parity, 8 bit data bits and 1 stop bit. The default baud rate is 9600. Changes to baud rate can be made using special procedure via the DIP switch used to select the node address during initialization at power up. During this special baud rate selection procedure, the number of averages used during the data acquisition is also selected.

The application software developed using the Lab VIEW (shown in Fig. 3.3) links the host computer to the pressure scanner via RS 232 communication. The application software performs all the required functions like initialize, reset, rezero calibration and read pressure. The detailed description of this application software is described in Appendix A.

3.3 Experimental Setup

A schematic sketch of the experimental setup is shown in Fig. 3.5. The test plate is flat plate with the injector mounted on it. The lip of the main nozzle exit is inline with the plate surface. The gas supply for the main nozzle was provided from the stagnation chamber, and was ensured to give an uniform flow at the exit of the main nozzle. The air for secondary injection nozzle was supplied from a separate stagnation chamber, which is connected to main storage tank through pressure regulating valve (PRV). There was a long tube connecting the stagnation chamber with the secondary nozzle. A stagnation probe was located in the jet air supply line from stagnation chamber to the nozzle. Thus pitot pressure at the entry to the injection nozzle was measured just before the entrance to the secondary injection nozzle. This was essential since the pressure drop between the secondary settling chamber and the secondary injection nozzle was found to be significant as reported by Spaid[14]. The static and the stagnation pressure probes are connected to pressure transducer, which is directly connected to a computer. A stagnation probe connected to a transverse mechanism was used to calibrate the main and the secondary injection nozzles. The traverse has six degrees of freedom, which also includes a probe-yawing mechanism. The traverse has spatial resolution of 0.1 mm in all the three-dimensions. The Pitot probe used had an inner diameter of 0.4 mm and an outer diameter of 0.6 mm.

3.4 Model Construction

In the present study rectangular Laval nozzles were used to simulate the free stream flows. The rectangular Laval nozzles were constructed from brass, since it is easy for soldering. For both designed Mach numbers of 1.6 and 2, the contour surfaces were made from CNC lathe, by using the program developed for method of characteristics for the design of supersonic nozzles[22]. On calibration, the nozzles designed for Mach 1.6 and 2 gave Mach 1.72 and 1.95 respectively. The nozzle exit area for the rectangular Laval nozzle is 25×30 mm.

The axisymmetric C-D nozzles made by brass were used to inject the air perpendicular to the freestream. On calibration, the secondary injection nozzles designed for Mach 1.3, 1.5 and 1.7 gave Mach 1.35, 1.41, and 1.52 respectively. The exit area of the secondary injection nozzle was fixed as 4 mm and the throat area was varied to generate different Mach numbers of 1.35, 1.41 and 1.52.

The flat plate used for the present study was made from brass plate of thickness

10 mm. Dimensions of the flat plate were 180 mm long and 25 mm wide. The static tapings were located along the center line of the plate and around the injection hole. The dimensions of the plate and the location of the pressure tapings are shown in Fig. 3.4. The width of the plate is taken such that it fits correctly with the main rectangular laval nozzle. The flat plate is fitted with the rectangular nozzle at its exit plane. The location of the injection point was the one height of the rectangular nozzle from the nozzle exit plane.

3.5 Measurements and Experimental Procedure

The stagnation pressure in the settling chambers and the static pressure on the plate surface, during the experimental runs were monitored on a computer screen through the VI based application software. The temperature in the settling chamber was measured by a sensitive thermometer. The ambient pressure was measured by a mercury barometer. Experiments were conducted for all the combinations of main stream Mach numbers and the secondary injection Mach numbers, for different nozzle pressure ratios(NPR) of injection nozzle.

The rectangular Laval nozzle and the axisymmetric straight secondary nozzle were calibrated by using pitot pressures at the exit plane of the nozzles. The pitot pressures were acquired at different locations in the exit plane moving the pitot tube by a traversing mechanism. The normal shock relation

$$\frac{P_t}{P_0} = \left[\left[1 + \frac{2\gamma}{\gamma+1}\left(M^2 - 1\right)\right]^{\frac{-1}{\gamma-1}}\right]\left[\frac{(\gamma+1)M^2}{(\gamma-1)M^2+2}\right]^{\frac{\gamma}{\gamma-1}}$$

is used to calculate the Mach number from the pitot pressure reading. In the above relation, P_{01} and P_{02} are the pitot pressures downstream and upstream of the shock, respectively. M is the Mach number upstream of the shock and γ is the ratio of specific heats.

3.6 Shadowgraph System

It is well known that optical methods are an easy but powerful way to study supersonic flows. The flow field produced by supersonic injection in to a supersonic cross flow lends itself particularly well to study by optical means. These flows produce large density variations that lead to index of refraction variations in light passing through

supersonic flow. Both the flow features and the interaction between flow fields can be studied by using shadowgraph technique. Shadowgraphs are usually considered mainly useful for revealing strong features of the flow. The penetration height can be directly obtained from the shadowgraph and this could be a measure of effect of the secondary jets.

Shadowgraph system at the High Speed Laboratory of IIT Kanpur was used in the present study to capture features of interaction flow field. The mirror used is of high quality with a focal length of 1.6 m. A light source is placed one focal length away from a 20 cm diameter cocave mirror. Light source used is an arc lamp. A still camera was used to capture the image.

3.7 Precautions Observed

In addition to the measures taken to minimize errors, like linearity checks, rezero calibrations, etc. the following precautions were also observed during the experiments:

- The horizontal alignment of the settling chamber was ensured.
- Care was exercised in the alignment of the models, to ensure proper positioning of the measurement planes.
- The nearest wall is 150 diameters hence wall effects are negligible.
- The pressure lines and the settling chamber ports were ensured to be leak- free.
- During the experiment the stagnation pressure reading was constantly monitored.

3.8 Data Accuracy

The possible sources of error of the present investigation are due to

- The settling chamber stagnation pressure measurement.
- The error in the measurement of total pressure of secondary injection
- The possible inaccuracies in nozzle dimensions.

The room temperature was almost constant with maximum variation of $a \pm 0.50°C$ during one experimental run. The nearest wall from the apparatus was as far as 3.5 m so that wall effects could be neglected. The stagnation pressure was maintained with an accuracy of $a \pm 0.1\%$

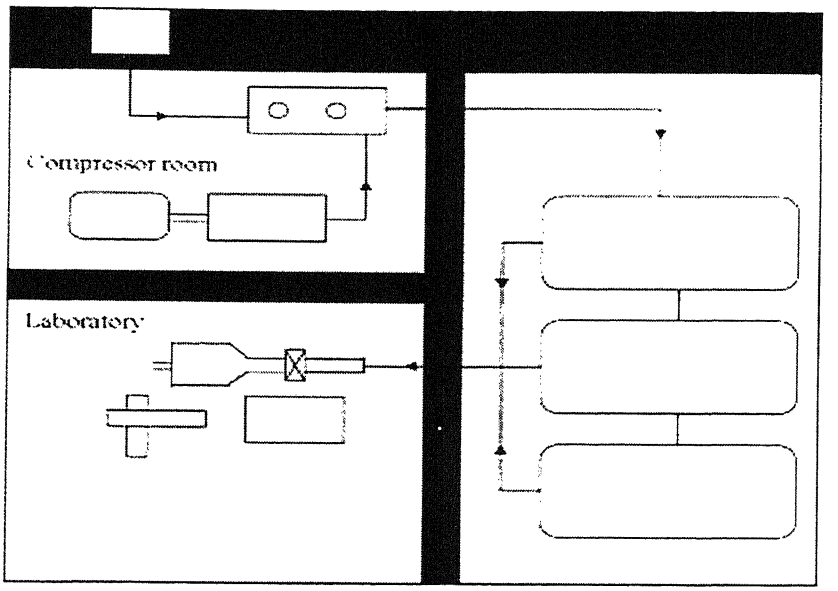

Figure 3.1 A view of the laboratory layout

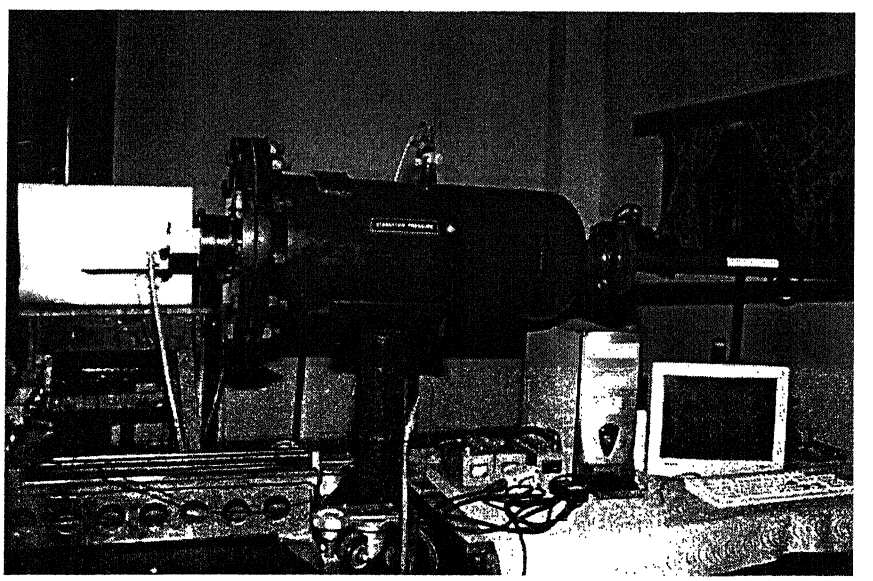

Figure 3.2 Schematic of jet test facility at IIT K

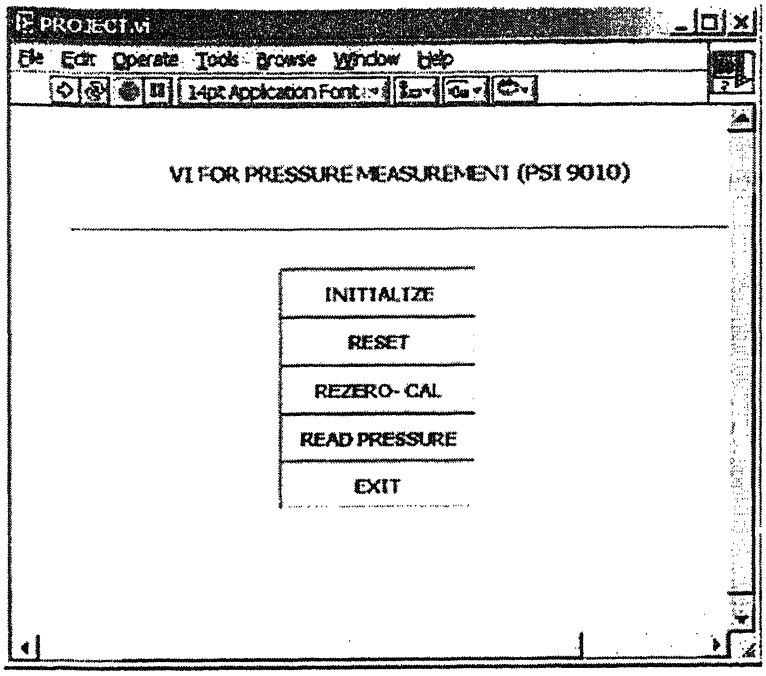

Figure 3.3 VI main program front panel

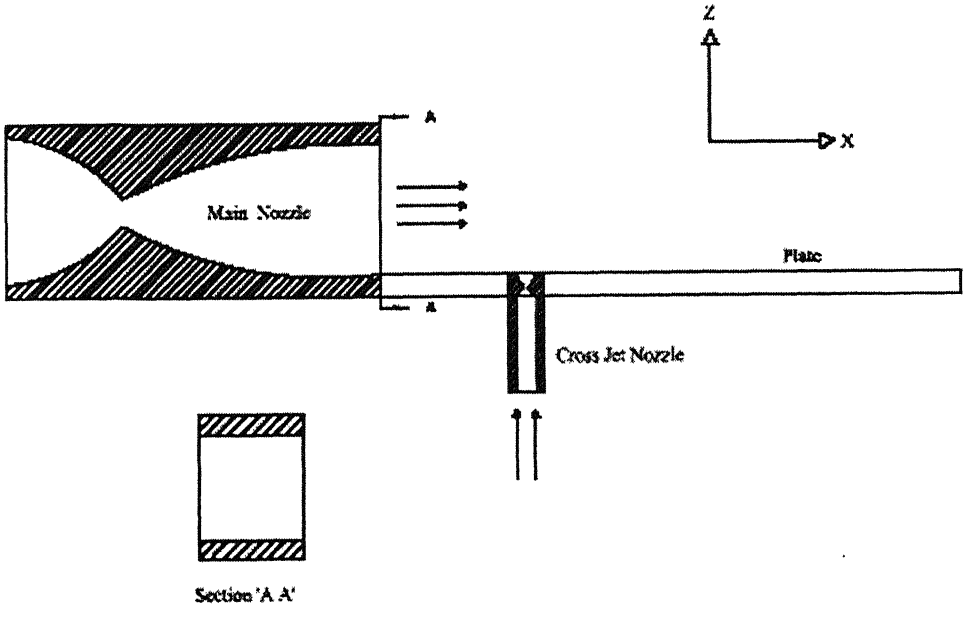

Figure 3.4 Schematic of experimental setup

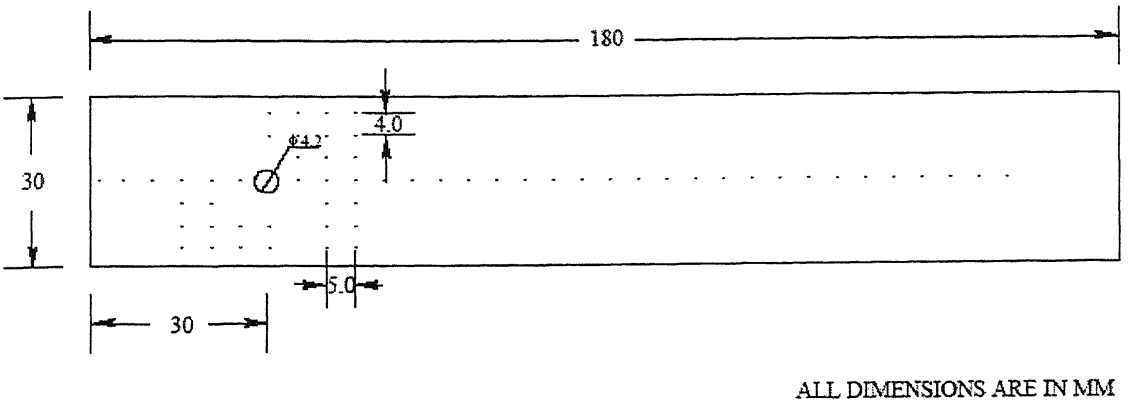

Figure 3.5 Flat plate on which static pressure is measured for nozzle Mach numbers 1.72 and 1.95

Chapter 4

Results and Discussion

4.1 Wall Pressure Distribution

The wall pressures measured along the centerline of the plate upstream and downstream of injection, and along the plate width. A number of static pressure taps were placed in the near field of secondary injection. The pressure data is non-dimensionalised as follows. For the centerline pressure, dP/P_{c0} was used as the non-dimensional parameter where dP is $(P - P_{c0})/P_{c0}$. Here P is the static pressure over the plate with secondary jet injection and P_{c0} without secondary injection i.e., when there is only main stream flow. This is done essentially to get an insight on the effect of secondary injection. For the pressure around the injection, the following expression $(P - P_{co})/P_a$ where P_a is the atmospheric pressure was used. The axial and transverse distance of the plate are non-dimensionalised with secondary jet nozzle exit diameter.

4.1.1 Mach 1.72 Main Flow

The non-dimensional wall pressure along plate centerline for Mach 1.35 secondary jet at nozzle pressure ratio 4 to 9, in steps of one, is shown in Figs. 4.1-4.4. The freestream was with NPR 7. It is seen that, the flow field is of uniform pressure up to a location upstream of the injection, where the bow shock is positioned, as shown in Fig. 1.2. After the shock the pressure experiences a jump in accordance with the shock theory. This pressure jump gets enhanced with NPR. Just downstream of the injection a low pressure region is established. This is because, as the secondary jet propagates, it forms a barrel shock with Mach disk when there is no freestream flow,

as seen in visualization Figs . 4.11a-b. But when the secondary jet propagates in the presence of freestream, a barrel shock with a Mach disk or shock crossing point encounters a supersonic field which is wave dominated, as seen in the Figs. 4.12a-f. It is seen that there is an incident shock just ahead of the injection point due to the freestream. The main flow with supersonic Mach number makes the barrel shock of the secondary jet to take a bend downstream. In turn, the leading barrel shock makes the trailing wave of the barrel to deflect downstream. The separated bubble tries to lift this deflecting trailing wave to lift-up in the vicinity of the bubble. These processes make a barrel wave zone as seen in the visualization pictures in Figs. 4.12a-f. The leading and trailing waves of the barrel shock get reflected from the free boundary of the main flow. It is well known that, the reflection from a free boundary will be **unlike**[22], that is, a compression wave will get reflected as an expansion fan and vice-verse. In accordance with this, the leading and trailing compression waves of the barrel shock reflect as expansion waves. Also, the expansion rays reflect as compression waves and coalease to form a shock on approach to the plate, seen as dark zone in the visualization figures Fig. 4.12a-f. The shock on reflection from the plate with a boundary layer on its surface, forms a "Mach reflection". Few such Mach reflections are seen in the above visualization figures. The flow experiences a jump in pressure while passing through the *lambda* waves at the Mach reflection zone. It is essential to note that, in the Mach reflection the waves are not straight as in a free field, because of the viscous action. Due to this the pressure rise through the Mach reflection zone can be gradual over a distance. This is seen predominantly at the last zone of pressure rise at x/d around 20 in Figs. 4.12a-f. The corresponding pressure zone is seen in Fig. 4.1. Therefore, injection of a secondary jet into a supersonic flow over a flat plate causes few zones of compression and suction on the plate. The net effect of secondary injection on the plate can be understood if the pressure field over the plate is analyzed with reference to the corresponding pressure due to the uniform flow alone, as in the present discussion. The compression is acting towards the plate and the suction away from the plate. Therefore, the moment about the injection location can easily be computed by taking moments of the forces due to these pressures about the injection point.

The centerline wall pressure distribution due to Mach 1.72 freestream at NPR 7 and secondary jet of Mach 1.35 at the NPR 4 to 9, in steps of one, is shown in Fig. 4.1. The physical feature of the flow field discussed above are clearly seen from these results. The shock ahead of the injection becomes progressively stronger with injection NPR. Also, the suction downstream of the shock greatly increases with

NPR. The initial zone upstream of the injection point is insensitive to secondary jet. This is natural, since the flow is supersonic and also the boundary layer on the plate in the initial zone is thin. Because of this, the disturbances are not in a position to propagate upstream. After the suction zone, the pressure recovers to the level of that without injection. But the flow field exhibits an oscillatory nature, this is because of the vortices being shed from the separated zone. Further, towards the end of the plate there is a steep rise in the pressure. This may be due to a strong compression wave hitting the plate. The strength of the wave is influenced by the injection NPR, but this influence is much smaller than that on the shock ahead of the injection point. This can easily be understood from the flow physics, that is the momentum imparted to the secondary jet, with increase of NPR has gone through a large number of interacting zones, before reaching the end of the plate. Therefore, their effect is bound to come down as the flow moves downstream. Another important feature seen at the high pressure zone near the plate end is that, the pressure peaks shift upstream with increase of secondary jet NPR. After the high pressure near the plate end, the flow gradually moves, exhibiting decrease in pressure as it moves to the plate end.

The results for Mach 1.41 secondary jet is shown in Fig. 4.2. For this case also the pressure field is not influenced by injection up to some distance on the plate. A shock is positioned ahead of the injection point. Compared to Mach 1.35 injection these shocks are much stronger. The suction downstream of the injection is also higher than that of Mach 1.35 injection. The flow field downstream of the suction zone exhibits considerable oscillations. Pressure rise due to shock interaction with the plate, is seen distinctly at two locations. But the pressure jump experienced due to the shock interaction are much lower than that for Mach 1.35 injection. Another important feature for this injection is that, unlike Mach 1.35 injection, there are two strong shock reflections in between the separation behind the injection and the plate location where another suction peak is located. Results for Mach 1.52 injection is shown in Fig. 4.3 reveals that, the pressure field up to a location ahead of the injection point is similar to the previous cases. The strength of shock upstream of the injection is much greater than the previous cases at all NPRs. Similarly, the suction is also powerful than the previous cases. But the two pressure peaks downstream of the separation zone exhibited by Mach 1.41 is not seen for this case. As in the case of Mach 1.35 there is a compression zone near the plate, exhibiting the upstream shift of pressure peak with increase of injection NPR.

From the above results it is clear that, with increase of injection Mach number the

blockage offered by the secondary jet increases. Due to this the shock ahead of the injection becomes stronger with increase of injection Mach number, also the suction after injection becomes powerful with the increase of injection NPR.

4.1.2 Mach 1.95 Main Flow

The pressure distribution results for Mach 1.95 freestream with secondary injection jet of Mach number 1.35, 1.41 and 1.52 at NPR 4 to 9 are shown in Figs. 4.5-4.8. Results for Mach 1.35 injection is shown in Fig. 4.5. It is seen that, up to x/d 8 from the nozzle exit, the pressure on the plate is uniform, and just after that there is a marginal jump in the pressure, this may be due to some compression wave hitting the plate. Upstream of the secondary jet a strong shock is positioned. This shocks causes a pressure jump and the jump is strongly influenced by secondary jet NPR. Downstream of the secondary jet there is a powerful suction zone. The extent of the suction zone is much wider compered to Mach 1.72 freestream. Also, the pressure field over the plate becomes significantly oscillatory compared to Mach 1.72 freestream. This may be because, the previous case of Mach 1.72 freestream is underexpaned at NPR 7 and hence the nozzle should have an expansion fan at the nozzle exit. The expansion fan at the nozzle exit plane would establish a favorable pressure gradient causing the boundary layer to be thin. But for Mach 1.95 at NPR 7 is slightly overexpanded and there would be an oblique shock at the nozzle exit, and hence the boundary layer on the plate would be relatively thicker. This might enable the disturbance due to the secondary flow to propagate upstream through this layer. There are number of pressure peaks of positive and negative values all over the plates, indicating that the shock reflection points on the plate have become many and, they can be viewed up to the end of the plate.

The pressure variations over the plate centerline for injection Mach 1.41 is shown in Fig. 4.6. Here, once again it is seen that, the shock ahead of the injection becomes much stronger, compared to Mach 1.35 injection with increase of NPR. Also, the suction behind the injection becomes powerful for this case. The extend of suction zone also increased compared to injection Mach number 1.35. Even though the number of pressure peaks has come down, the flow continuous to be oscillatory all over the plate. Results for Mach 1.52 secondary jet are shown in Fig. 4.7. The shock ahead of the injection becomes much stronger than that of Mach 1.41 injection for all NPRs. Similarly, the suction zone behind the injection become more powerful and also the extent of suction zone. As in the case of injection Mach 1.41, here again the number

of peaks are less than those for Mach 1.35 injection but the flow continuous to be oscillatory throughout the plate.

4.2 Flow Visualization

The visualized picture of the flow field of Mach 1.72 freestream without secondary injection at NPR 7 over the flat plate is shown in Fig. 4.9. This is an underexpanded flow at nozzle exit. Expansion fan at the nozzle exit, is getting reflected from the free boundary as compression waves and shock wave hitting the plate is reflecting as shock wave are clearly seen from the picture. That is, the entire flow field over the plate is wave dominated. The waves in the secondary jet with injection Mach numbers 1.35, 1.41 and 1.52 are shown in Figs. 4.11a-b. It is seen that the secondary jet in the absence of freestream is propagating as a typical free jet, possessing a number of shock cells and Mach disk and showing dissipation of shock strength with increase in axial distance. The shock cell strength increases with increase of injection NPR. Also, supersonic core increases with increase of NPR. It is seen that, the underexpansion level plays a significant role on the Mach disk height. Mach disk height increases with injection NPR for all the three secondary injection nozzles. The complex flow field due to the combination of Mach 1.72 freestream and Mach 1.35 secondary injection at NPR 4 to 9, in steps of one, are given in Figs. 4.12a-f. It is seen that, the secondary jet possessing number of shock cells is forced to get deflected by the mainstream. This interaction results in the formation of a strong shock ahead of the injection point termed as leading or bow shock and a less prominent trailing shock far downstream of the injection point extending upto the edge of the free boundary. Boundarylayer separation ahead of the injection is also seen from the visualization figures. The trailing shock is found to interact with the separated zone downstream of the injection. The leading shock end point with free boundary moves upstream with increase of NPR indicating that the shock becomes stronger with increase of NPR as discussed in centerline pressure variations. The pressure jump location downstream of the injection point, closer to the plate end was envisaged due to reflection of compression waves from the plate with boundary layer. This can also be viewed from visualization figures. Results for the combination of Mach 1.72 freestream and injection Mach 1.52 are shown in Figs. 4.13a-f. From these figures it is evident that the leading shock strength progressively increases with increase of NPR. Also, the Mach reflection from the flat plate downstream of separation zone, are clearly seen at all NPRs. Here again

the visualized leading edge wave authenticate the results presented in the centerline pressure, stating that the strength goes up with increase in NPR.

Visualization pictures for Mach 1.95 freestream with secondary injection Mach numbers 1.35, 1.41 and 1.52 are shown in Figs. 4.14-4.16. Here the main flow is at NPR 7 and it is slightly overexpanded for Mach 1.95. From these results it is seen that, for Mach 1.95 freestream with Mach 1.35 injection, the shock shape changes continuously with injection NPR. This indicates shock strength increases with increase in NPR.

4.3 Penetration Height

The penetration height of the injected secondary fluid into the primary stream was scaled directly from the shadowgraph photographs. The penetration height in the present study is taken as the maximum height reached by the bent-over of the highly underexpanded secondary jet. In other words, the first kink observed in the secondary jet trajectory is taken as the penetration height. The penetration height(h) normalized by the exit diameter(d) of the secondary injection nozzle is given as a function of the ratio of secondary injection stagnation pressure to mainstream stagnation pressure($\frac{P_{0j}}{P_{0u}}$). Penetration heights are directly measured from the shadowgraphs for both the mainstream Mach numbers, with combination of different secondary injection Mach numbers.

4.3.1 Mach 1.72 Main Flow

For mainstream Mach number 1.72, injection Mach numbers were 1.35, 1.41, and 1.52, and mainstream stagnation pressure was held constant as NPR 7 for all experimental runs. The secondary injection stagnation pressure was varied from NPR 4 to 9, in steps of one. Figure 4.17 shows the non-dimensionalized penetration height for mainstream Mach 1.72 with injection Mach 1.35 and 1.52. The penetration height for secondary injection Mach 1.41 with the mainstream Mach 1.72 was not measured, because the photographs taken for this experimental setup were not of the quality required for this. Figure 4.17 is a linear fit for the penetration heights obtained for different stagnation pressure ratios for mainstream Mach 1.72 with injection Mach 1.35 and 1.52. For both the cases, i.e. for secondary injection Mach numbers 1.35 and 1.52, the penetration height is increasing with the ratio of injection stagnation pressure to

mainstream stagnation pressure. This is also seen clearly from the visualization photographs shown in Figs. 4.12-4.13. The reason for this increase in penetration height with increase in stagnation pressure ratio is the following. The increase in stagnation pressure ratio increase the mass flow rate through the secondary injection nozzle and the level of underexpansion for the given Mach number also increases. When the mass flow rate increases it imparts an increase in momentum for the secondary jet, and this momentum would help in penetrating more into the mainstream. The level of expansion also plays a significant role in penetration. When underexpansion level increases for a given secondary injection nozzle as it does with increase of stagnation pressure ratio, the Mach disk height formed in the secondary jet increases. This can be clearly seen from visualization photographs of secondary injection alone as shown in Figs. 4.11a-b.

An interesting observation made with penetration heights for Mach 1.72 case is that, with different secondary injection Mach numbers, penetration height remains almost the same for a stagnation pressure ratio. As seen in Fig. 4.17, at high stagnation pressure ratios penetration height shows some deviations for the two secondary injection Mach numbers. At small pressure ratios, both the curves give same penetration heights. The penetration height is determined by the momentum of the secondary injection jet for a given mainstream Mach number. Momentum of the secondary jet depends up on both the mass flow rate through the nozzle and the exit velocity or Mach number of the nozzle. In the present study the secondary injection nozzle exit diameter was held constant and throat area was varied to get different design Mach numbers. So, for a given nozzle, the mass flow rate and the Mach number determines the injectant momentum. When Mach number increases for a fixed exit diameter nozzle, its throat area must decrease. This in turn effects the mass flow through the nozzle, as mass flow rate is proportional to the throat area for a given stagnation pressure. So, in the case of a fixed exit diameter nozzle, mass flow rate decreases when Mach number increases, and vice-versa. Since momentum is proportional to both mass flow rate and exit velocity, the combination of these two important parameters determines the penetration. In the present study, for the injectant Mach numbers 1.35 and 1.52, the total momentum is coming to almost the same value, with negligible difference. Since the penetration height increases with injection NPR, the NPR plays a dominant role in dictating the strength of the shock ahead of the injection. This clearly reflects as the "pressure jump", upstream of the injection, as seen in the plate centerline pressure plots given in Figs. 4.1-4.4. In other words, the increase of penetration height can be viewed as stiffening of the virtual fluid cylinder

formed by the injection. Due to the increased stiffness with NPR increase, both the high pressure zone upstream of the injection and the suction zone downstream of the injection are strongly influenced as discussed in wall centerline pressure section.

4.3.2 Mach 1.95 Main Flow

Figure 4.18 shows the normalized penetration heights for Mach 1.95 freestream with secondary injection Mach numbers 1.35, 1.41 and 1.52 as a function of stagnation pressure ratio. Here also the stagnation pressure ratio is varied by varying the NPR for the secondary injection jet. It is seen from the figure, that the results are showing same trend as that of Mach 1.72 freestream case. The penetration height increases with stagnation pressure ratio for all secondary injection Mach numbers. The reason for this is same as that explained in the case of Mach 1.72 freestream. Here also, for all secondary injection Mach number nozzles penetration height remains the same and the physical reason for this is same as described in the previous case with Mach 1.72 freestream. In Fig. 4.18 reference is made to Zukoski and Spaid theory[1] for penetration height. From figure it is seen that the trend of the penetration heights for different experimental tests, showing agreement with the reference given. Hence jet momentum plays a significant role on penetration height. To get an insight into the effect of main stream Mach number variation on penetration height, graphs are plotted for both the main stream flow. Here the penetration height is higher for main stream Mach number 1.95 for the same NPR and the same injection Mach number. The reason for this could be as follows. The exit area for Laval nozzle used for generating mainstream was held constant for both the main flow Mach 1.72 and 1.95. The throat area is more for Mach 1.72 nozzle and the higher mass flow rate for the Mach 1.72 nozzle due to larger throat compared to the Mach 1.95 nozzle, pushes the secondary jet more. Also, the momentum imparted by the mainstream is more for Mach 1.72 case. From this it is evident that, the penetration height of the secondary jet also depends on the momentum of the mainstream flow. How much the secondary jet penetrated into the mainstream is a measure of mixing of the secondary jet with the main flow. This is an important parameter from the mixing point of view, as in the case of supersonic combustion ramjet. In addition to the initial penetration of the transverse jet as given in terms of penetration height, the subsequent trajectory of the jet and mixing along the trajectory are also of interest.

4.4 Shock Strength and Shape

The shape and the strength of the bow shock, introduced when a secondary jet injected into a main flow is often important, as it determines the pressure losses in fuel injection problems and the surface pressure for attitude control applications. The shock radius R_s of the interaction field is measured perpendicular to the flat plate axis at distances (x_i) downstream from the main nozzle exit. The shape of the leading bow shock is an essential input parameter in several of the analytical models of secondary injection and therefore, deserves separate consideration. To get an insight into shock strength and its effect on the complex interaction field, strength of the shock is defined as follows

$$\frac{P_2'}{P_1'} = \frac{(P_2 - P_{2c0})}{(P_1 - P_{1c0})}$$

where P_1 and P_2 are the pressures on the plate before and after the pressure jump location and P_{1co} and P_{2c0} are the surface pressures with main flow alone (without secondary injection) at respective points on the plate. The shock strength gives an idea of the pressure jump occurred with the injection, and its variation with different NPRs and injection Mach numbers.

4.4.1 Shock Strength for Mach 1.72 Main Flow

The shock strength found out using the above expression is plotted against the secondary jet NPR in Fig. 4.19 for Mach 1.72 freestream with injection Mach numbers 1.35, 1.41 and 1.52. The variation of shock strength with NPR shows a monotonic increase of shock strength for all injection Mach numbers. This is because, the secondary jet can be viewed as a truncated right circular cone kept upside down in the freestream. Since it is a fluid cone it is bound to deflect when the freestream is present. However, the increase of NPR can be viewed as enhancement of stiffness of flexible cone. Therefore, with increase of NPR the deflection tendency of cone goes down, thereby tries to offer more resistance to freestream. This increase of resistance is reflected in the form of erection of the upstream shock. This is reflected as increase of shock strength and hence pressure jump after the shock, as seen in the centerline pressure plots. The stiffening effect with NPR also reflected as increase of suction behind the secondary jet. The increase in shock strength with NPR is the greatest for Mach 1.35 injection, and progressively decreases with increase of injection Mach number M_j. Also it is seen that, at low NPRs shock strength increase is much

higher than that at high NPRs. For Mach 1.52 injection at higher NPR, variation in shock strength is not much predominant and this indicates that, the pressure jump for higher NPRs, for Mach 1.52 injection is not increasing like that of Mach 1.35 injection. The reason for this could be the following. For a supersonic main flow the maximum jump in pressure occurs theoretically for a normal shock. But in actual case there won't be a normal shock in a solid boundaryless flow. So the shock produced will be oblique in nature and with increase of injection Mach number, the stiffness of the flexible cone as discussed above increases and this results in increase of shock strength. Theoretically there is a limit for the maximum pressure jump for an oblique shock, determine by the oblique nature of the shock produced for a mainstream Mach number. It appears that the increase in NPR and injection Mach number make the oblique shock to reach a limiting strength. The injection Mach number which drives the shock to the limiting strength for Mach 1.72 main flow appears to be about 1.52 and NPR above 9, in the present study. A cross plot of shock strength variation with secondary jet Mach number at different NPR is shown in Fig. 4.20. These results authenticate the physics described above.

4.4.2 Shock Strength for Mach 1.95 Main Flow

The shock strength variation for Mach 1.95 freestream with injection NPR for different injection Mach numbers is shown in Fig. 4.21. It is seen that, as in the case of Mach 1.72 freestream the variation shows a similar trend indicating that the shock strength increases with increasing NPR and also, the rate of increase becomes smaller with NPR. These behaviors are clarified in the cross plots of shock strength with M_j, plotted in Fig. 4.22. For this case, even though the oblique shock strength shows a tendency to approach a limiting value, as in the case of Mach 1.72 freestream, the injection NPR at which this will happen seems to be much greater than that for Mach 1.72.

4.4.3 Shock Shape

The variation of the bow shock strength maximum (along the centerline) with injection NPR and injection Mach number was found to get influenced significantly with both M_j and NPR as seen in the visualization pictures. The measurement of shock radius quantified this effect. Radius (R_s) of the leading bow shock measured perpendicular to the plate is an important parameter, which can be used for the

prediction of jet interaction flow field. Figure 4.23 shows the shock radius for main flow of Mach 1.72 with injection Mach number 1.35 for different NPRs from 4 to 9, against the distance measured from the main nozzle exit. It is seen that, the shock shape is changing continuously with M_j and NPR, exhibiting increase of shock radius with NPR. Shock radius plotted in Fig. 4.24 for Mach 1.95 freestream with Mach 1.35 injection also exhibits similar variation. Figure 4.25 shows the variation of shock radius for Mach 1.95 freestream with different injection Mach numbers for NPR 9. It is evident from these results that the shape and thus strength of the shock depends on both NPR and injection Mach number in accordance with the reason described in the previous section.

The most promising analytical model for the radius of the leading shock is based on analogy with Blast wave theory which gives the following relation for the shock radius $R_s{}^2$.

$$\frac{R_s}{R_{s0}} = K \frac{1}{(M_\infty)^{1/2}} \left(\frac{X_s}{R_{s0}}\right)^{1/2} \tag{1}$$

where X_s is the shock stream wise coordinate measured from its origin, M_∞ is the freestream Mach number and K is a numerical constant called shock radius correction factor. The reference radius R_{s0} was computed with the following interpretation of the blast energy per unit length[2].

$$R_{s0} = \frac{1}{(2\pi)^{1/2}} \left(\frac{E}{P_\infty}\right)^{1/2}$$

$$E = \frac{M_j h_{j0}}{V_\infty} = \frac{m_j c_p T_{j0}}{V_\infty}$$

$$p_\infty V_\infty = m_\infty \frac{RT_\infty}{A_\infty}$$

$$R_{s0} = \frac{1}{(2\pi)^{1/2}} \left[\left(\frac{T_{j0}}{T_0}\right)^{1/2} \frac{\gamma}{\gamma-1} \left[\frac{T_0}{T_\infty}\frac{A_\infty}{A^*_\infty}\right] \frac{P_{j0}}{P_0}\right]^{1/2} \left(A^*_j\right)^{1/2}$$

$$R_{s0} = \frac{1}{(2\pi)^{1/2}} \left[\frac{T_{j0}}{T_0^{1/2} P_0} \frac{\gamma}{\gamma-1} \left[\frac{T_0}{T_\infty}\frac{A_\infty}{A^*_\infty}\right]\right]^{1/2} (\dot{m}_j)^{1/2}$$

The above equation is simplified for application in the present study, to result in

$$R_{s0} = \frac{1}{\sqrt{2\pi}} \left[\frac{\gamma}{\gamma - 1} \left(1 + \frac{\gamma - 1}{2} M_\infty^2 \right) \left(\frac{1}{M_\infty} \left(\frac{\gamma + 1}{2} \right)^{\frac{-(\gamma+1)}{2(\gamma-1)}} \left(1 + \frac{\gamma - 1}{2} M_\infty^2 \right)^{\frac{\gamma+1}{2(\gamma-1)}} \right) \right]^{1/2}$$

$$\left(NPR \left(\frac{P_a}{P_{0u}} \right) \right)^{1/2} \sqrt{A_j} \left[\frac{1}{M_j} \left(\frac{\gamma + 1}{2} \right)^{\frac{-\gamma+1}{2(\gamma-1)}} \left(1 + \frac{\gamma - 1}{2} M_j^2 \right)^{\frac{\gamma+1}{2(\gamma-1)}} \right]^{1/2}$$

In order to relate *Eq.*(1) to experimental results it is expressed in the following form.

$$\frac{R_s}{R_{s0}} = K \frac{1}{(M_\infty)^{1/2}} \left(\frac{x - x^*}{R_{s0}} \right)^{1/2}$$

where x^* is the distance between the physical coordinate and the origin of the bow shock. From shadowgraph pictures it is not possible to find out the exact position of the origin of the leading shock, because the starting point of the leading bow shock is in a complex interaction field with shock boundary layer interaction and due to this lambda shocks are formed. So it is assumed that the origin of blast wave as 3 mm upstream from the injection point, by extending the radius to meet the axis. The above equation is applied to all experimental combinations of mainstream Mach numbers with all injectant Mach numbers for different NPRs. The shock correction factor K found out for all these combinations are plotted against injection Mach numbers in Fig. 4.26. In this figure K is computed for all secondary injection Mach numbers at injection NPR 5, 7 and 9. This was done for both freestream Mach numbers. For example, in the plot, $M_j = 1.35$, there is a cluster showing a band for K from 3.65 to 4.2. Similarly for other M_js.In this plot reference is made to Charwat and Allegre[2]. It is interesting to note that, the value of K remains almost the same for all experimental tests, and the variation is small. According to Blast wave theory for shock radius, for the analogy to be completely valid the shock correction factor K should remains constant for all tests. In this sense the trend exhibited by shock correction factor K based on present study is reasonable. The K value obtained by Charwat and Allegre for their different experimental runs comes very near the value obtained in the present study and shown in Fig. 4.26a-b. In the present study the shock correction factor obtained is coming between 3.6 and 4.2 for different experimental runs.

4.5 Force and Moment on the Plate due to Secondary Jet

The force and moment caused by the flow field generated by the injection of a secondary jet through a small opening in a wall over which a supersonic freestream is flowing is of considerable interest, since this can be exploited for imparting linear shift and attitude control for a flying vehicle like a missile. Therefore, after gaining an insight into the physics of the flow field due to the combination of freestream and the injection, an attempt is made to estimate the force and moment due to this combined field. Before venturing into force and moment calculation, the pressure measured over the surface of the plate around injection location are presented in the form of surface plots. The pressures measured at locations shown in Fig. 3.5 are presented as isobaric contours in Figs. 4.31-4.35. The measured pressures were non-dimesionlised with ambient atmospheric pressure, that is the pressure is expressed as $\frac{P-P_{c0}}{P_a}$, where P is the wall pressure due to interaction between freestream and injection, P_{c0} is the wall pressure due to freestream alone without injection and P_a is the atmospheric pressure. In the plots, the injection point is at $x/d = 7.5$ along the centerline i.e., $y/d = 0$. The pressure levels are shown as different shades. The results for Mach 1.72 freestream with 1.35 injection at NPR 5, 7 and 9 are shown in Fig. 4.31. As we saw in the centerline pressure plots, here also it is seen that, the pressure upstream of injection goes up with increase of NPR. Also, the pressure in the suction zone goes down with increase in NPR. Similar results for Mach 1.72 with Mach 1.5 injection are shown in Fig. 4.31. Compared to previous case, this case the effect of NPR on the positive as well as negative zones are predominant in accordance with shock strength influence discussed. The results for Mach 1.72 freestream with Mach 1.41 injection at different NPRs from 4 to 9, are shown in Fig. 4.32. The plots reveal the strong influence of NPR on increase in shock strength and the suction, with NPR increase. The surface pressure plots for Mach 1.95 freestream with 1.35, 1.41 and 1.52 injection at NPR 5, 7 and 9 are shown in Figs. 4.33-4.34. In addition to increase of shock strength and suction strength, the extent of suction varying with NPR is clearly seen from these plots. Some specific results for Mach 1.72 and 1.95 freestream are compared in Fig. 4.35. These results clearly authenticate the discussions about shock strength and suction zone made based on centerline pressure and flow visualization.

The surface pressures were used to estimate the force and moment acting on the plate. In the force estimation, the thrust of the secondary injection jets are not

included. The force was determined as follows

$$F = \sum P_i \, (x_{i+1} - x_i) \, \Delta y$$

where subscript i refers to pressure at a port and $i + 1$ refers to pressure at the next immediate downstream port, Δy is the lateral distance, which is constant of 4 mm in the present case. The force acing over the plate extending 3.7 times the injection diameter on either side of the injection point were computed with the above expression. The force for Mach 1.72 freestream with injection Mach numbers 1.35, 1.41 and 1.52 is plotted against NPR in Fig. 4.27. It is seen that, for Mach 1.35 injection the negative force increases with increase of NPR continuously. For injection Mach 1.41 the force is not influenced by NPR significantly but for injection Mach 1.52 once again the negative force increases with increase of NPR. The force acting on the plate is due to the positive pressure zone upstream of injection and negative pressure zone downstream of injection, therefore the magnitude and extent of the positive and negative pressure zones put together dictate the force. These results for injection Mach numbers 1.35 and 1.52 clearly show that, the magnitude of negative pressure downstream of injection and the extent of negative zone are predominant over positive pressure in positive zone at all NPRs. But for Mach 1.41 injection the positive and negative pressures are influenced almost identically with increase of NPR causing the total force to be at a constant level.

The moment due to the forces at each grid on the surface about the injection point is estimated for all the injection Mach numbers. The non-dimensionalised moment $M_c$is calculated using the expression below $\frac{M-M_{c0}}{M_{c0}}$ where M is the moment due to the local force with injection and M_{c0} is the moment due to local force without injection. The moment for Mach 1.72 freestream is shown in Fig. 4.28. It is seen that the net moment is always negative for all cases indicating that tendency is nosedown. The nosedown moment increases with NPR for all M_j. Also, the moment increases with M_j at all NPRs.

The forces computed for Mach 1.5 freestream at different NPRs with injection Mach numbers 1.35, 1.41 and 1.52 are shown in Fig. 4.29. Unlike Mach 1.72 freestream, for this case the negative force increases continuously with NPRs for all M_j. Also, the magnitude of the force is significantly higher compared to 1.72 at all NPRs. This clearly reveals that, the freestream Mach number dominance over in the suction zone is much higher than the positive zone. The moment result for Mach 1.95 freestream is shown in Fig. 4.30. For all M_j the nosedown moment increases monotonically with NPR. Like force the moment for this case is much higher than

that for freestream Mach number 1.72 at all NPRs. The M_js are found to influence the moment significantly at all NPRs.

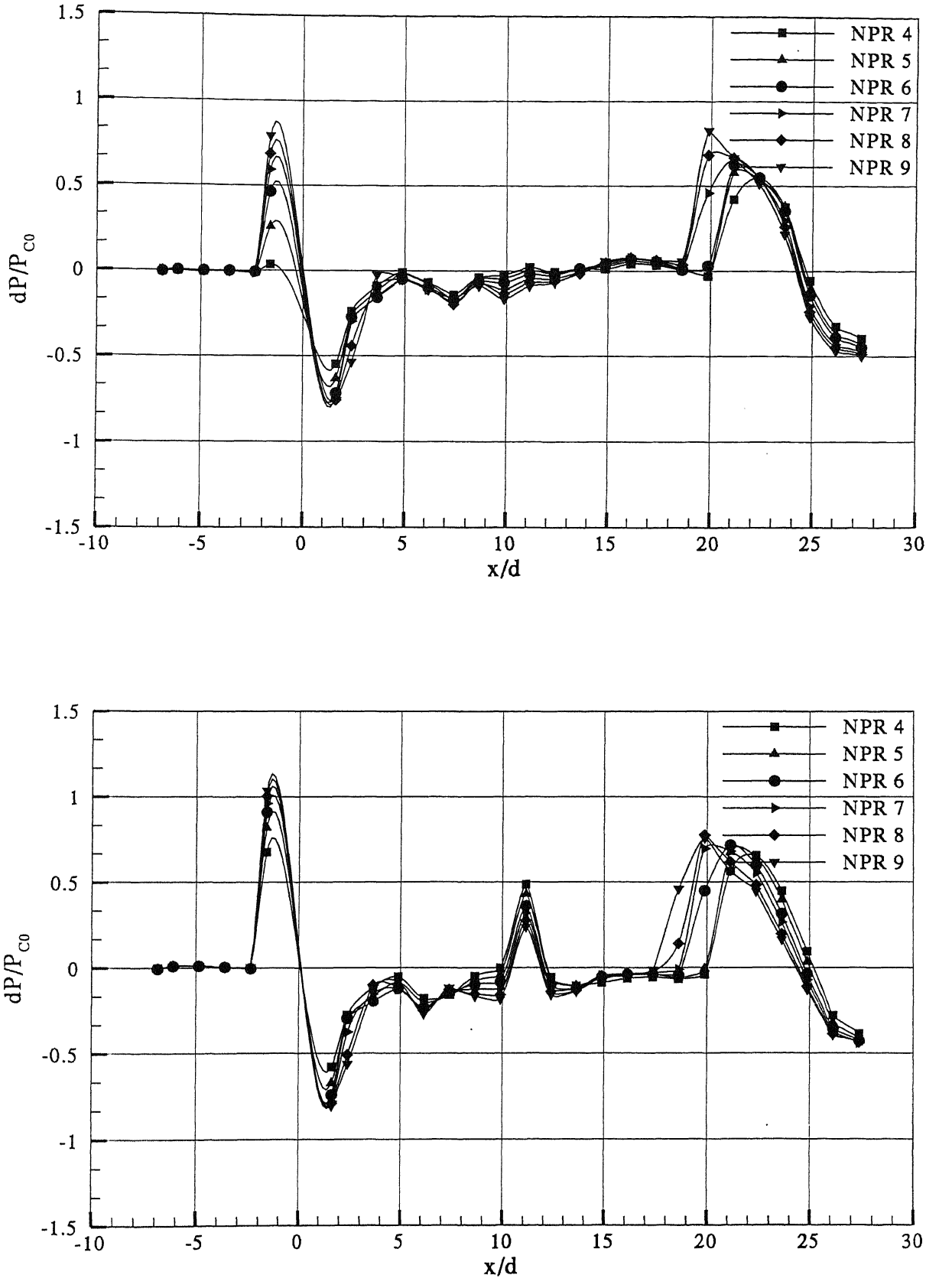

Figure 4.2 Centerline pressure plot for Mach 1.72 freestream with M_j 1.41

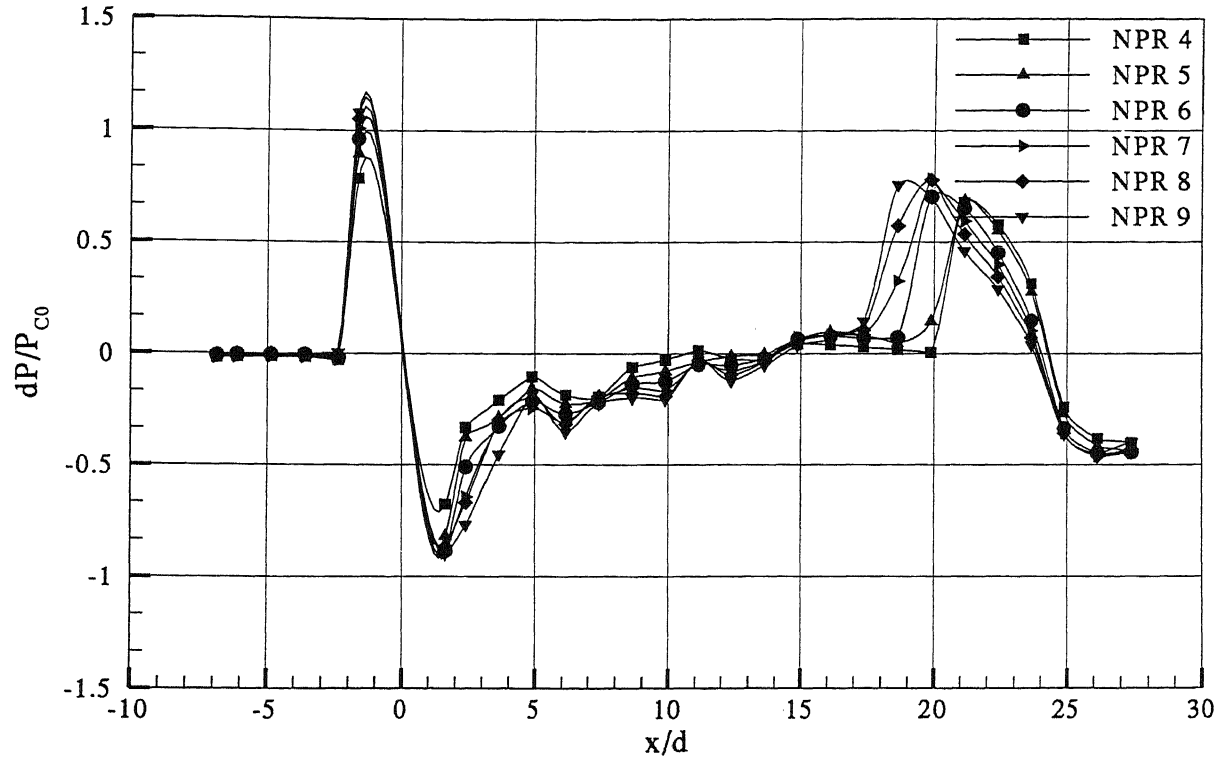

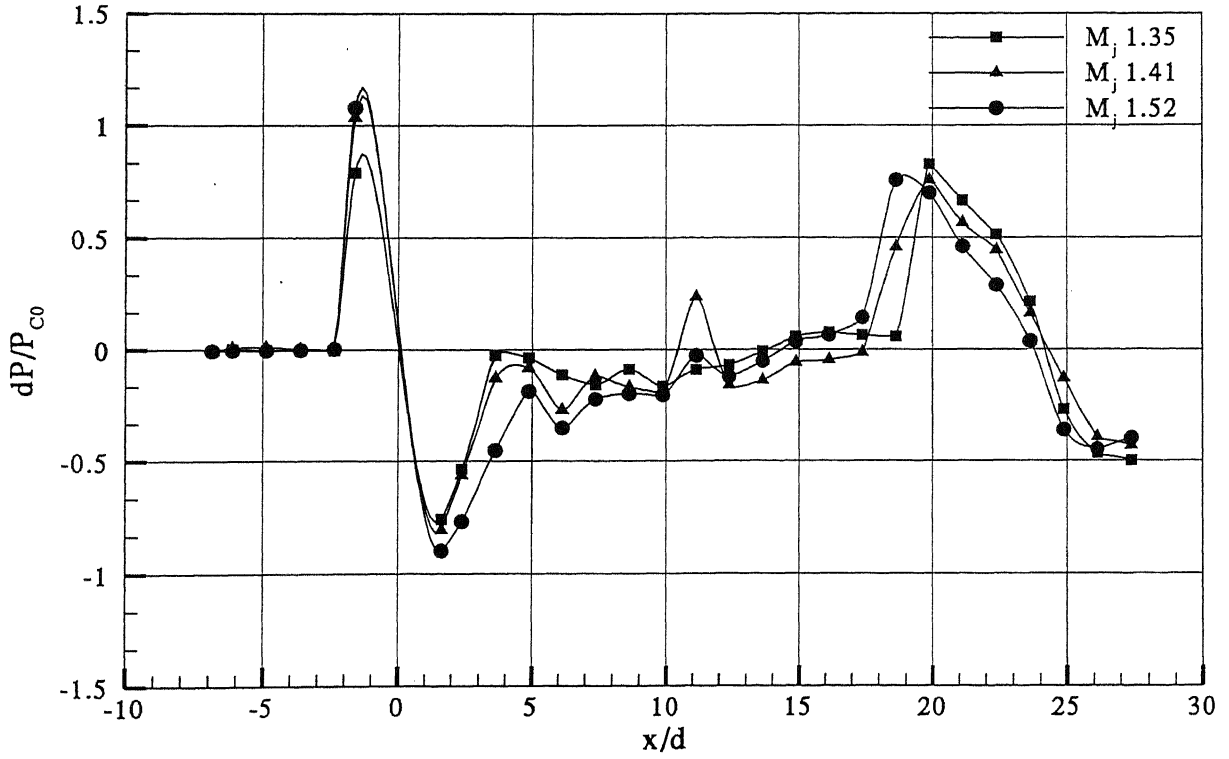

Figure 4.4 Centerline pressure plot for Mach 1.72 freestream, injection NPR 9

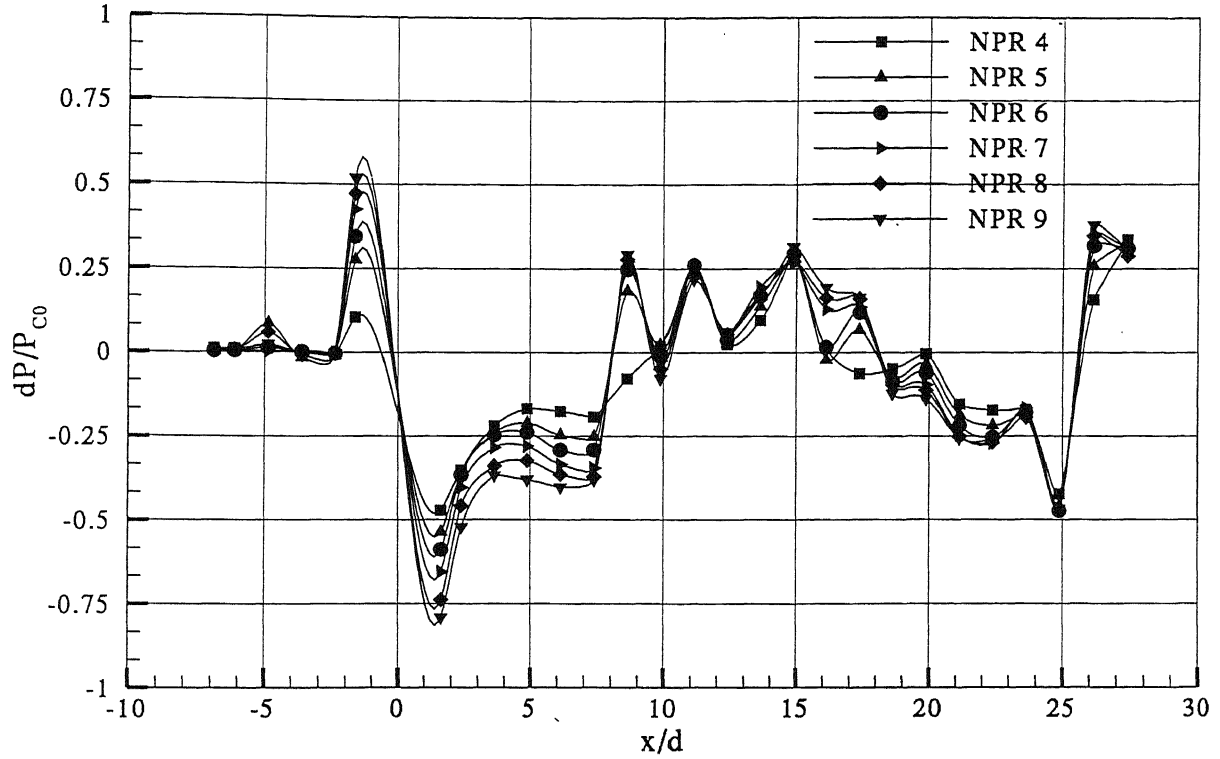

Figure 4.5 Centerline pressure plot for Mach 1.95 freestream with M. 1.35

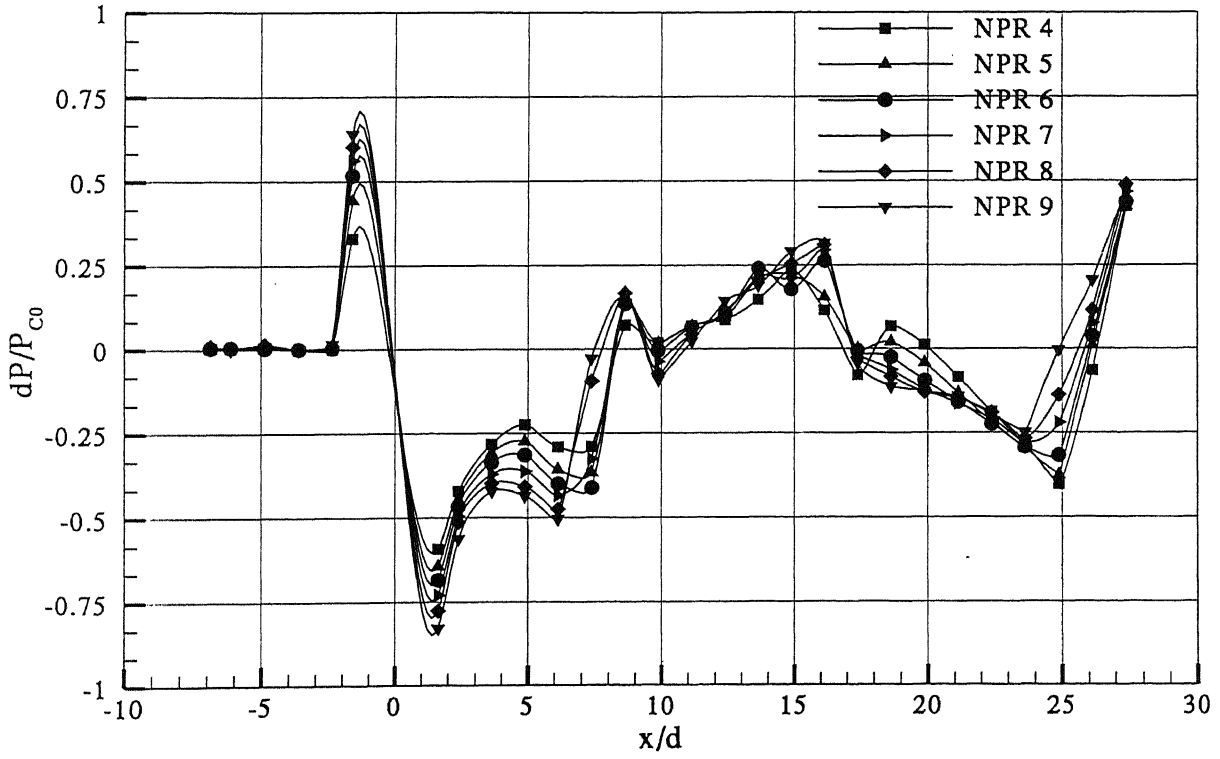

Figure 4.6 Centerline pressure plot for Mach 1.95 freestream with M_j 1.41

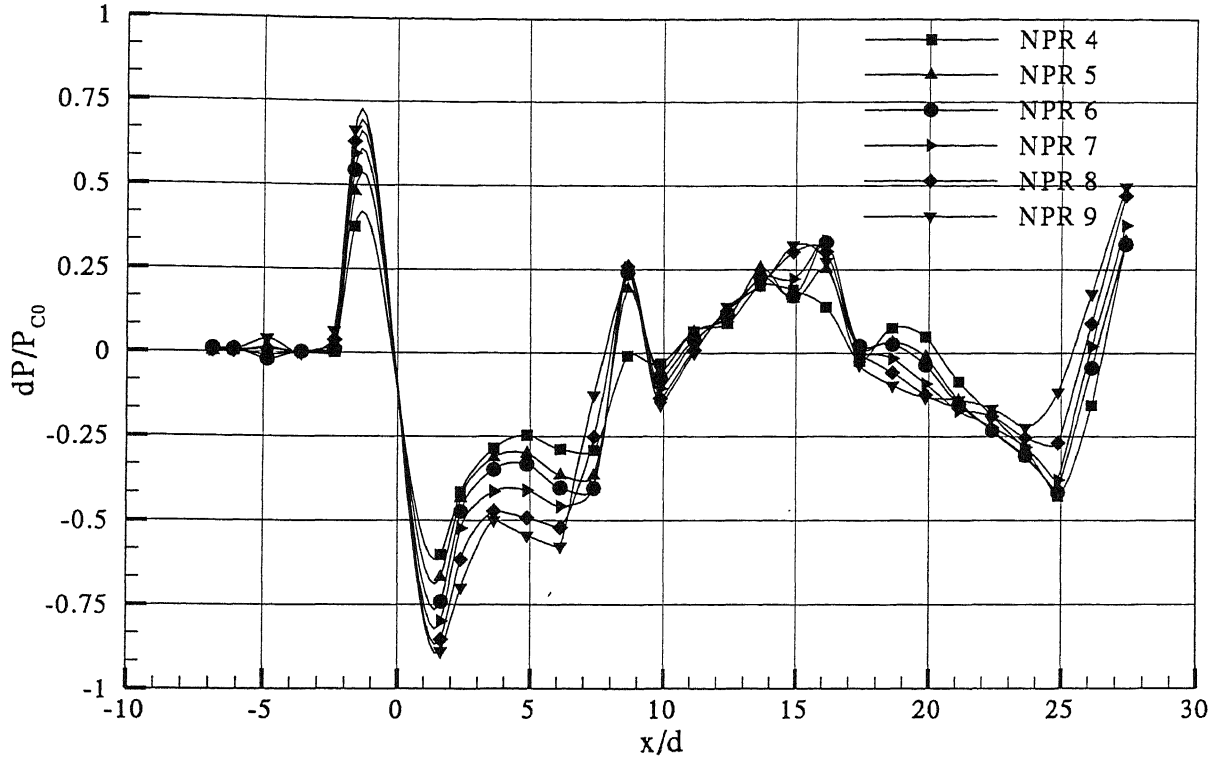

Figure 4.7 Centerline pressure plot for Mach 1.95 freestream with M$_j$ 1.52.

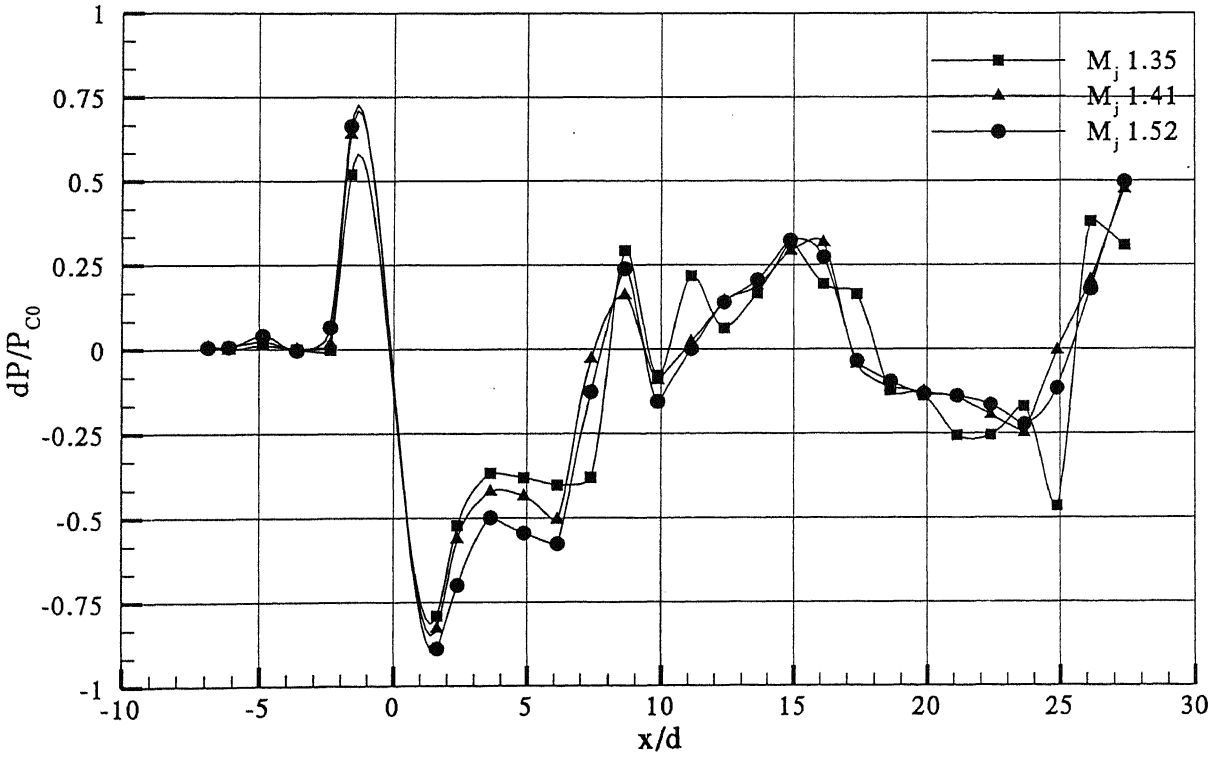

Figure 4.8 Centerline pressure plot for Mach 1.95 freestream, injection NPR 9

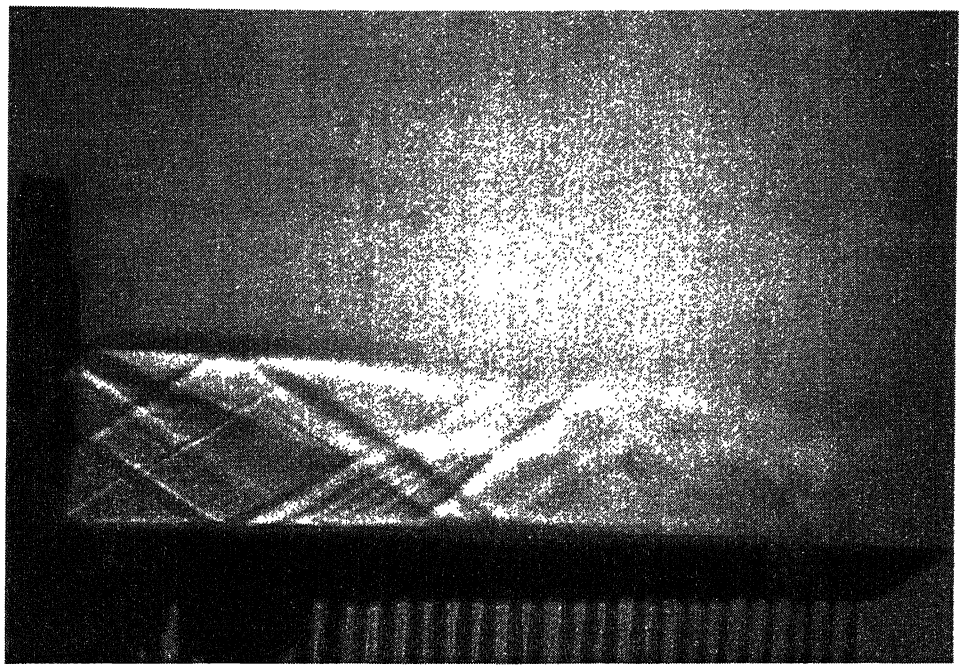

Figure 4.9 Flow field of Mach 1.72 mainstream with out secondary injection.

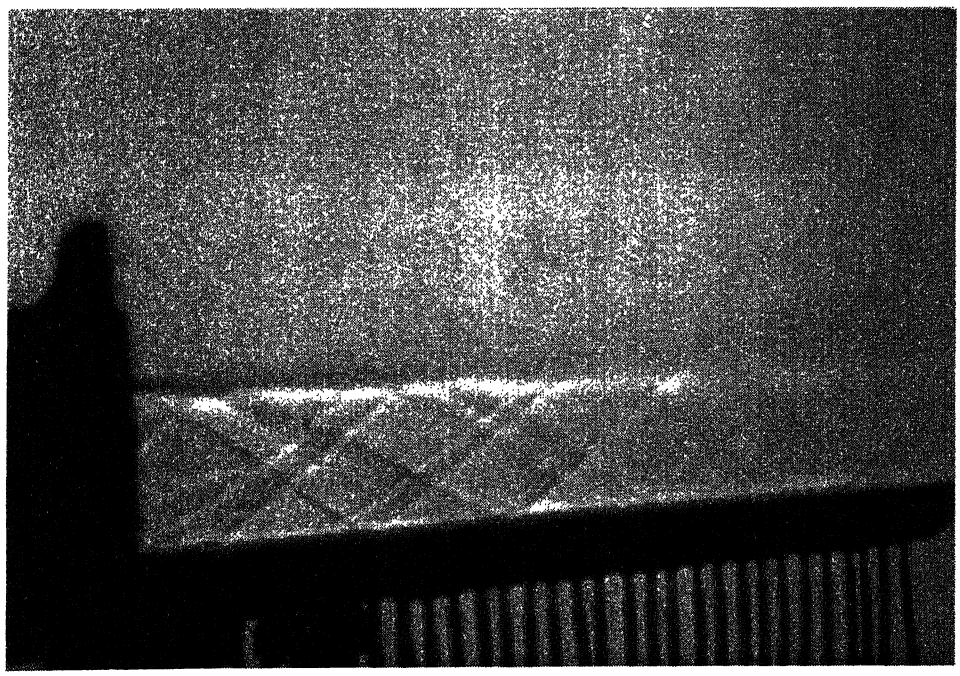

Figure 4.10 Flow field of Mach 1.95 mainstream with out secondary injection.

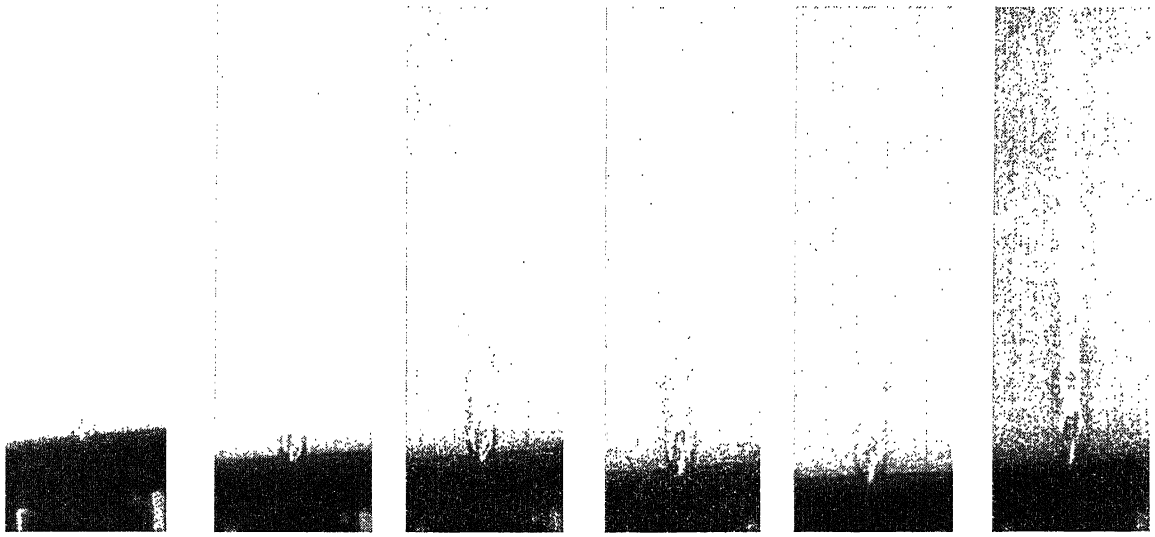

Fig 4.11a Shadowgraph of flow field with Mach 1.35 secondary injection alone.

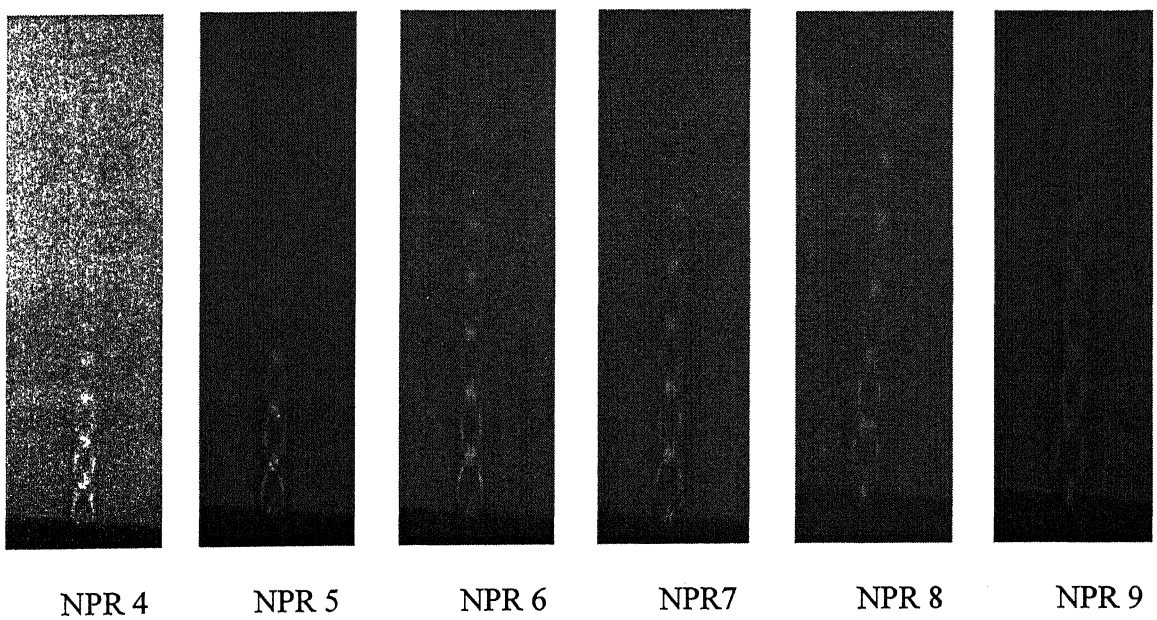

Fig 4.11b Shadowgraph of flow field with Mach 1.52 secondary injection alone.

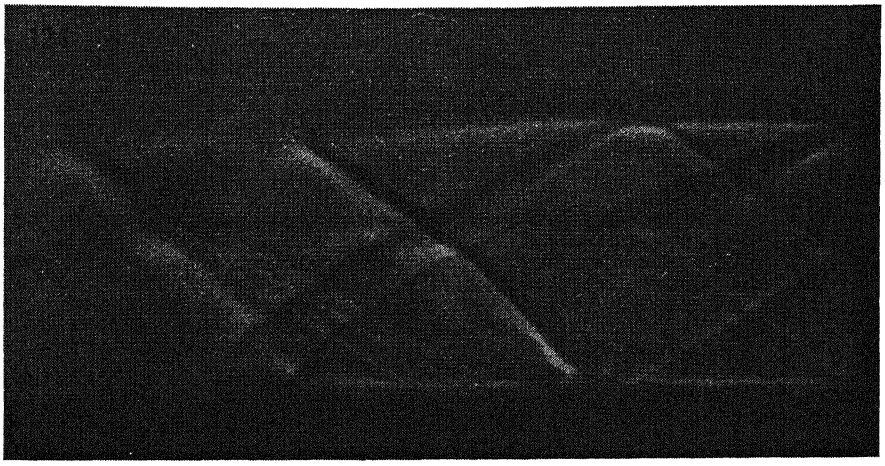

Figure 4.12a Shadowgraph of flow field with main stream Mach 1.72 , Mj 1.35 (NPR 4)

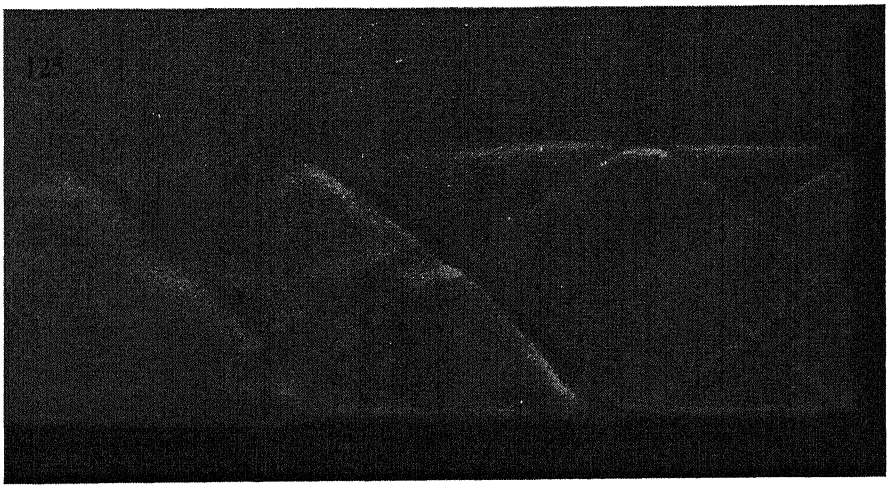

Figure 4.12b Shadowgraph of flow field with main stream Mach 1.72, Mj 1.35 (NPR 5)

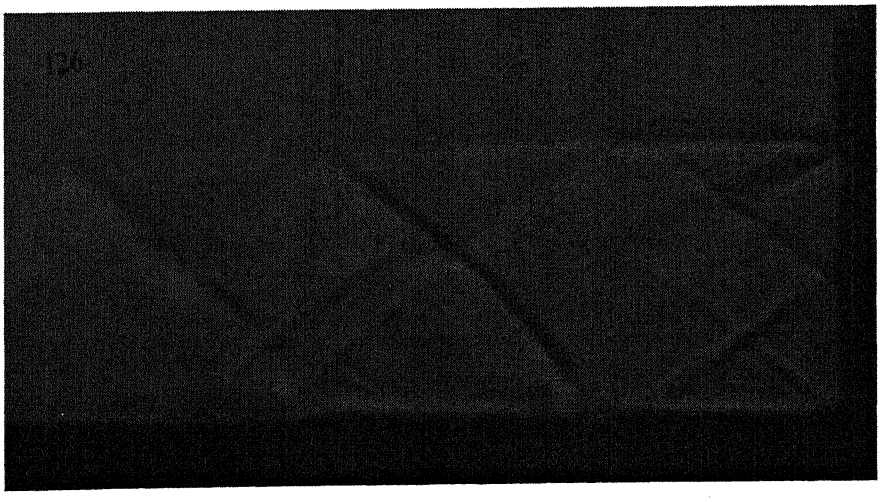

Figure 4.12c Shadowgraph of flow field with main stream Mach 1.72, Mj 1.35 (NPR 6)

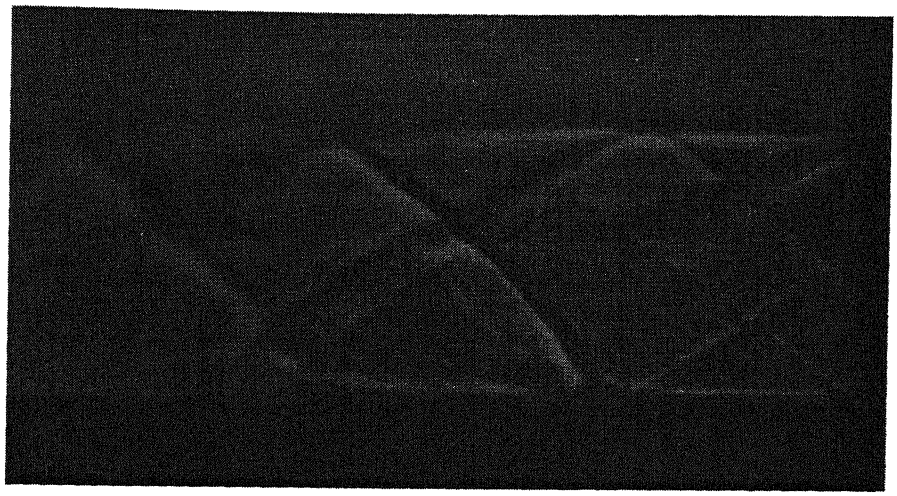

Figure 4.12d Shadowgraph of flow field with main stream Mach 1.72, Mj 1.35 (NPR 7)

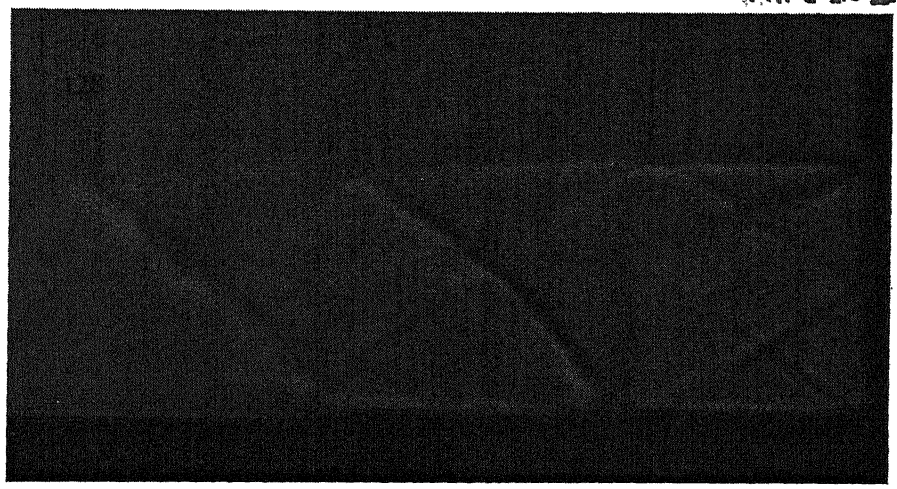

Figure 4.12e Shadowgraph of flow field with main stream Mach 1.72, Mj 1.35 (NPR 8)

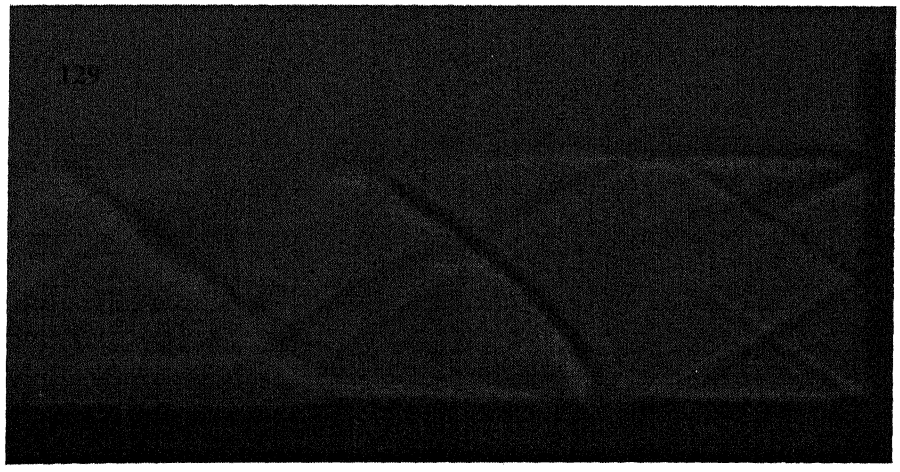

Figure 4.12f Shadowgraph of flow field with main stream Mach 1.72, Mj 1.35 (NPR 9)

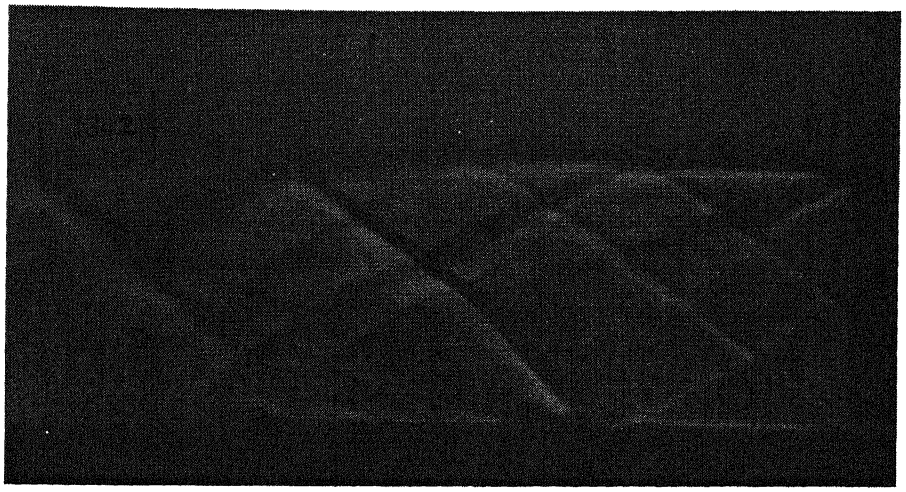

Figure 4.13a Shadowgraph of flow field with main stream Mach 1.72, Mj 1.52 (NPR 4)

Figure 4.13b Shadowgraph of flow field with main stream Mach 1.72, Mj 1.52 (NPR 5)

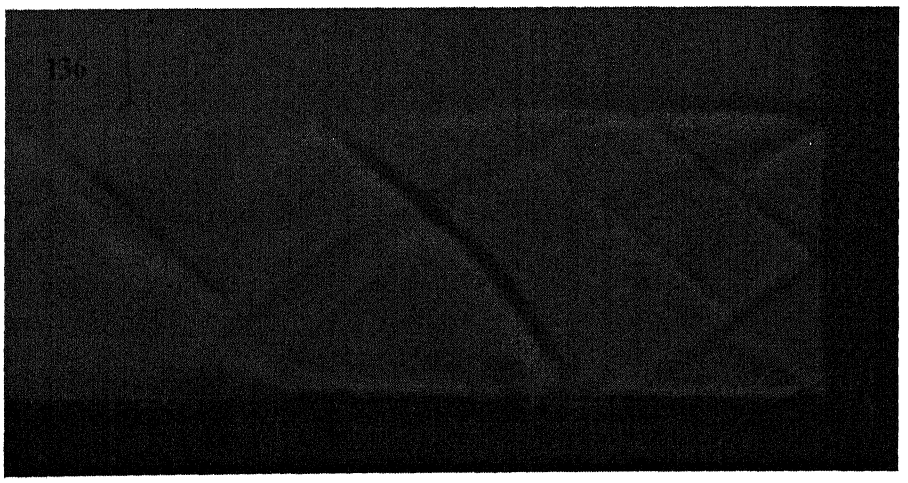

Figure 4.13c Shadowgraph of flow field with main stream Mach 1.72, Mj 1.52 (NPR 6)

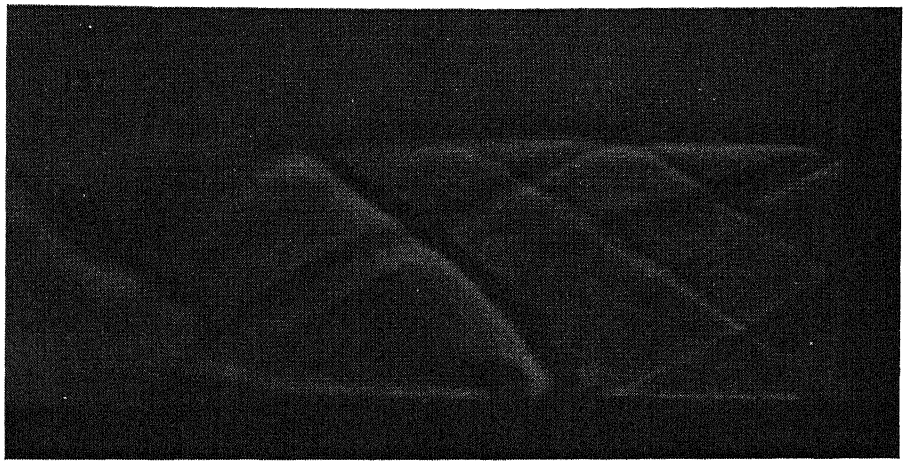

Figure 4.13d Shadowgraph of flow field with main stream Mach 1.72, Mj 1.52 (NPR 7)

Figure 4.13e Shadowgraph of flow field with main stream Mach 1.72, Mj 1.52 (NPR 8)

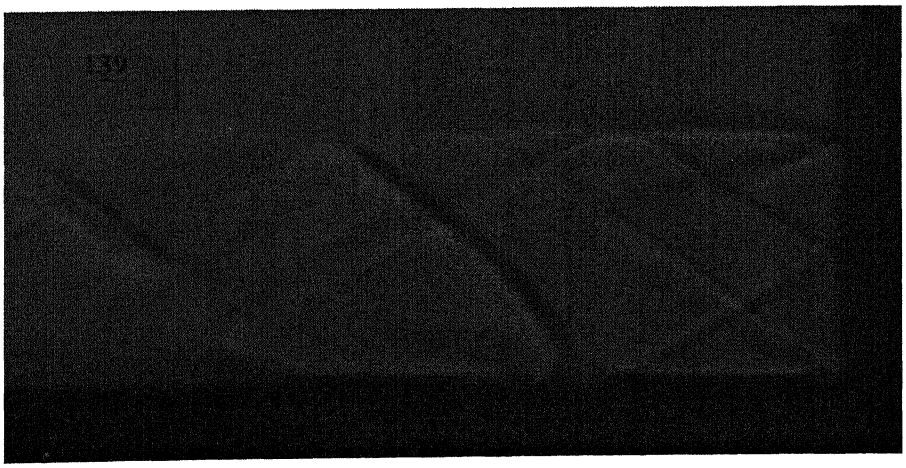

Figure 4.13f Shadowgraph of flow field with main stream Mach 1.72, Mj 1.52 (NPR 9)

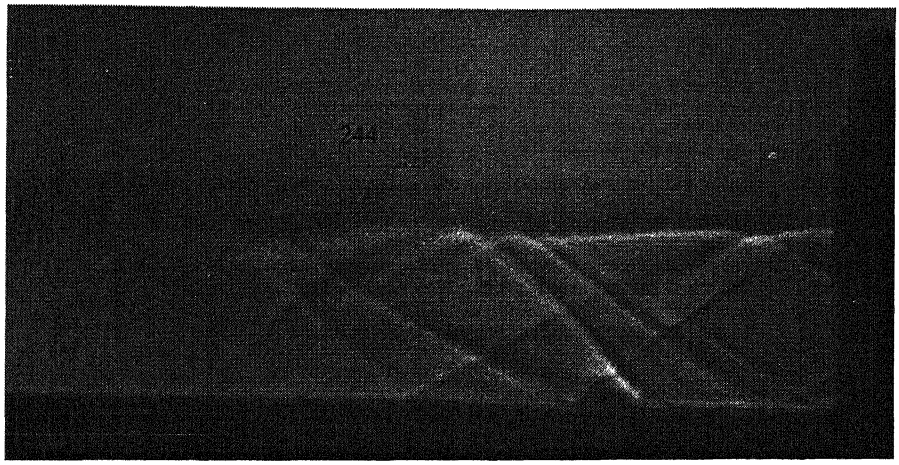

Figure 4.14a Shadowgraph of flow field with main stream Mach 1.95, Mj 1.35 (NPR 4)

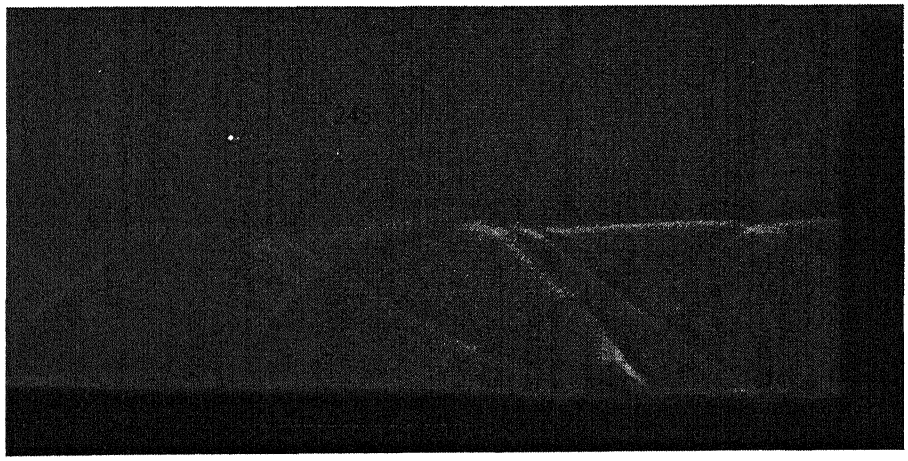

Figure 4.14b Shadowgraph of flow field with main stream Mach 1.95, Mj 1.35 (NPR 5)

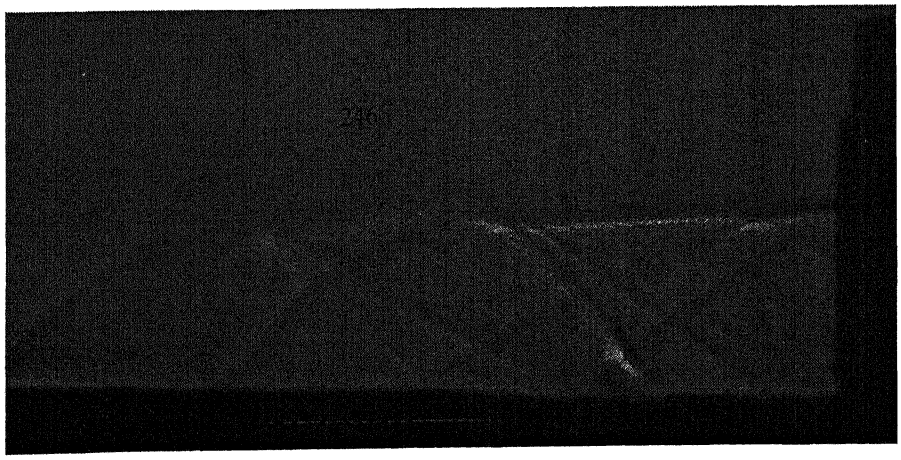

Figure 4.14c Shadowgraph of flow field with main stream Mach 1.95, Mj 1.35 (NPR 6)

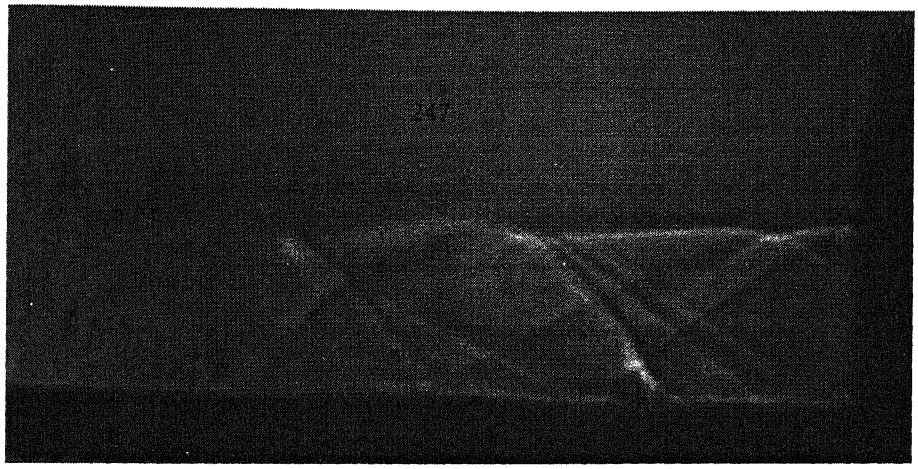

Figure 4.14d Shadowgraph of flow field with main stream Mach 1.95, Mj 1.35 (NPR 7)

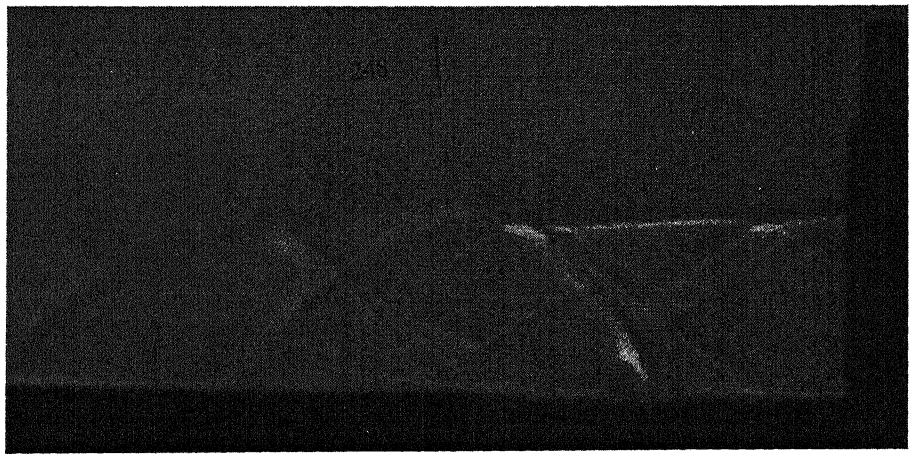

Figure 4.14e Shadowgraph of flow field with main stream Mach 1.95, Mj 1.35 (NPR 8)

Figure 4.14f Shadowgraph of flow field with main stream Mach 1.95, Mj 1.35 (NPR 9)

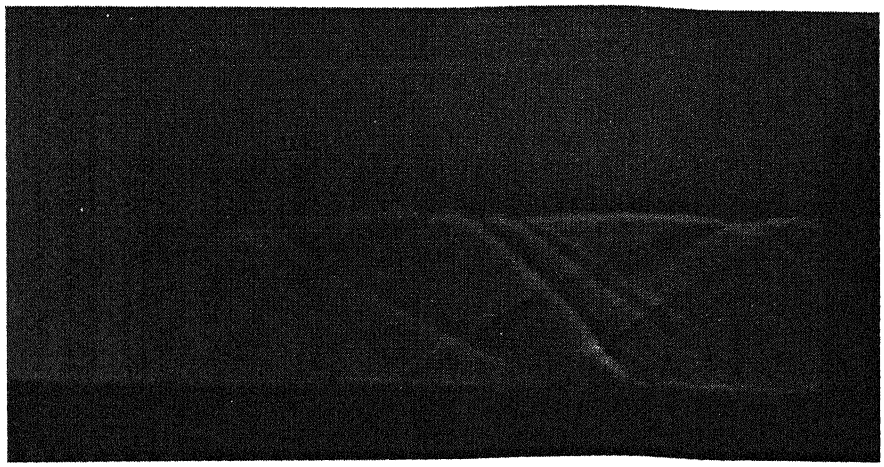

Figure 4.15a Shadowgraph of flow field with main stream Mach 1.95, Mj 1.41 (NPR 4)

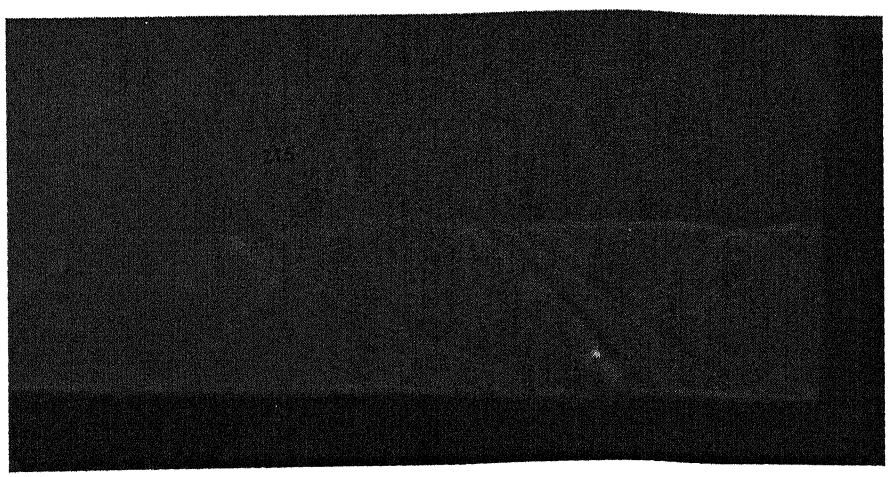

Figure 4.15b Shadowgraph of flow field with main stream Mach 1.95, Mj 1.41 (NPR 5)

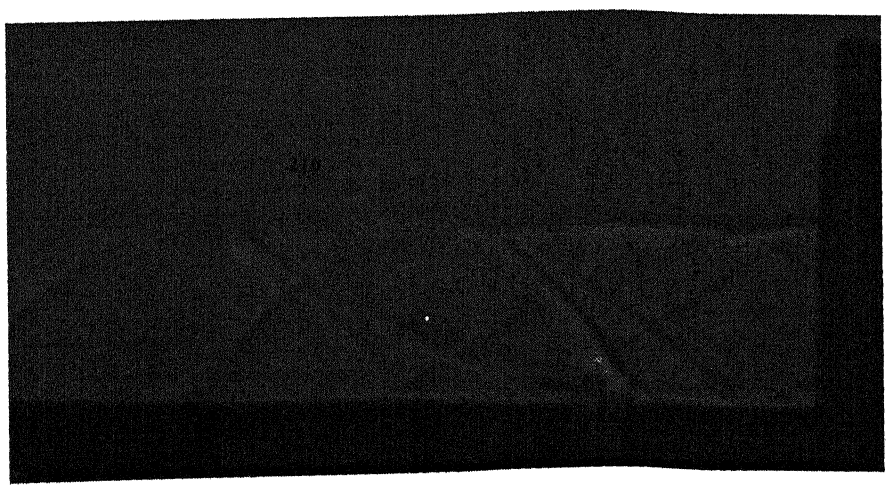

Figure 4.15c Shadowgraph of flow field with main stream Mach 1.95, Mj 1.41 (NPR 6)

Figure 4.15d Shadowgraph of flow field with main stream Mach 1.95, Mj 1.41 (NPR 7)

Figure 4.15e Shadowgraph of flow field with main stream Mach 1.95, Mj 1.41 (NPR 8)

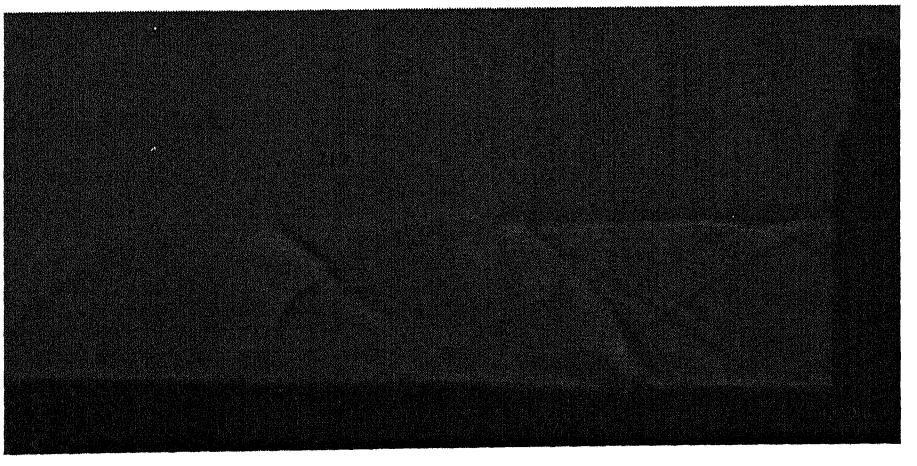

Figure 4.15f Shadowgraph of flow field with main stream Mach 1.95, Mj 1.41 (NPR 9)

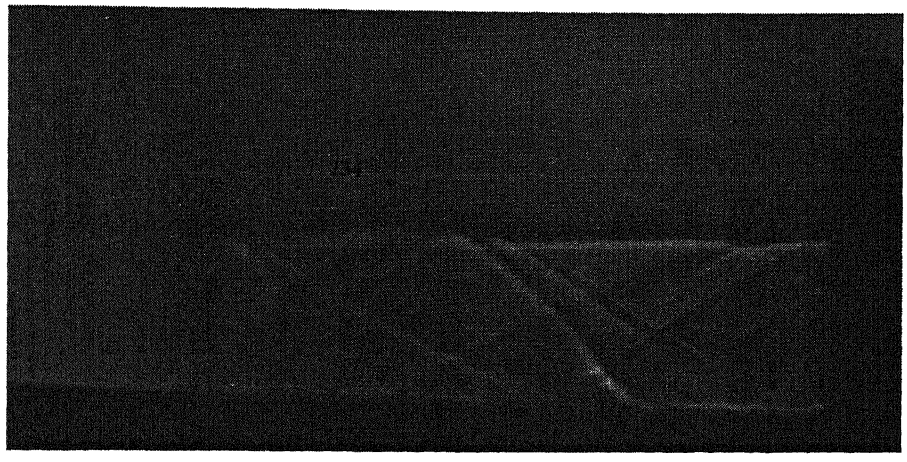

Figure 4.16a Shadowgraph of flow field with main stream Mach 1.95, Mj 1.52 (NPR 4)

Figure 4.16b Shadowgraph of flow field with main stream Mach 1.95, Mj 1.52 (NPR 5)

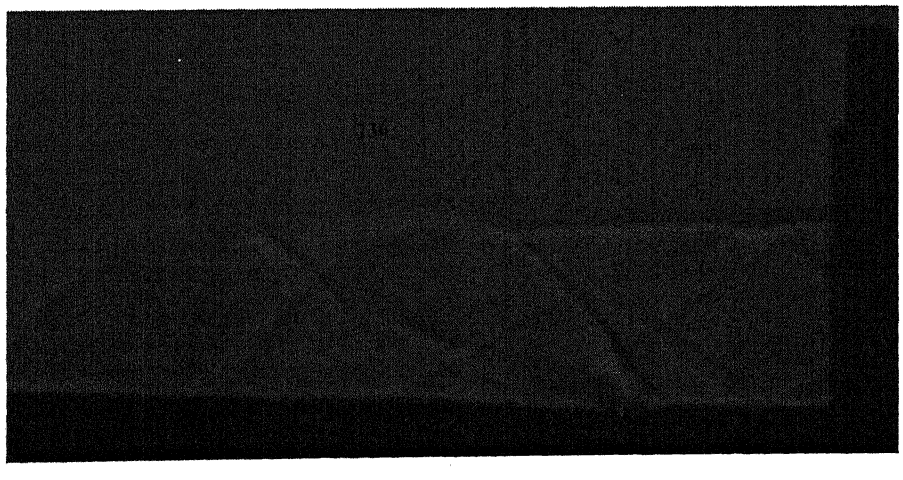

Figure 4.16c Shadowgraph of flow field with main stream Mach 1.95, Mj 1.52 (NPR 6)

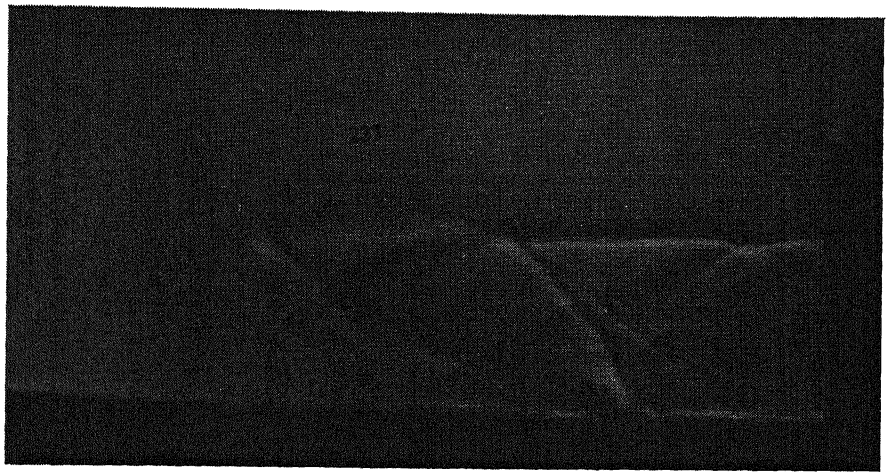

Figure 4.16d Shadowgraph of flow field with main stream Mach 1.95, Mj 1.52 (NPR 7)

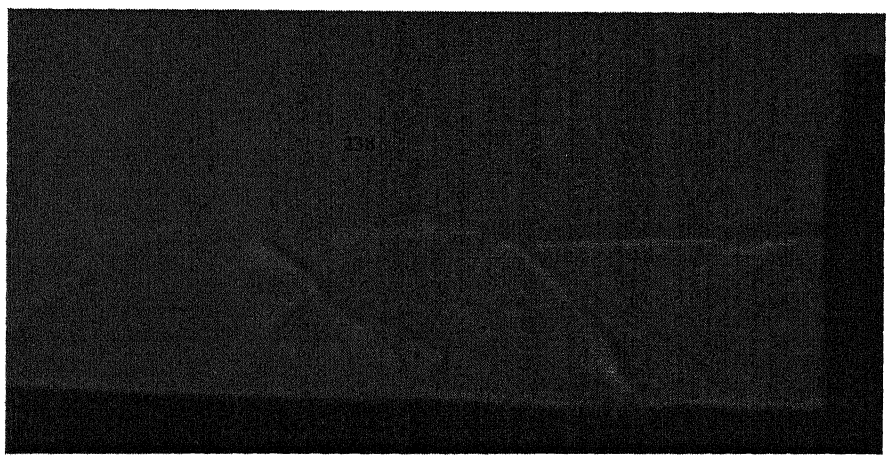

Figure 4.16e Shadowgraph of flow field with main stream Mach 1.95, Mj 1.52 (NPR 8)

Figure 4.16f Shadowgraph of flow field with main stream Mach 1.95, Mj 1.52 (NPR 9)

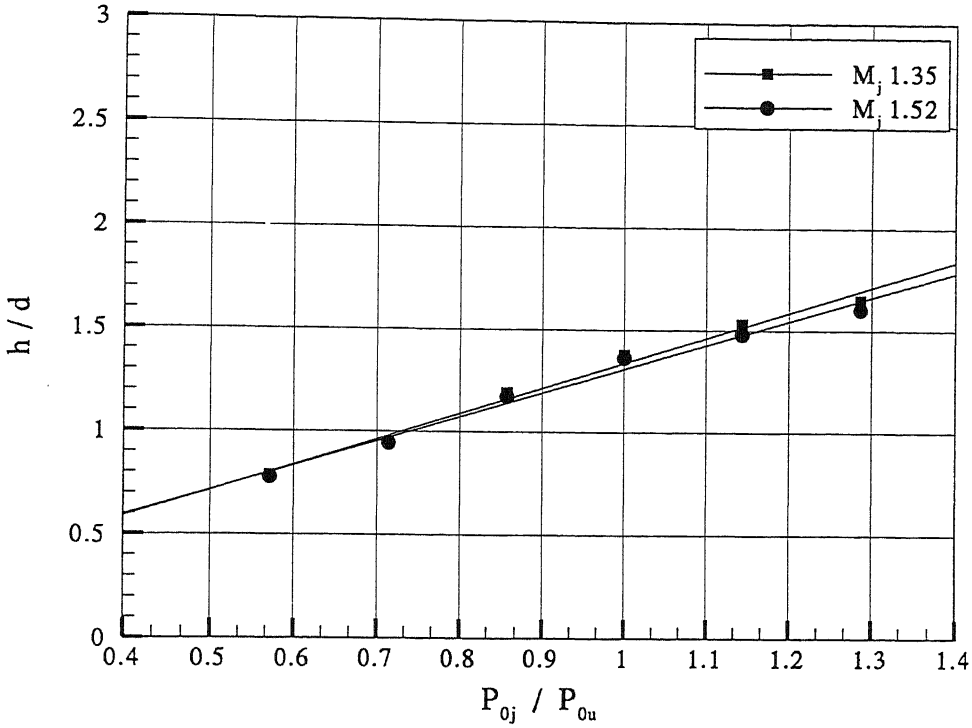

Fig 4.17 Penetration height for main stream Mach 1.72

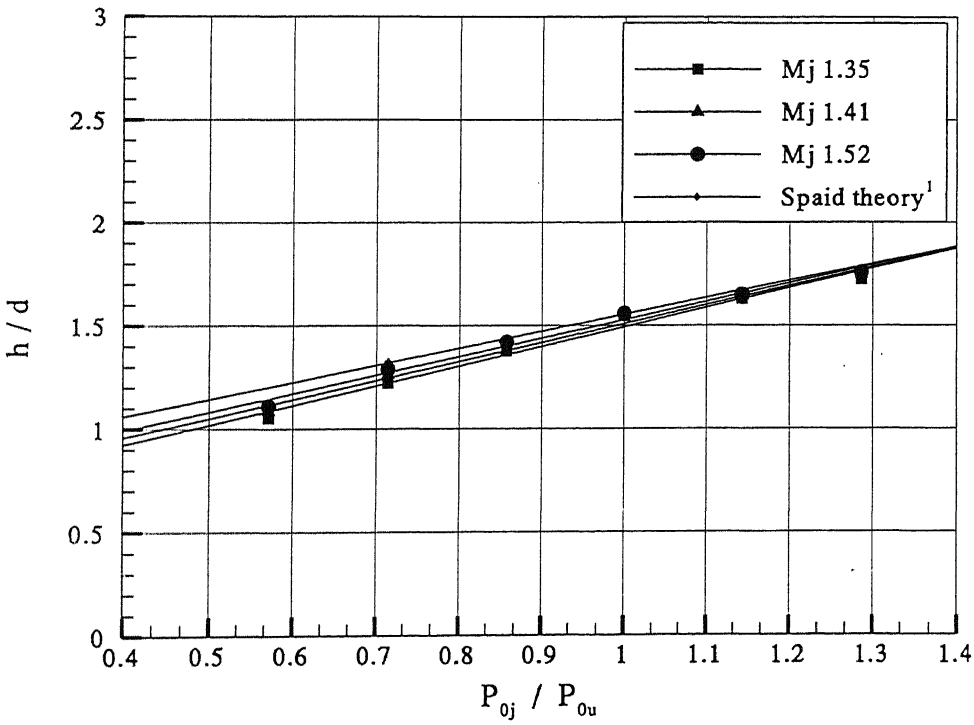

Fig 4.18 Penetration height for main stream Mach 1.95

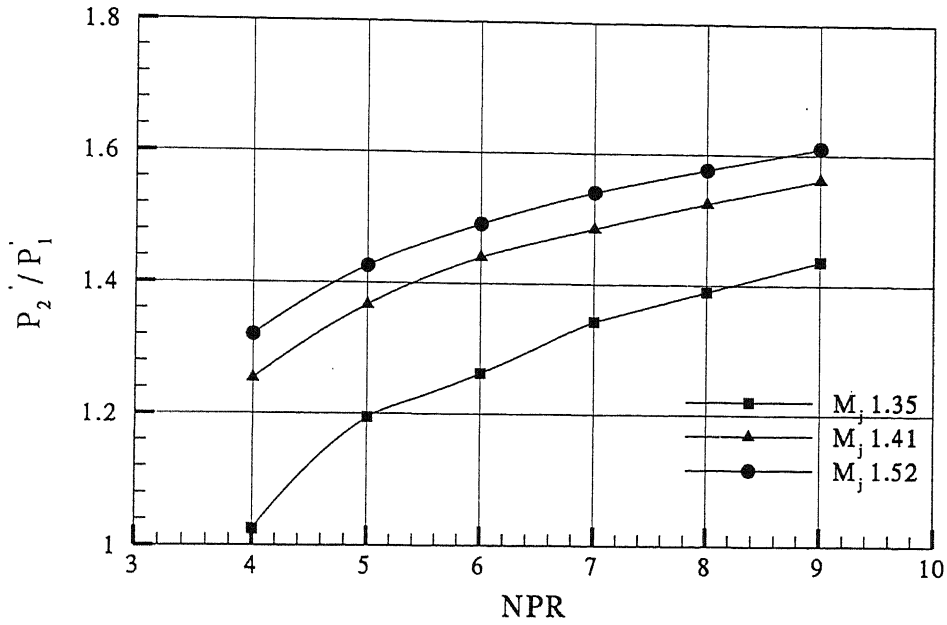

Figure 4.21 Shock strength of Mach 1.95 freestream with NPR.

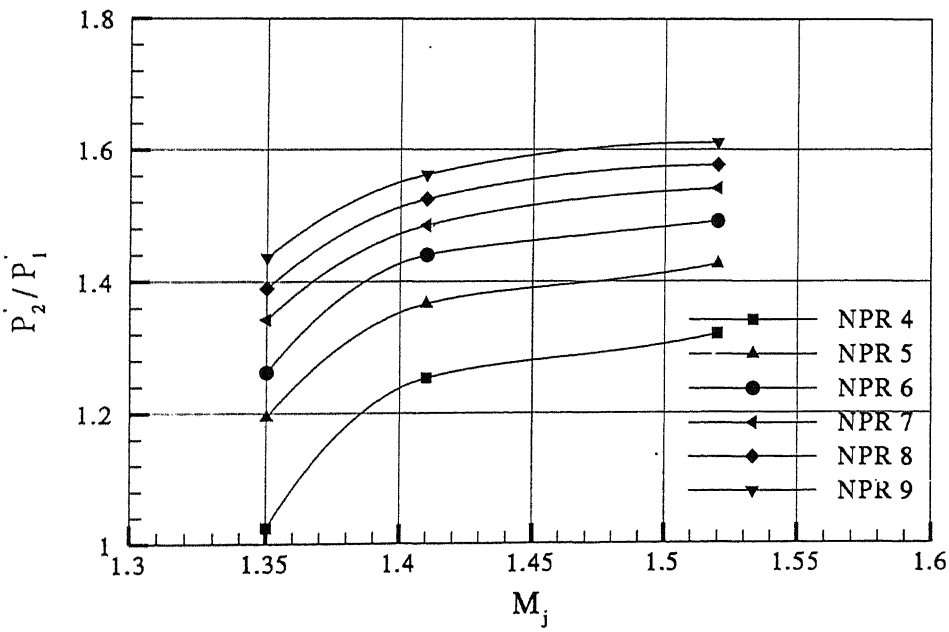

Figure 4.22 Shock strength of Mach 1.95 freestream with M_j.

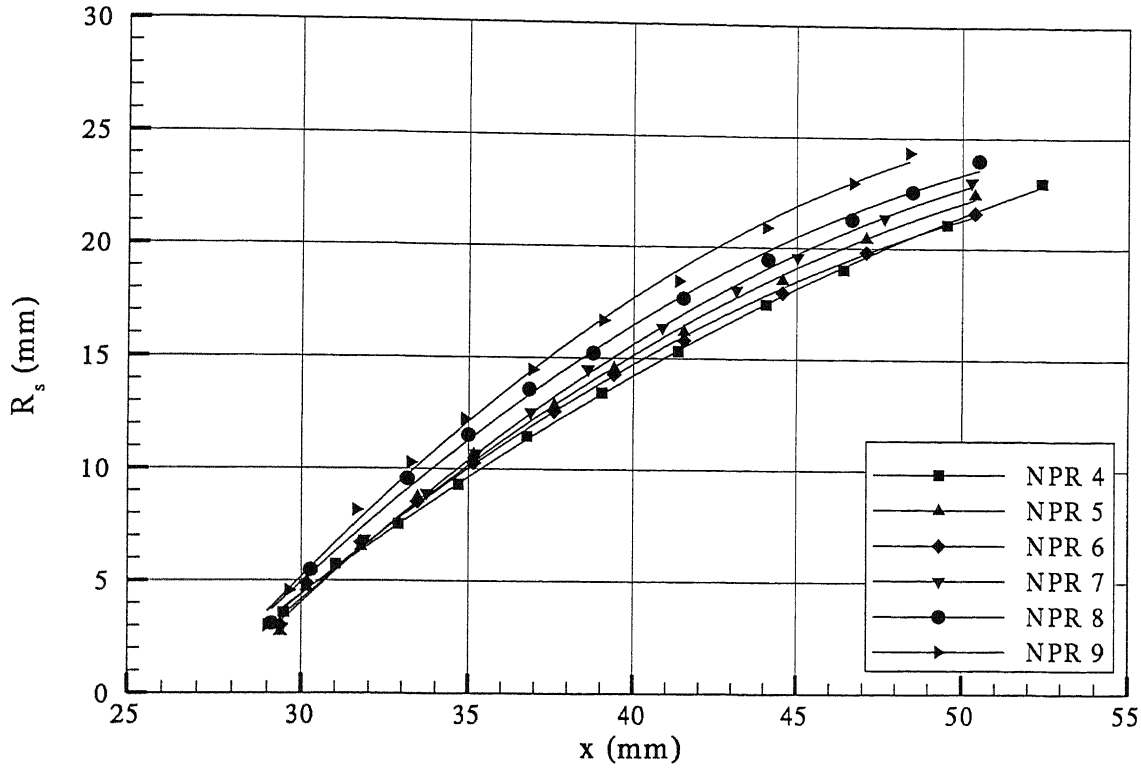

Figure 4.23 Shock radius for Mach 1.72 freestream with M_j 1.35

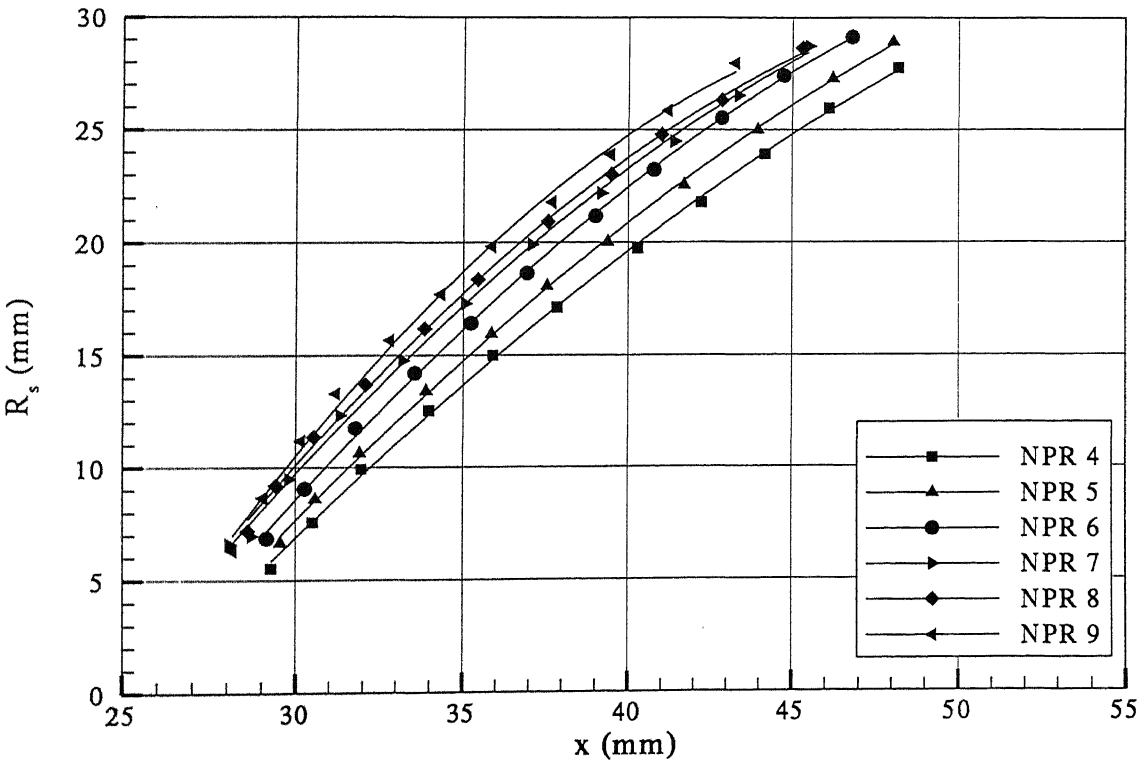

Figure 4.24 Shock radius for Mach 1.95 freestream with M_j 1.41

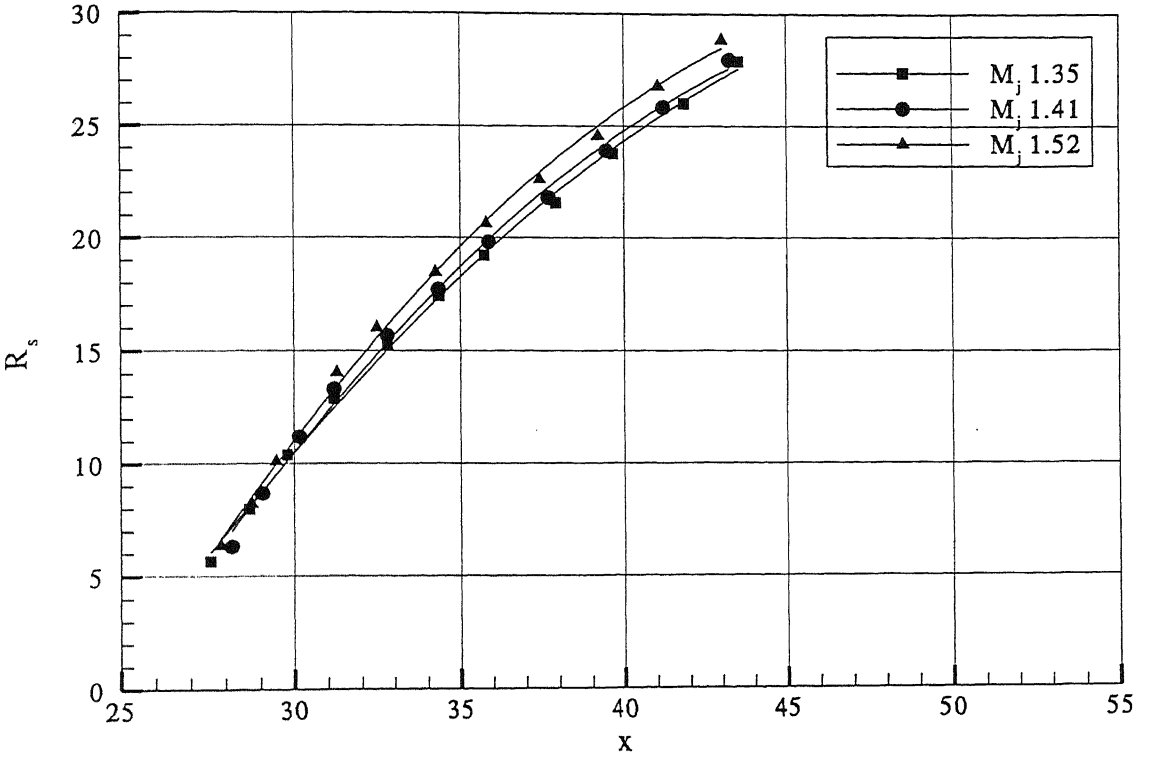

Figure 4.25 Shock radius in mm for Mach 1.95 freestream with injection NPR 9

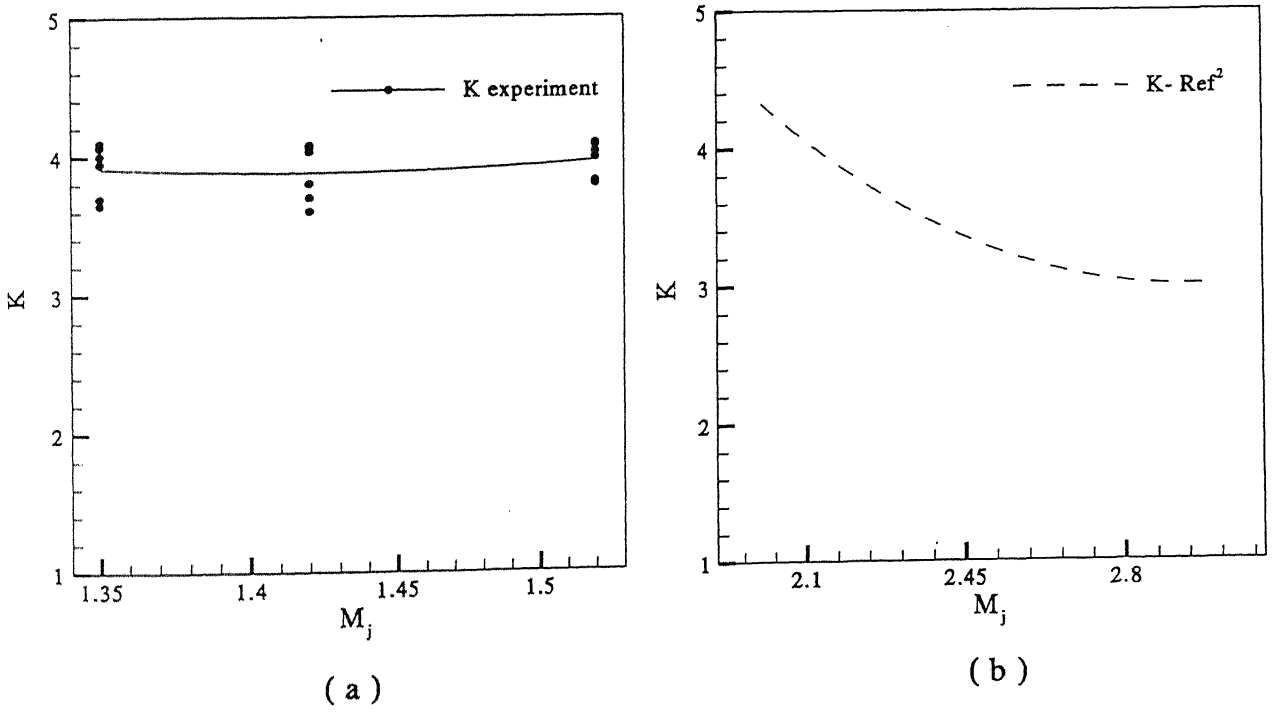

Figure 4.26 Shock correction factor K. a). Experimental, b). Charwat^2

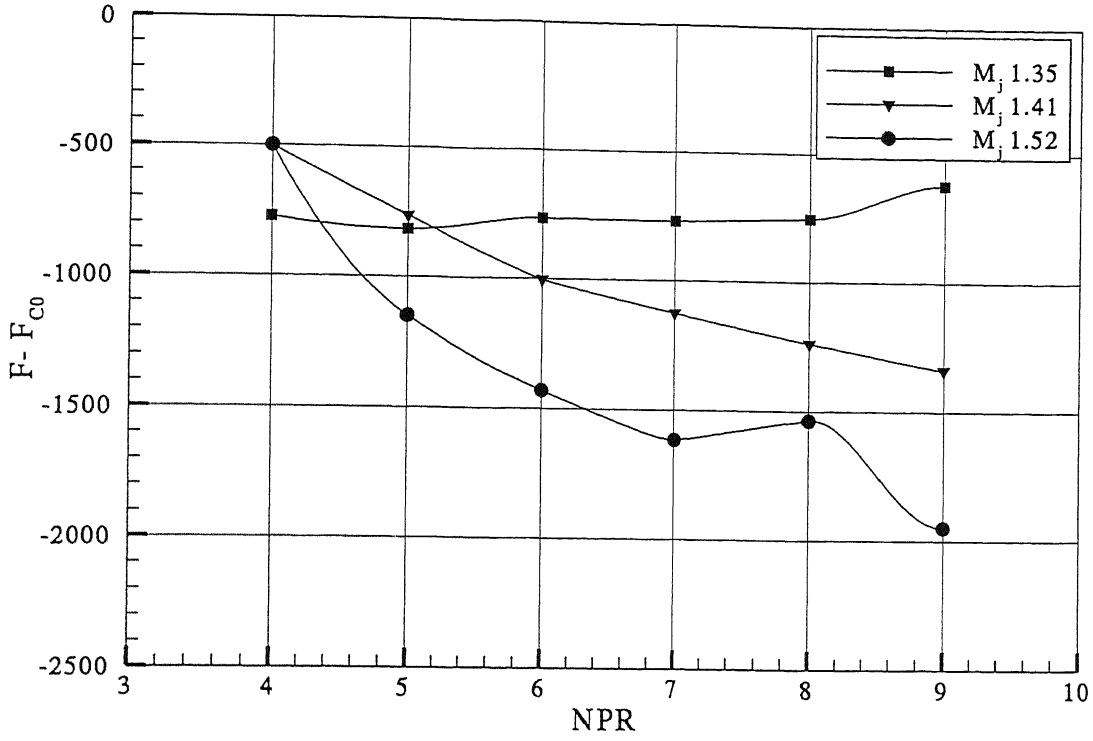

Figure 4.27 Force for Mach 1.72 freestream with injection NPR

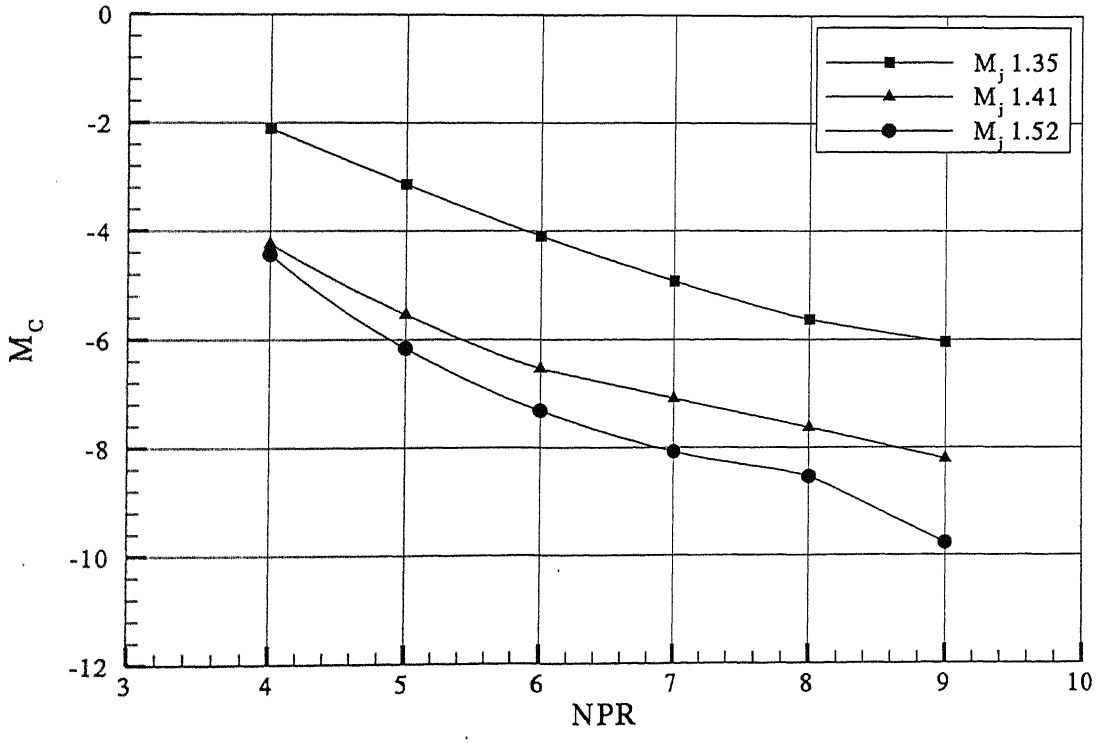

Figure 4.28 Moment for Mach 1.72 freestream with injection NPR

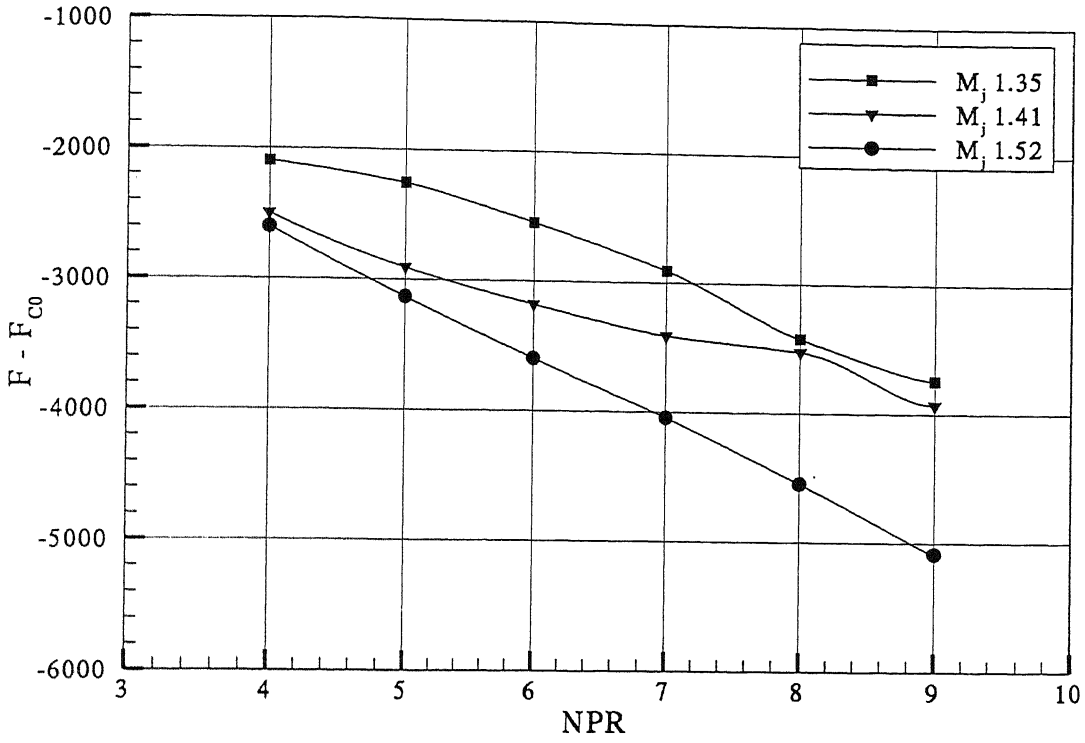

Figure 4.29 Force for Mach 1.95 freestream with injection NPR

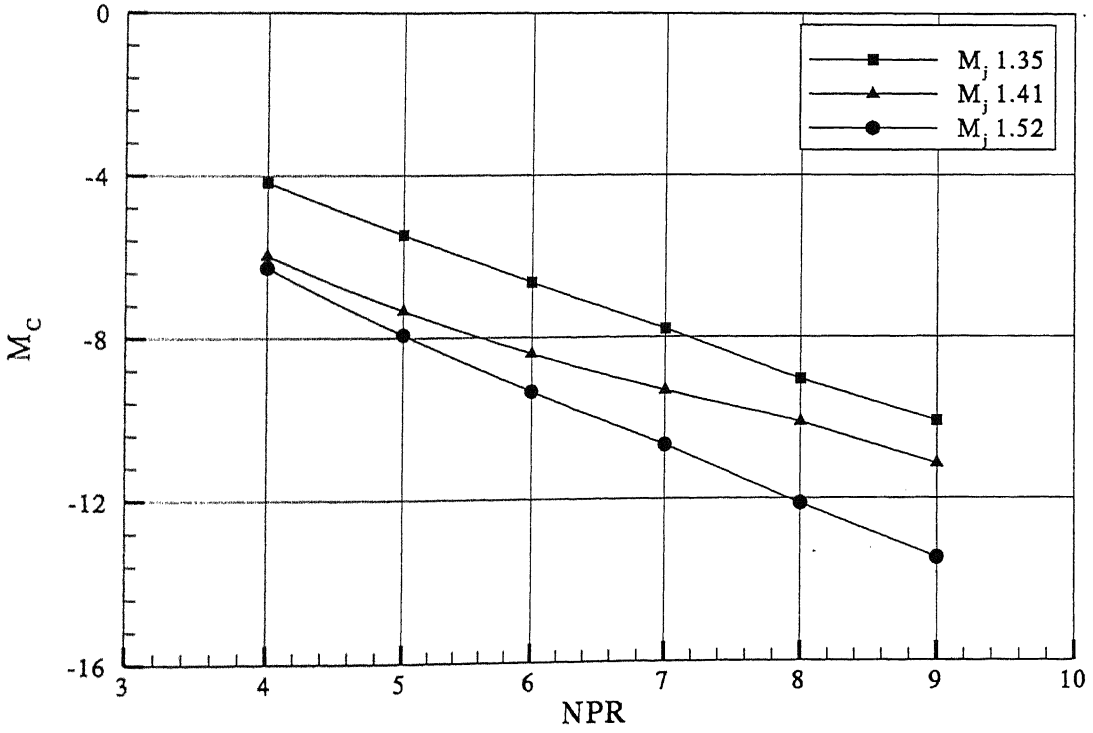

Figure 4.30 Moment for Mach 1.95 freestream with injection NPR

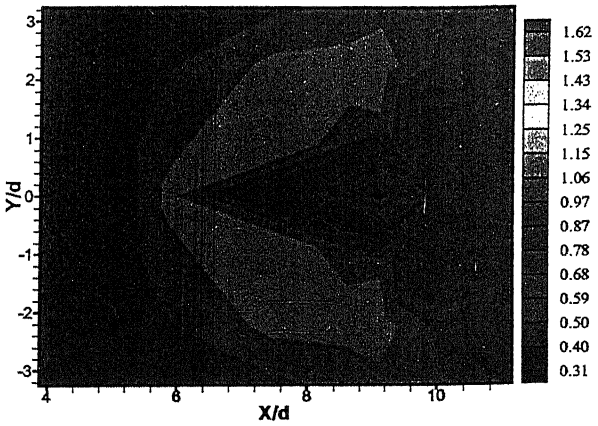

M 1.72, Mj 1.35, NPR 5

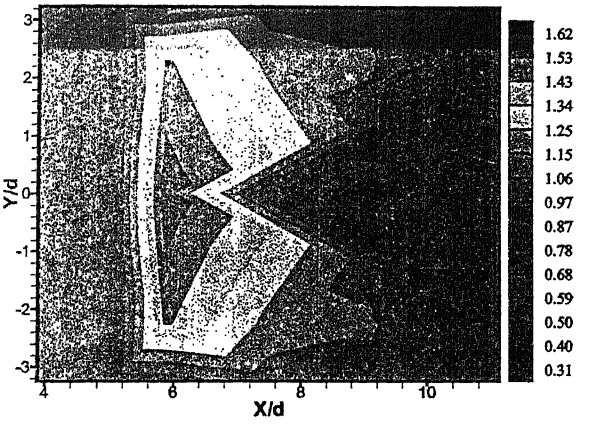

M 1.72, Mj 1.52, NPR 5

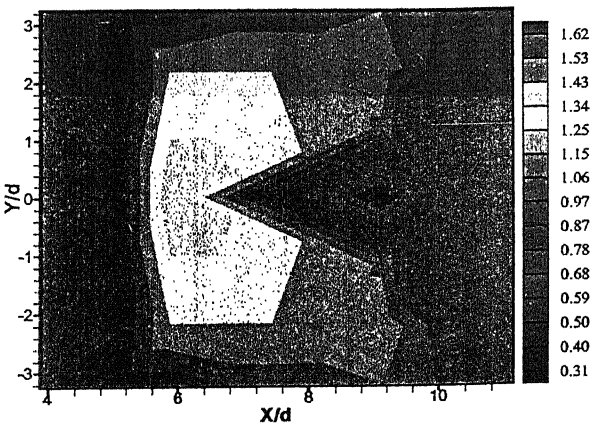

M 1.72, Mj 1.35, NPR 7

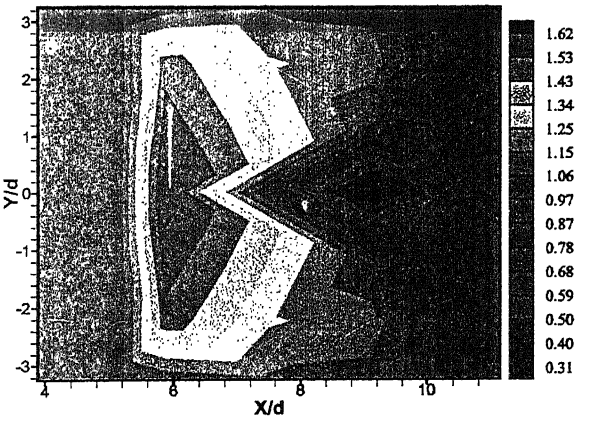

M 1.72, Mj 1.52, NPR 7

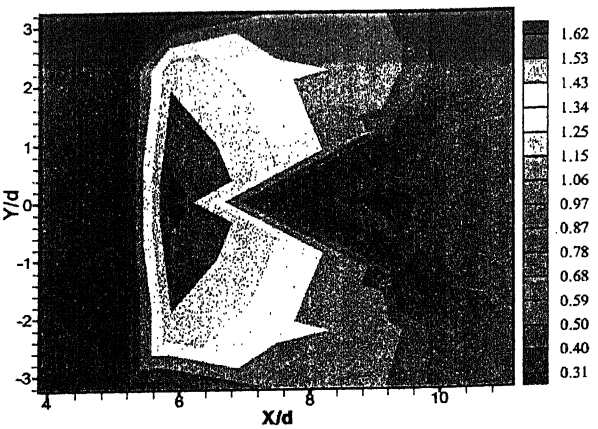

M 1.72, Mj 1.35, NPR 9

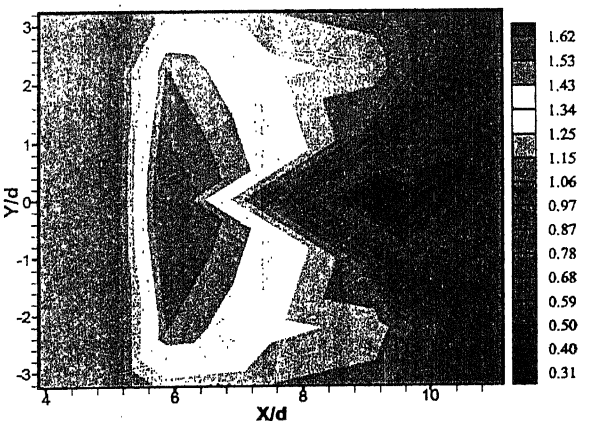

M 1.72, Mj 1.52, NPR 9

Figure 4.31 Pressure distribution around the injection for Mach 1.72 freestream with M_j 1.35 and 1.52

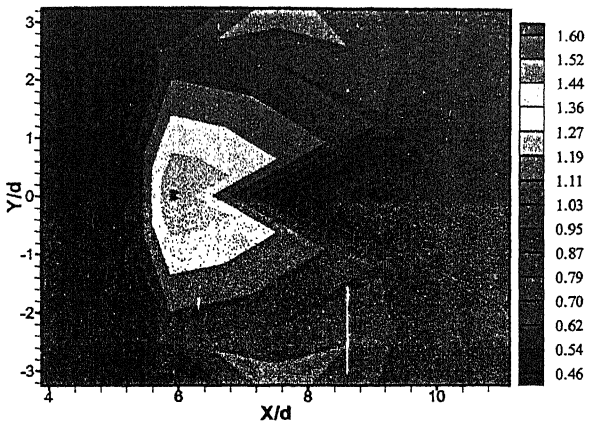

M 1.72, Mj 1.41, NPR 4

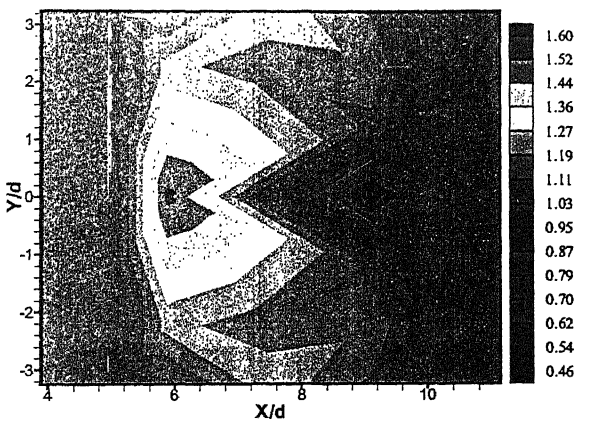

M 1.72, Mj 1.41, NPR 5

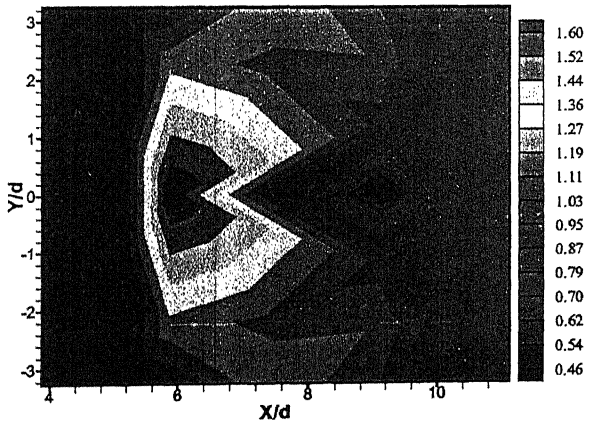

M 1.72, Mj 1.41, NPR 6

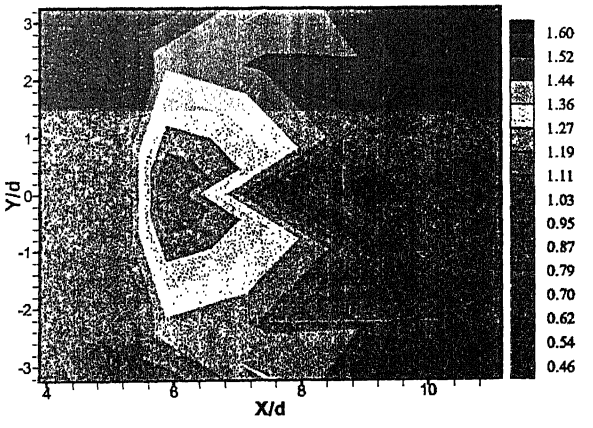

M 1.72, Mj 1.41, NPR 7

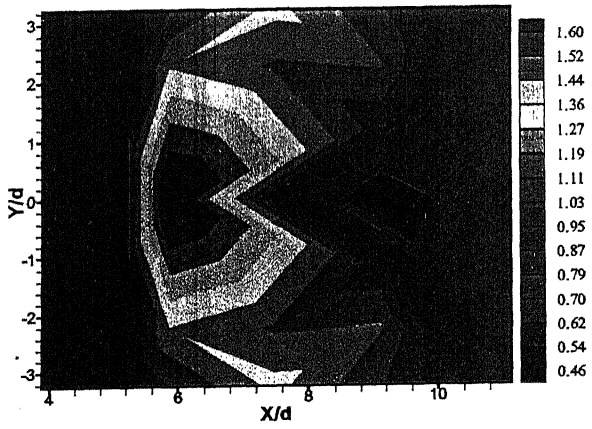

M 1.72, Mj 1.41, NPR 8

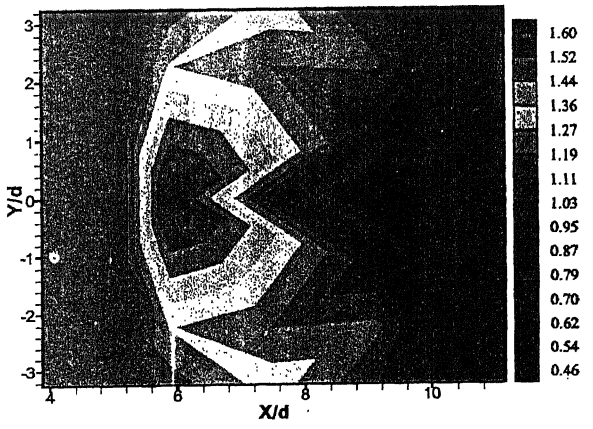

M 1.72, Mj 1.41, NPR 9

Figure 4.32 Pressure distribution around the injection for Mach 1.72 freestream with M_j 1.41

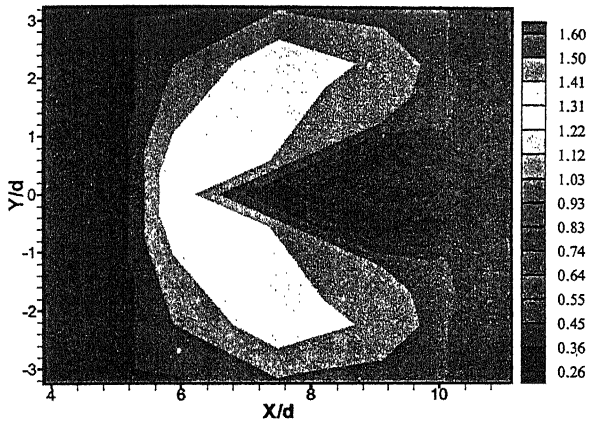

M 1.95, Mj 1.35, NPR 5

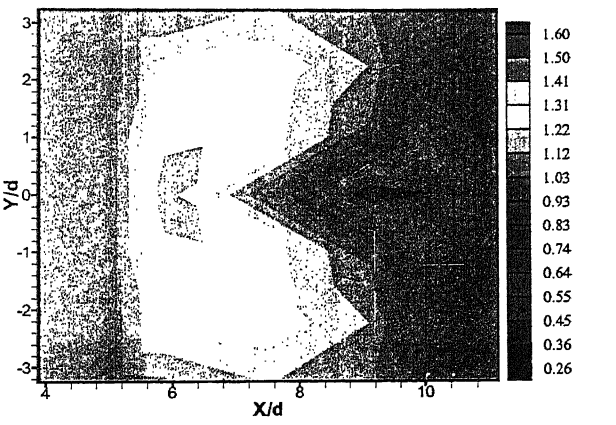

M 1.95, Mj 1.41, NPR 5

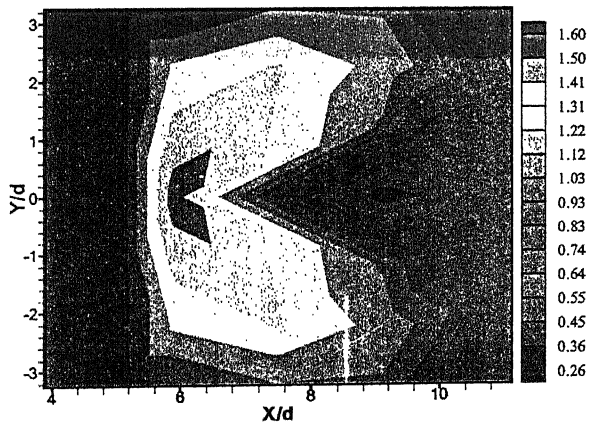

M 1.95, Mj 1.35, NPR 7

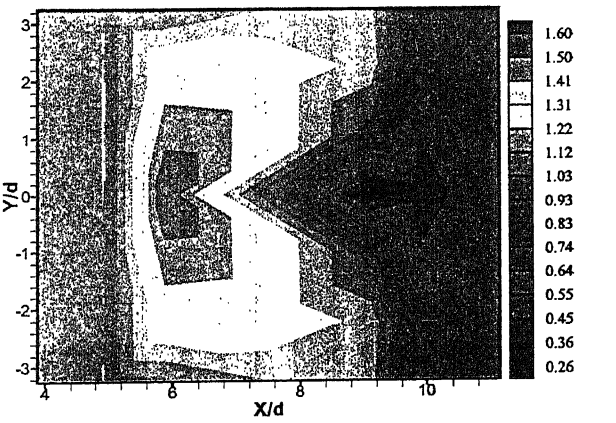

M 1.95, Mj 1.41, NPR 7

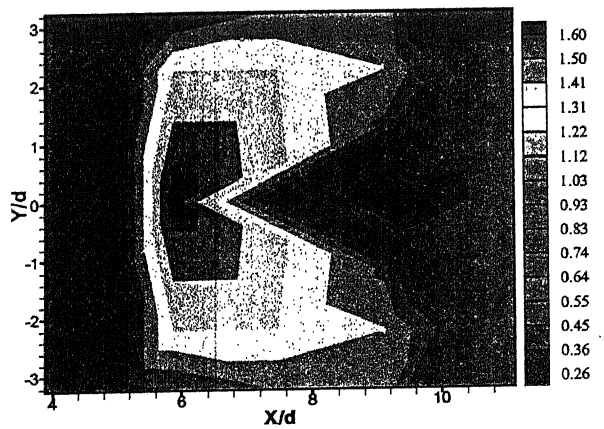

M 1.95, Mj 1.35, NPR 9

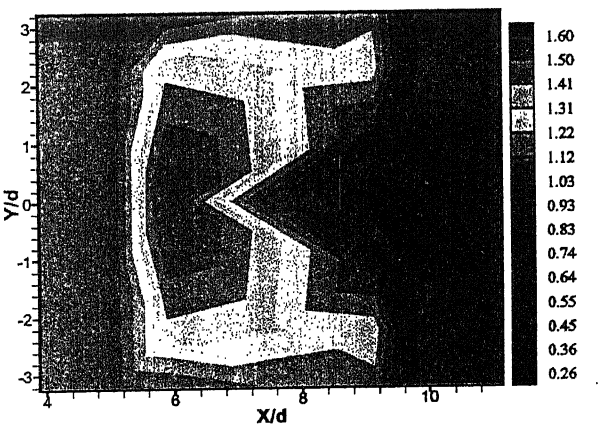

M 1.95, Mj 1.41, NPR 9

Figure 4.33 Pressure distribution around the injection for Mach 1.95 freestream with M_j 1.35 and 1.41

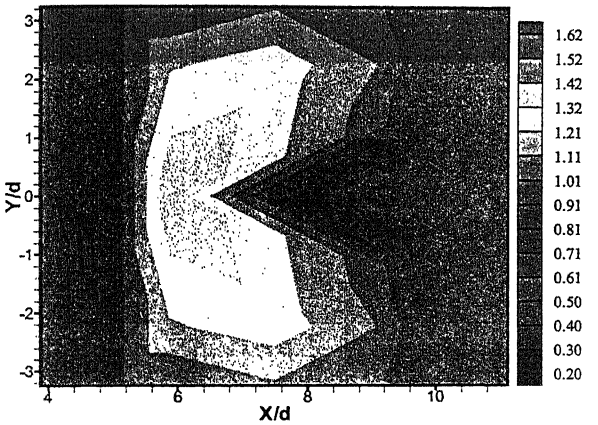

M 1.95, Mj 1.52, NPR 4

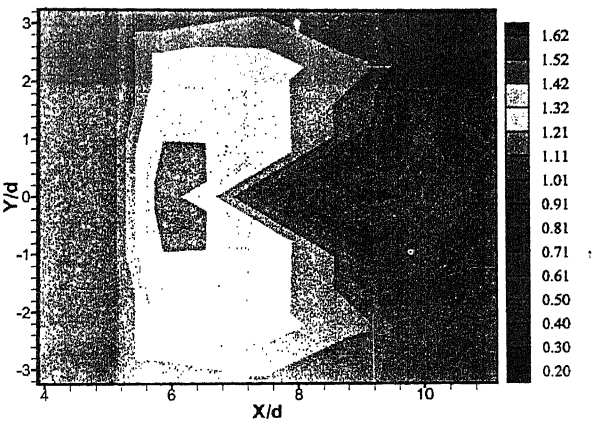

M 1.95, Mj 1.52, NPR 5

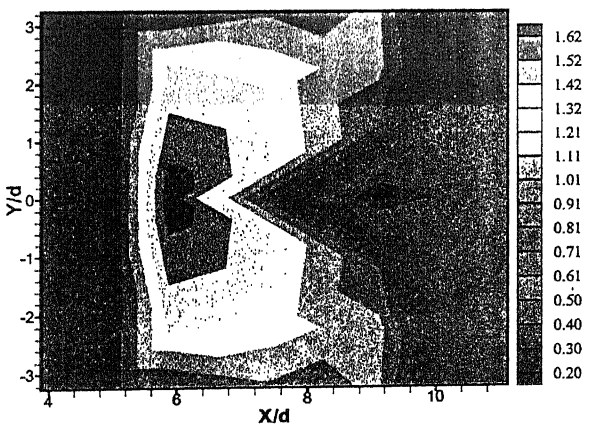

M 1.95, Mj 1.52, NPR 6

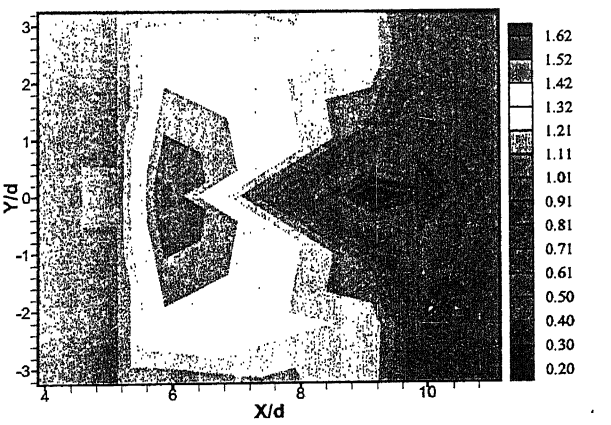

M 1.95, Mj 1.52, NPR 7

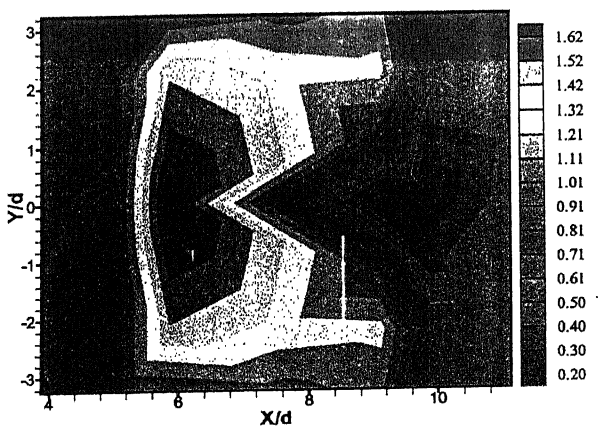

M 1.95, Mj 1.52, NPR 8

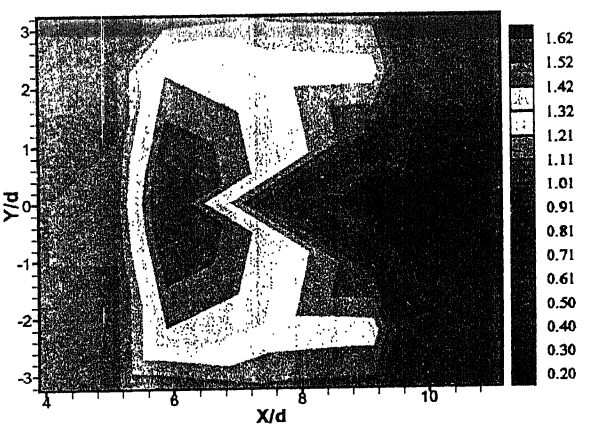

M 1.95, Mj 1.52, NPR 9

Figure 4.34 Pressure distribution around the injection for Mach 1.95 freestream with M_j 1.52

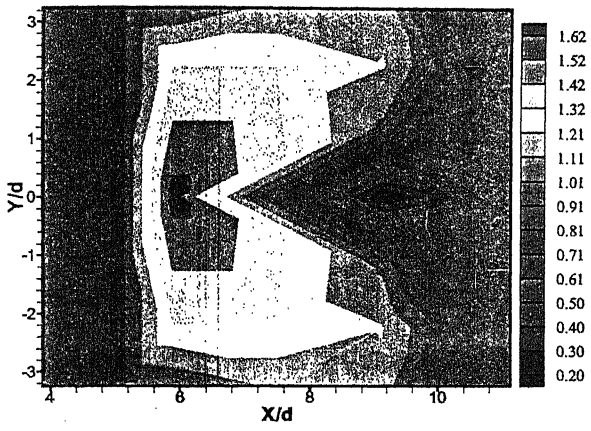

M 1.95, Mj 1.35, NPR 9

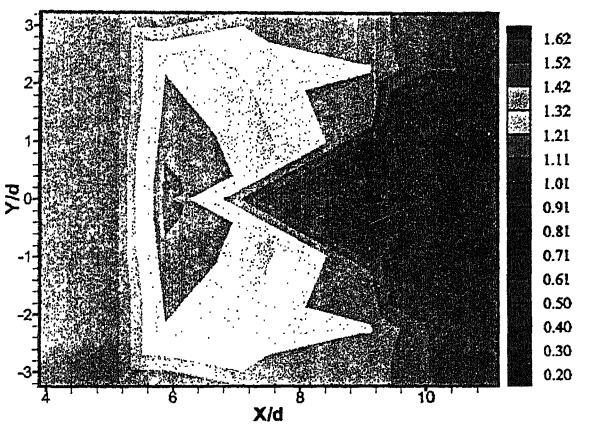

M 1.72, Mj 1.35 NPR 9

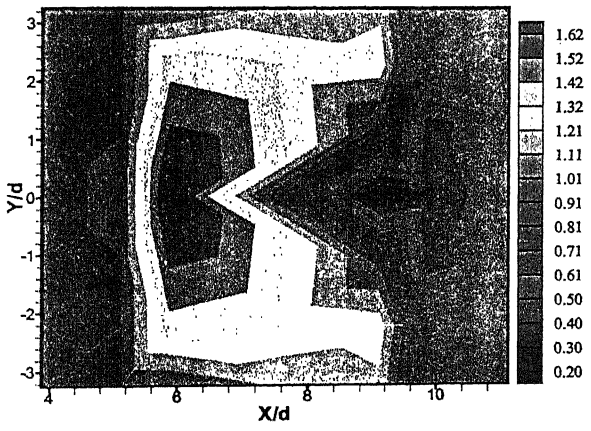

M 1.95, Mj 1.41, NPR 9

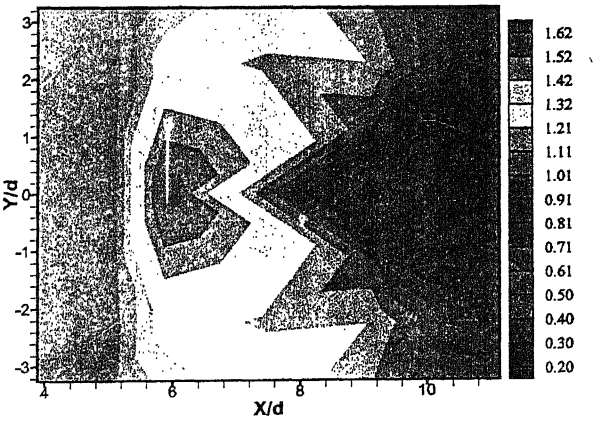

M 1.72 Mj 1.41, NPR 9

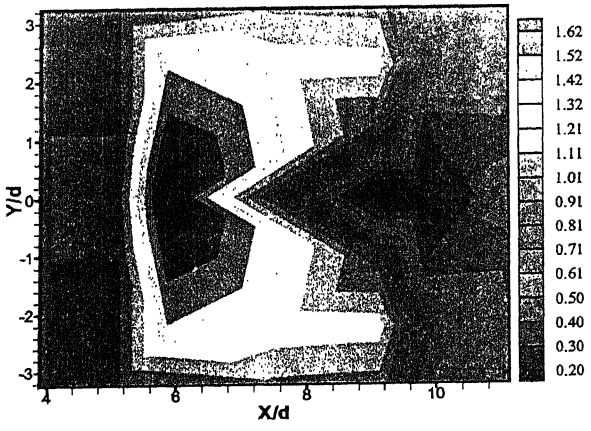

M 1.95, Mj 1.52, NPR 9

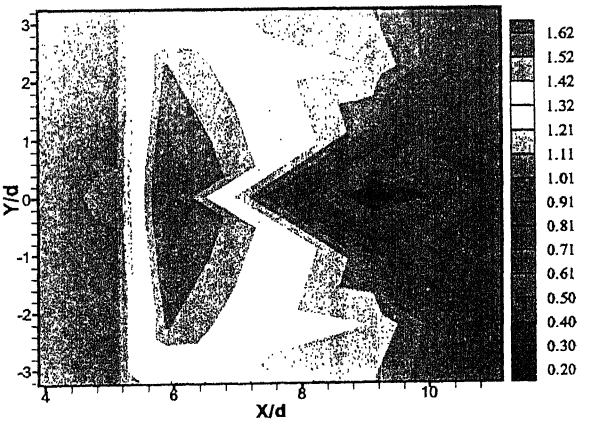

M 1.72, Mj 1.52, NPR 9

Figure 4.35 Pressure distribution around the injection for Mach 1.72 and Mach 1.95 freestream with M_j at NPR 9

Chapter 5

Conclusions

Experiments were carried out to study the resultant flow field over a flat plate due to a supersonic freestream and a secondary injection. Injection of supersonic secondary jet from the plate, transverse to supersonic freestream acts as an obstruction for the main stream and results in the formation of a strong bow shock ahead of injection. A separation shock is also formed due to the boundary layer separation ahead of the bow shock because of the adverse pressure gradient casued by the bow shock. Two separation regions are formed due to the injection of supersonic secondary jet into the supersonic main stream. One is ahead of the injection, which is due to the adverse pressure gradient generated by bow shock. Another separated region is formed behind the injection port and is due to the wake formed behind the secondary jet.

The positive maximum and the extent of that zone ahead of the injection and negative maximum and the extent of the negative zone behind the injection increases with increase in NPR (momentum flux) of the secondary jet for the same freestream Mach number and injection Mach number, and also increases with injection Mach number for a particular M_∞ and NPR. The parameters, penetration height, shock radius and shock strength, force and moment are increasing with increase in NPR for constant freestream Mach number M_∞ and injection Mach number M_j i.e. the expansion level of the secondary jet plays a dominant role on the penetration of the jet into the mainstream. It is founded that, the penetration height is independent of secondary injection Mach number for same injection momentum flux and increases with freestream Mach number. The shock strength increases with increase in secondary injection Mach number and NPR for the same freestream Mach number. Increase in NPR and M_j makes the oblique shock to reach a limiting strength. The magnitude of the moment generated due to the secondary jet is found to increase with both NPR

and M_j and this can be exploited for the maneuvering of a flying object like a missile.

5.1 Scope for future work

- Different shapes of secondary injection nozzle like elliptic, diamond, rectangular may be tested.
- injection can be made at angles instead of transverse to plate, to minimize total pressure loss.
- Number of secondary jets can be made more to study the effect of multiple jets on interaction flow field.
- Axisymmetric body like missiles may be used instead of flat plate.
- Similar study with higher range of freestream and injection Mach numbers will be of wider application.

References

[1] Spaid, F.W. and Zukoski, E.E., "Secondary injection of gases into a supersonic flow", *AIAA Journal*, Vol. 2, pp. 1689–1696, 1964.

[2] Charwat, A.F. and Allegre, J., "Interaction of a supersonic stream and a transverse supersonic jet", *AIAA Journal*, Vol. 2, pp. 1965–1971, 1964.

[3] Cohen, L.S.," Penetration and mixing of multiple gas jets subjected to cross flow", *AIAA Journal*, Vol. 2, pp. 1965–1971, 1964.

[4] Orth. R.C. and Funk, F.A., "An experimental and comparative study of jet penetration in supersonic flow", *Journal of Spacecraft*, Vol.4, pp. 1236–1242, 1967.

[5] Schetz, J.A. and Billing, F.S., "Penetration of gaseous jets injected into a supersonic flow", *Journal of Spacecraft* Vol.3, pp. 1658–1665, 1966.

[6] Heister, S.D. and Karagozian, A.R., "Gaseous jets in supersonic crossflow", *AIAA Journal*, Vol. 28, pp. 819–827, 1990.

[7] Billig, F.S., Orth, R.C and Lasky, M., "A unified analysis of gaseous jet penetration", *AIAA Journal*, Vol. 9, pp. 1048–1058, 1971.

[8] Gruber, M.R., Nejad, A.S., Chen, T.H. and Dutton, J.C., "Bow shock/jet interaction in compressible transverse injection flow fields", *AIAA Journal*, Vol. 34, pp. 2191–2193, 1996.

[9] Gruber, M.R., and Goss, L.P., "Surface pressure measurements in supersonic transverse injection flowfields", *Journal of Propulsion and Power*, Vol. 15, pp. 633–641, 1999.

[10] Chrans, L.J., and Collins, D.J., "Stagnation temparature and molecular weight effects in jet interaction", *AIAA Journal*, Vol. 8, pp. 287–293, 1970.

[11] Papamoschou, D. and Hubbard, D.G., "Visual observations of supersonic transverse jets", *Experiments in Fluids*, Vol. 14, pp. 468–471, 1993.

[12] Everett, D.E., Dutton, J.C. and Morris, M.J., "Wall pressure measurements for a sonic jet injected transversely into a supersonic cross flow", *Journal of Propulsion and Power*, Vol. 14, pp. 861–868, 1998.

[13] Brandies, J. and Gill, J., "Experimental investigation of side-jet steering for supersonic and hypersonic missles", *Journal of Spacecraft and Rockets*, Vol. 33, pp. 346–352, 1996.

[14] Spaid, F.W., "Two-dimensional jet interaction studies at large values of Reynolds and Mach numbers", *AIAA Journal*, Vol. 13, pp. 1430–1434, 1975.

[15] Sakima, F., Fei, H., Arai, T. and Kasahara, J., "Interaction phenomena between a supersonic cross flow and a transverse soinc jet" *AIAA paper 2002-5181*, 2002.

[16] Broadwell, J.E. and Roshko.A., "Structure and mixing of a transverse jet in incompressible flow", *Journal of Fluid Mechanics*, Vol. 148, pp. 405–412, 1984.

[17] Dcwdy, M.W. and Newton, J.F., "Investigation of liquid and gaseous secondary injection phenomena on a flat plate with M=2.1 to M=4.54", *California Institute of Technology* Rep. 32-542, 1963.

[18] Sutton, O.G., "A theory of eddy diffusion in the atomosphere", *Proc. Roy. Soc.*, A(CXXXV), pp. 143–165 1932.

[19] Brown, G.L. and Roshko, A., "On density effect and large structure in turbulent mixing layers", *Journal of Fluid Mechanics*, Vol. 64, pp. 775–816, 1974.

[20] Hussian, A.K.M.F., "Coherent structures - reality and myth", *Physics of Fluids*, Vol. 26, pp. 2816–2849, 1986.

[21] Schluter, J.U. and Schonfeld, T., "LES of jets in cross fliw and its application to a gas turbine burner", http://www.cerfacs.fr

[22] Rathakrishnan, E., *Gas Dynamics*, Prentice Hall of India, 1995.

[23] Rathakrishnan, E., *Instrumentation, Measurements and Experiments in Fluids*, to be published.

[24] http://www.allstar.fiu.edu/aero/rocket3.html

Appendix A

Virtual Instrumentation Based Pressure Aquistion System

Pressure measurement in the supersonic field is one of the challenging tasks, it can not be measured directly by any means but it can be very easily measured by an indirect means through a Pitot probe. It is emphasized by many experimentalists and researchers in the high speed arena that Pitot pressure measurement is the best. The pressure obtained from the Pitot can be read by many means like manometers, Bourdon gauge etc. In high speed flows , pressure measurement is the one of the difficult tasks, as the pressure values are continuously oscillating in nature (especially in open flows) and also it is necessary to read the pressure at faster rate which is only possible with electronic sensing devices, and an automated data acquisition system which eliminates the human prone errors completely.

At aerodynamics lab IIT Kanpur the jet testing facility is equipped with 16 port pressure scanner (PSI 9010) with a range of 2.5kpa to 5200kpa. The main feature of this system is that it can average 256 readings by the time of scanning and gives the averaged value with in fraction of seconds, and also the data acquisition is done by LAB view based application software which is developed in such a fashion that it can acquire the data by mouse clicking and saves the data in a text file which will be processed and analyzed further. The complete pressure measurements system consists of pressure scanner, and a VI based software to acquire the pressure from different parts.

System description

Figure. A.1 shows the implementation of the Virtual Instrumentation based pressure measurement system. As shown in the Fig. A.1 The system mainly consists of the

following components

- System hardware.
- Host computer loaded with application software to acquire pressure.

Description of instrument

The system 9010 intelligent pressure scanner is a pressure measuring device intended for use in test and production environments. It consists of 16 channels and is working in differential mode. It has an asynchronous RS 422/485 host communication interface. It also includes a standard RS-232 diagnostic interface that may also be used as host interface. The optomux style command set is used to send commands and receives response from all ports. It may be configured to communicate in the multidrop network communication always at selected baud rate using the optomux protocol. The multidrop communication always operates with no parity, 8 bit data bits and 1 stop bit. The default baud rate is 9600. Changes to baud rate can be made using special procedure via the DIP switch used to select the node address during initialization at power up. During this special baud rate selection procedure, the Number of averages used during the data acquisition is also selected.

The application software developed using the Lab VIEW (shown in figure 3.3) links the host computer to the pressure scanner via RS 232 communication. The application software performs all the required functions like initialize, reset, rezero calibration and read pressure. The detailed description of these functions is given as follows.

Initialize

The initialize VI of the application software is intended to initialize the module address and check the power restart has occur or not, and also it displays the response of the scanner on the monitor of the host computer.

Reset

Reset VI is intended to instruct the scanner to reset and set all internal control variables to their default reset state.

Rezero calibration

This VI is intended to perform the calibration of the scanner with reference to the standard atmospheric pressure, finds the calibration coefficients (recalibrated offset coefficients) and stores them in nonvolatile transducer memory.

Read pressure

Figure A.3 shows the front panel of the read pressure VI. This VI performs the major task in the entire application software that is to acquired pressure. In this VI, it is provided with a flexible advanced file handling system so that all the acquire data will be saved in the form of text file along with the date time and the details of the channel numbers from which data has been acquired. It also displays the measured pressure value currently on the monitor of the host computer. The main attraction of this VI is that we can display the measured pressure in different units as per users choice like Pascal, inches of mercury and atmospheres etc., logic behind this program is shown in Fig. A.3.

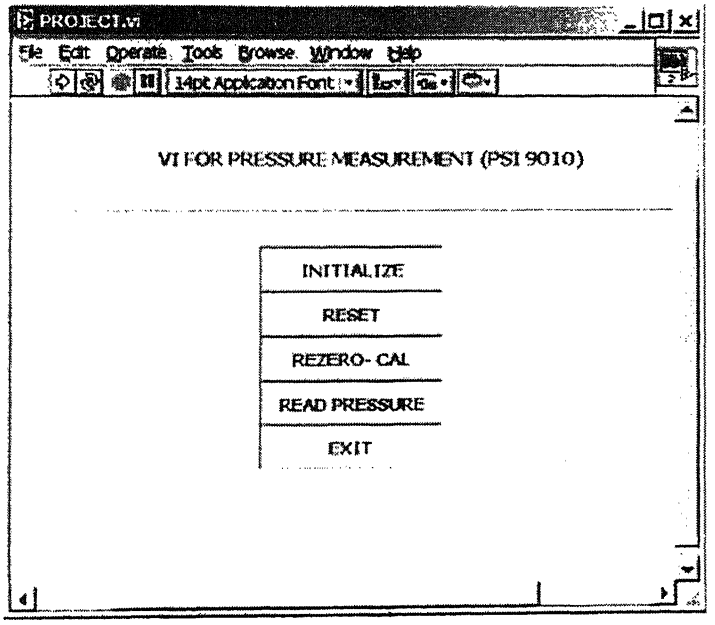

Figure A.1 VI main program front panel

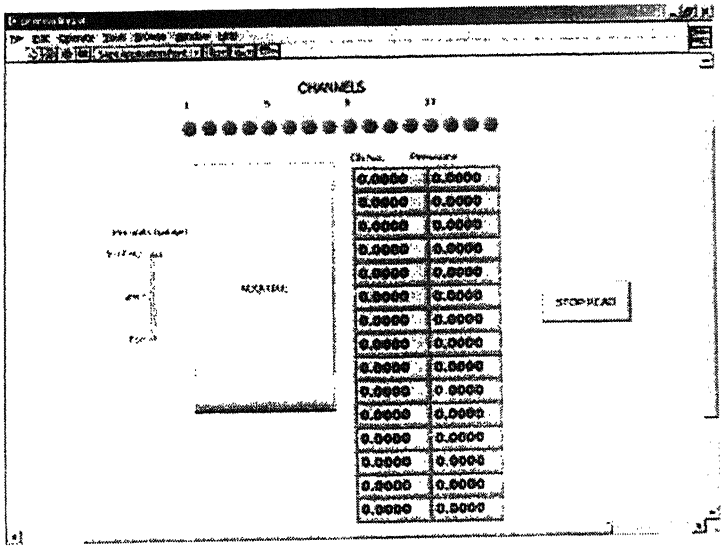

Figure A.2 Read function front panel

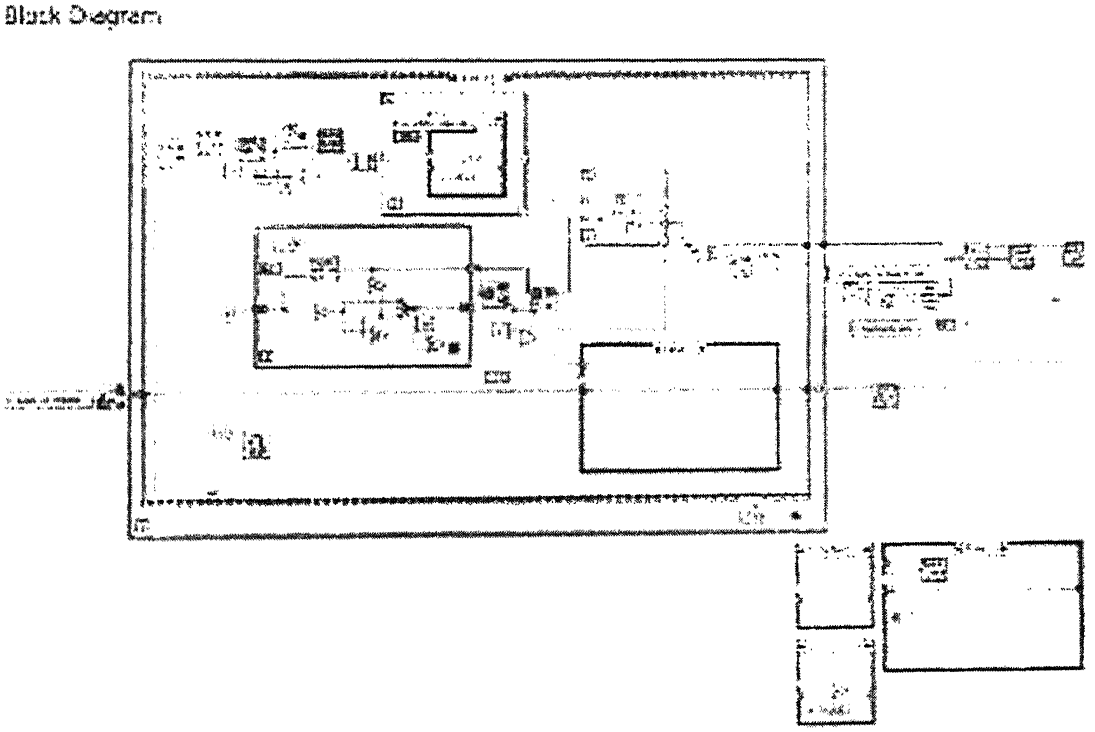

Figure A.3 Block diagram of the program